Molecular Models for Conductance in Junctions and Electrochemical Electron Transfer

by

Shobeir Khezr Seddigh Mazinani

A Dissertation Presented in Partial Fulfillment
of the Requirements for the Degree
Doctor of Philosophy

Approved November 2015 by the
Graduate Supervisory Committee:

Vladimiro Mujica, Co-Chair
Tarakeshwar Pilarisetty, Co-Chair
Charles A. Angell
Anne K. Jones

ARIZONA STATE UNIVERSITY

December 2015

ABSTRACT

This thesis develops molecular models for electron transport in molecular junctions and intra-molecular electron transfer. The goal is to identify molecular descriptors that afford a substantial simplification of these electronic processes.

First, the connection between static molecular polarizability and the molecular conductance is examined. A correlation emerges whereby the measured conductance of a tunneling junction decreases as a function of the calculated molecular polarizability for several systems, a result consistent with the idea of a molecule as a polarizable dielectric. A model based on a macroscopic extension of the Clausius-Mossotti equation to the molecular domain and Simmon's tunneling model is developed to explain this correlation. Despite the simplicity of the theory, it paves the way for further experimental, conceptual and theoretical developments in the use of molecular descriptors to describe both conductance and electron transfer.

Second, the conductance of several biologically relevant, weakly bonded, hydrogen-bonded systems is systematically investigated. While there is no correlation between hydrogen bond strength and conductance, the results indicate a relation between the conductance and atomic polarizability of the hydrogen bond acceptor atom. The relevance of these results to electron transfer in biological systems is discussed.

Hydrogen production and oxidation using catalysts inspired by hydrogenases provides a more sustainable alternative to the use of precious metals. To understand electrochemical and spectroscopic properties of a collection of Fe and Ni mimics of hydrogenases, high-level density functional theory calculations are described in the fourth chapter. The results, based on a detailed analysis of the energies, charges and molecular orbitals of these metal complexes, indicate the importance of geometric constraints imposed by the ligand on molecular properties such as acidity and electrocatalytic activity. Based on model calculations of several intermediates in the

catalytic cycle of a model NiFe complex, a hypothetical reaction mechanism, which very well agrees with the observed experimental results, is proffered.

Future work related to this thesis may involve the systematic analysis of chemical reactivity in constrained geometries, a subject of importance in the context of enzymatic activity. Another, more intriguing direction is related to the fundamental issue of reformulating Marcus theory in terms of the molecular dielectric response function.

To Annie.

ACKNOWLEDGMENTS

I want to express my deep gratitude towards many distinguished and accomplished scholars that educated, discussed, enlightened, and inspired me through out my academic life.

I would like to thank Prof. Vladimiro Mujica for his academic and non-academic role that he played in my life. He gave me the freedom to work on different topics and maintained a collaborative environment, while helping us to gain a guided mastery, albeit partial mastery as I still have a long path ahead of me. I have to mention the role of Professors Ranko Richert and Stuart Lindsay for graciously teaching me concepts of glassy materials and molecular electronics, respectively, through discussions and also working within their research groups.

I also feel indebted to the inspiring Prof. Austen Angell, for his priceless advice and comments throughout the years.

I also want to thank Dr. Tarakeshwar Pilarisetty, for putting his patience and setting up a practical foundations of computational chemistry for me. On the same note, I should thank Dr. Julio Palma for his role in clarifying many concepts through introducing literature or our fruitful debates. I also want to thank Dr. Thorsten Hansen and Dr. Arne Keller for sharing their experience and knowledge with me during their visits.

Dr. Anne Jones' role in my academic life goes beyond a PI and an educator. She rekindled my interest in inorganic chemistry that was initiated by Prof. Davar Boghaei during my undergraduate studies. But above all, she was generous with her time and helped me grow as a scientist.

I had the opportunity to get to know Prof. Will Heywood whom I learned extensively about creative process and design mindset.

I also want to mention my friends who kept me inspired, happy, and sane. I want

to thank doctors: Kayvan, Homayoun, Mohammad, and Hamed. Many of these great friendships were formed around Prof. Afshin Shafiee whom I learned to think deeper and beyond the buzzwords.

I want to thank Annie for her boundless support and understanding. The least I could do was to dedicate this thesis to her since we were both in this together. Finally, I love to show my great appreciation for all my family, my mom, dad, and two amazing brothers, have done for me through all my life.

> How restlessly I desire you,
> Whose absence is the bitter ordeal of being buried alive.
> How restlessly I ask for you,
> On the back of a horse, freshly saddled,
> Who seems to have no patience,
> And the distance is a pointless experience. [1]

[1] Ahmad Shamlou, English translation by Payman Akhlaghi

TABLE OF CONTENTS

CHAPTER Page

LIST OF TABLES

Table Page

Table Page

LIST OF FIGURES

Figure Page

Figure Page

Figure Page

Figure Page

Chapter 1

INTRODUCTION

A long-standing subject of substantial importance for both experimentalists and theorists is the understanding of how charge is transferred across molecules or interfaces. [69, 122, 149, 150, 188] While this seemingly simple process is of utmost importance in biology, chemistry, and material science, it is interesting to note that it does not involve bond breaking or bond formation. While charge transfer can involve both electron and hole transport, the latter is not considered in this dissertation. Intramolecular electron transfer is a chemical reaction involving a quantum tunneling process whereby an electron is transferred from a donor to an acceptor site either through chemical bonds or through space under the influence of a free energy gradient. Electron transport involves the passage of current when a molecule is connected in a circuit to two electrodes under an external voltage bias. While both processes involved electronic charge transfer, there are fundamental differences and they are described using different theoretical frameworks.[100, 101, 122] Under some simplifying assumptions it is possible to establish a simple proportionality relationship between molecular conductance and electron transfer rate.

Electron transfer and transport in biological systems are key to our existence. They are present in the cellular energy harvesting and storage that is the driving-force of all our activities. Electron transfer (ET) in photosystems (Figure 1.1), and mitochondria catalyzes the transformation of redox equivalents into usable ATP and are two processes that portray the importance of ET in biological systems.[24] Perhaps one of the most intriguing cases in biological ET is the extracellular respiration that some microbes have adapted. Through this process, they oxidize the organic matter

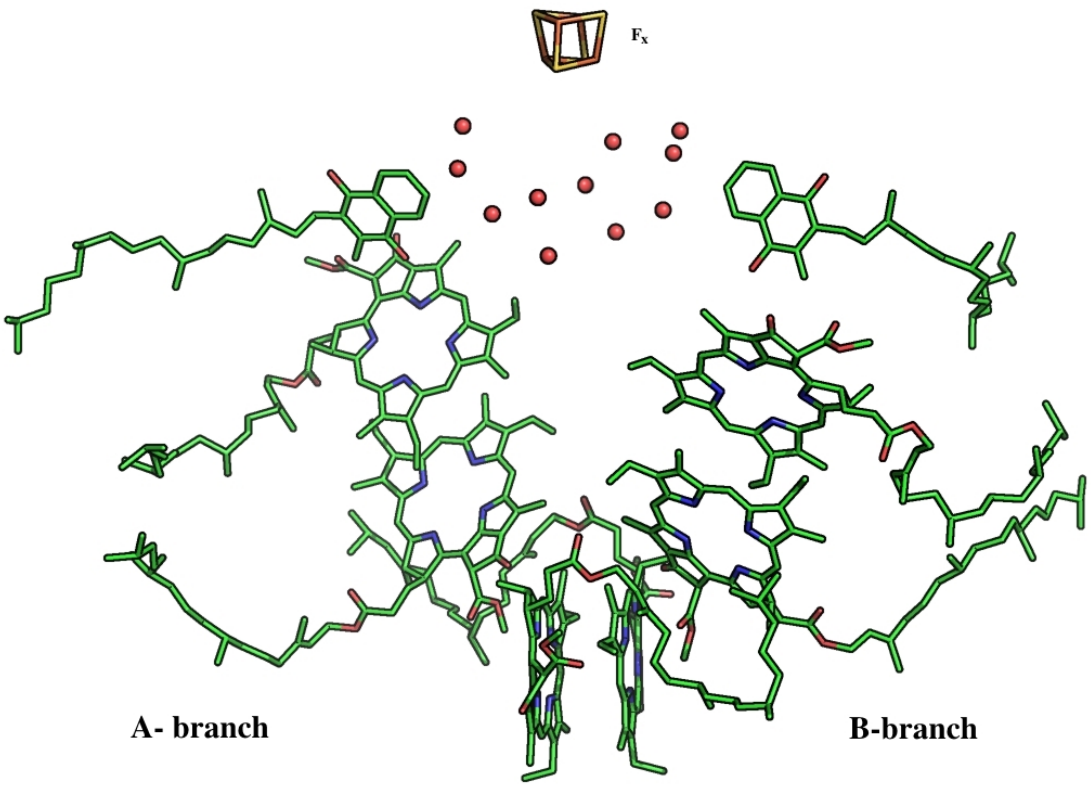

Figure 1.1: An Illustration of an Electron Transfer Chain in PSI (Pdb Entry 1jb0). The Electron Transport Rate in the Two Different Branches (a and B) Is Different.

inside the cell and use the electrons to reduce the transition metal oxides that are rocks!

Inspired by ET in biological systems, chemists have tried to tune the redox properties of metalloenzymes to produce renewable fuels.[74, 13, 221] In chapter four of this thesis, I discuss an example of a successful exploitation of an organometallic complex to produce an exquisite hydrogen production catalyst.

In the realm of material science, electron transfer/transport is the key to the fabrication of the next generation of diodes, wires, and sensors which can be hooked to biological systems. In fact the idea of using an organic molecule as a diode was at

the onset of the new field of molecular electronics.[10] Against this background, I will examine several aspects of electron transfer/transport in a diverse variety of systems throughout this dissertation.

In this chapter, I briefly address the theoretical prerequisites necessary for understanding the material discussed in the subsequent chapters. In the next chapter, I discuss our attempts to find a molecular descriptor that can capture the essence of electron transport which can be used as a screening parameter in designing molecular wires. We then shift into weak interactions and discuss our results in assessing and studying electron transport (ETP) through biologically-relevant hydrogen-bonded systems. We also discuss the effect of cations on conductance of a molecular system through weak interactions (not covalent bonding).

Lastly, I examine our use of computational tools in understanding the mechanism of several hydrogen-generating catalysts in an electrochemical realm.

1.0.1 Marcus Theory of Electron Transfer

A few expressions have been proposed within the framework of classical, semi-classical, and quantum mechanics, to explain electron transfer rate.[149, 122, 124, 24] Here, I briefly review the major expression that is often used, which is based on Marcus's groundbreaking work.[122]

For the purpose of this thesis, electron transfer is considered to occur between two ionizable chemical entities. These two groups can be classified as, the donor (D) and acceptor (A). In other words, the donor is in its reduced state (R) and the acceptor is oxidized (O).

$$\mathrm{RO} \longrightarrow \mathrm{OR}$$

Let us assume that two different electronic states, a and b, corresponding to the minima of two different potential energy surfaces associated with different charge distributions of the same molecule, are the initial and final states of associated with the electron transfer reaction. States a and b can be described by two charge localized, diabatic electronic states with energies E_a and E_b. These energies depend on the nuclear coordinates. A simple idea about these diabatic states is that they could can be related to resonant structures in valence bond theory, but in reality they correspond to real charge rearrangements induced by the fluctuations in nuclear polarization of the environment, typically a solvent. In some cases, e.g. photo-induced ET, these states depend on the experimental preparation details and they do not correspond to the Born-Oppenheimer adiabatic states that diagonalize the electronic Hamiltonian. The electronic Hamiltonian in the diabatic states basis can be cast into the following form:

$$\mathbb{H} = \begin{pmatrix} E_a & V_{ab} \\ V_{ba} & E_b \end{pmatrix} \tag{1.1}$$

where the V_{ab} is the electronic coupling matrix element. The eigenvalues of this Hamiltonian1.1 are the adiabatic electronic ground state (E_0) and charge-transfer excited states' energies (E_1). These energies are defined as:

$$E_{0/1} = \frac{E_a + E_b}{2} \pm \frac{1}{2}\sqrt{(\Delta E)^2 + 4|V_{ab}|^2} \tag{1.2}$$

where the vertical diabatic energy gap is defined as $\Delta E = E_b - E_a$. While diabatic states give a more clear representation of the problem, adiabatic states are more readily used and obtained from electronic structure calculations (Figure 1.2). In fact, all the density functional theory calculations that are described in the coming chapters are the adiabatic states, with E_0 being the outcome of DFT calculations and E_1 can be calculated within the time-dependent DFT formalism.

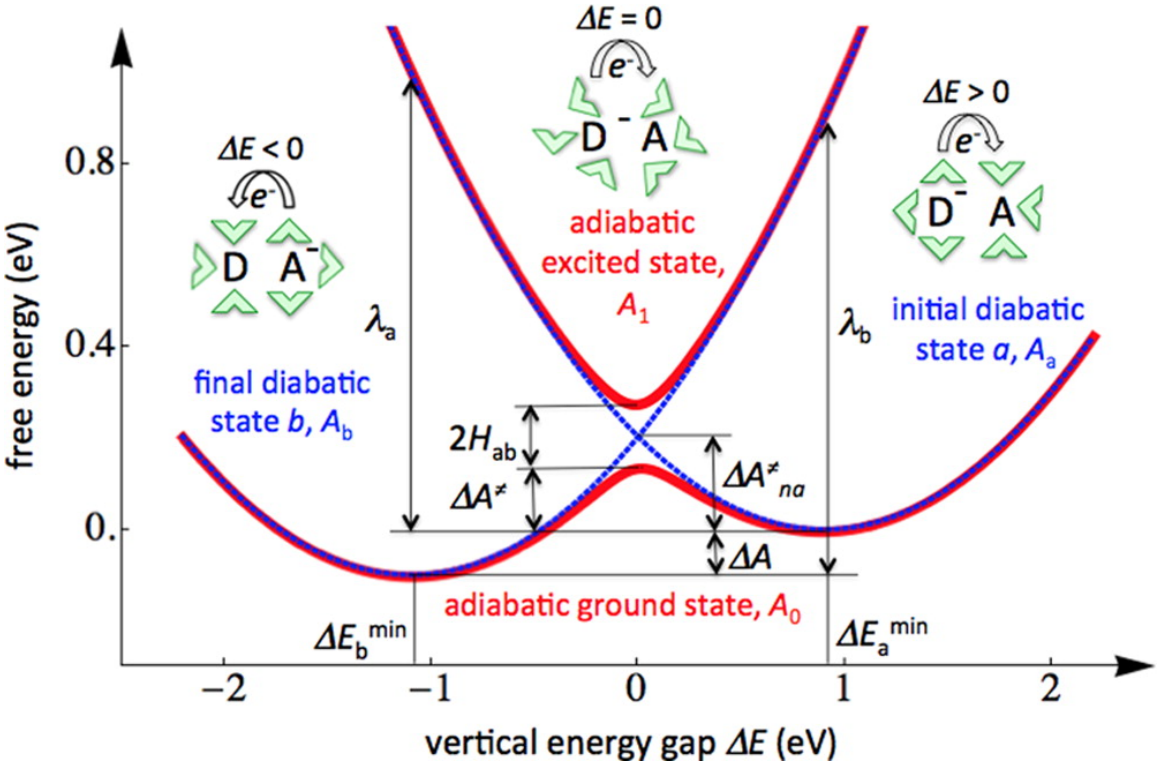

Figure 1.2: "Free Energy Curves for Electron Transfer Between Electron Donor (D) and Acceptor (a) in a Dielectric Environment (Solution Or Protein). Finite Temperature Fluctuations and Reorganization Of the Dielectric Environment along the Et Reaction Coordinate Are Indicated by Green Chevrons." Adapted with Permission from Reference [24].Copyright(2015) American Chemical Society.

The electronic coupling term, discussed above, is a key parameter. In the small coupling regime, V_{ab} is small in comparison to the reorganization energy, λ which is the Gibbs energy expended when the chemical system that has gone through a vertical electron transfer relaxes to the equilibrium state for the new charge distribution, the D and A groups to a good approximation save their individual identity. This corresponds to the non-adiabatic regime. In the adiabatic regime where the coupling is substantial this causes the system to stay in the lower potential energy curve (Figure 1.2) because of the large gap between the adiabatic ground and excited states.

In this sense, Marcus theory is corresponds mostly to a non-adiabatic process. Hence the Landau-Zener theory is applicable to find the probability that the system goes from state a to state b through the intersection of potential energy curves. This approximation together with Fermi Golden Rule can be used in the derivation of the basic equation of Marcus theory for electron transfer rate:

$$k_{ET} = \frac{2\pi}{\hbar}|V_{ab}|^2 \frac{1}{\sqrt{4\pi\lambda K_b T}} exp(-\frac{(\lambda + \Delta G^\circ)^2}{4\lambda K_b T}) \tag{1.3}$$

where k_{ET} is the rate of ET reaction, V_{ab} is the electronic coupling between the initial (a) and final (b) states, λ is the reorganization energy, ΔG° is the Gibbs free energy change for the electron transfer reaction, K_b is the Boltzmann constant, and T is the absolute temperature. Reorganization energy is the energy needed to reorganize the system (compound + its environment) from state a to the structure of state b in the absence of charge transfer.

Marcus's theory follows and enhances the Arrhenius ideas for the rate of a chemical reaction. It neatly defines the activation energy of the reaction through the reorganization energy and Gibbs free energy for the formation of the transition state. It also defines a pre-exponential factor based corresponding to the thermally averaged overlap of the electronic wave functions of states a and b. In the final section of the next chapter, I will mention how we believe we can improve on this equation to provide more time-dependent and dynamical equation.

1.1 History and Background of Molecular electronics

How do electrons move in and through a molecule? What is the electronic conductance of a single molecule sandwiched between metal electrodes? How can we build an electronic device using individual molecules? Molecular electronics (ME) is an interdisciplinary effort of scientists and engineers to answer these questions.

The early efforts in molecular electronics can be traced back to the 1950s, where it was recognized as a potentially promising subject by the United States Department of Defense.[135] In 1974, Arieh Aviram and Mark Ratner proposed, theoretically, that a molecule can act as a device, molecular rectifier (i.e. a molecule that shows diode behavior).[10] This paper was revolutionary because it laid out a schema for calculating molecular conductance through a molecule.

How can someone attach a molecule to a metallic electrode? This was the number one challenge that the field faced in the 1970s. Several conferences devoted to the field, in the 1980s, that were hosted by Forrest Carter and Aviram, stimulated some seminal (and some borderline science-fiction) ideas that popularized molecular electronics.[135] But perhaps the major breakthrough ensued by the IBM laboratories' discovery of the scanning tunneling microscope (STM) and later the atomic force microscope (AFM). It was soon clear that these tools, that help us 'touch' and manipulate individual molecules, can be used to observe and measure conductance (current versus voltage behavior) of a single molecule conencted to, for instance, two gold electrodes (i.e. STM tip and substrate). The first earnest attempt at measuring electron transport through a single-molecule was carried out by Mark Reed and James Tour's groups.[170] Also Robert Metzger's group experimentally proved the feasibility of a molecular rectifier.[136] These experiments taught us, how to measure the conductance of a single-molecule, but the importance and dominance of the fluctuations in the experimental data remained unrecognized.

A collaborative effort among synthetic and physical chemists along with physicists and theoreticians was and is needed to overcome the issues that the molecular electronics community faces. The synthetic problems are more or less resolved. The main challenge for chemists were to coming up with anchoring groups that can robustly connect the molecule to the electrodes. In most cases, sulphur and amine or other

groups with lone-pairs are used. Gold and platinum are commonly used as the electrodes due to their resistance to oxidation and degradation and also their ability to easily form nanometer-sized STM tips. The inescapable problem that experimentalists and device-makers face, is the considerable size of the fluctuations. This problem was solved by using the break-junction techniques that enabled scientists to make thousands of measurements. By theoretical and statistical analysis of the outcome of those measurements, in form of histograms, we can reproducibly measure molecular conductance.[188]

The theoretical and computational efforts in the realm of quantum transport are mostly around the non-equilibrium Green's function techniques. I would briefly discuss the theoretical framework to describe electron transport.

1.1.1 Theoretical Overview

Theoretically, there are different regimes that depending on the applied voltage, the thermal energy, length of the molecule, etc. I briefly describe the formalism to compute the molecular conductance based on the non-equilibrium Keldysh Green's function method.[216]

1.1.2 Problem Set up

Figure 1.3 presents the setup that is used to calculate electron transport in an electrified junction. The junction comprises of left and right semi-infinite electrodes and a molecule, [6]helicene. It is assumed that the metal electrodes are defect free, periodic crystallines with the unit cell defined in the direction of transport.

Thermodynamically, we have two bulk gold electrodes and a region in the middle. Mostly for computational reasons the molecular device is considered to incorporate some parts of the electrodes. This will be clarified later. We treat the combination of

the main molecule and the parts of the leads as one system and we name it 'extended molecule'. The two electrodes normally have different chemical potentials (in the presence of bias voltage), μ_L and μ_R, and they are able to exchange electrons with the extended molecule.

Electrostatic view of the problem can clarify the reason we need to include few (2 to 4) layers of gold atoms in the extended molecule. The conductance depends on the spatial profile of the electrostatic potential, which in principle has to be determined self-consistently through the simultaneous solution of Schrödinger equation to calculate the charge density $\rho(\vec{r})$ and Poisson equation to determine the electrostatic potential $\Phi(\vec{r})$. This is expressed schematically as the following set of equations.

$$\begin{cases} H\Psi = E\Psi \\ \Psi \rightarrow \rho \\ \nabla^2\Phi = -\frac{\rho}{\epsilon_r} \end{cases} \tag{1.4}$$

Where ϵ_r is the dielectric constant of the inter-electrode medium.This scheme, described by the set of equations 1.4, was used for a one dimensional tight-binding system, and Mujica et al. found that the self-consistent charge distribution for a finite applied voltage corresponded essentially to that of a polarizable dielectric.[66] Similar conclusions using three-dimensional models and *ab initio* electronic structure methods have been found by Ratner et al. [216] These results strongly hinted to the importance of explicitly including the molecular polarization in a conductance model, a topic that is explored extensively in this dissertation and in particular in chapter 2.

To avoid the discontinuity, the self-consistent electrostatic potential that is calculated for the extended molecule should be equal to the electrodes'. Hence we add several layers of the electrode to form the extended molecule. This is also consistent with the physical picture of a molecule adsorbed on an electrode surface which would

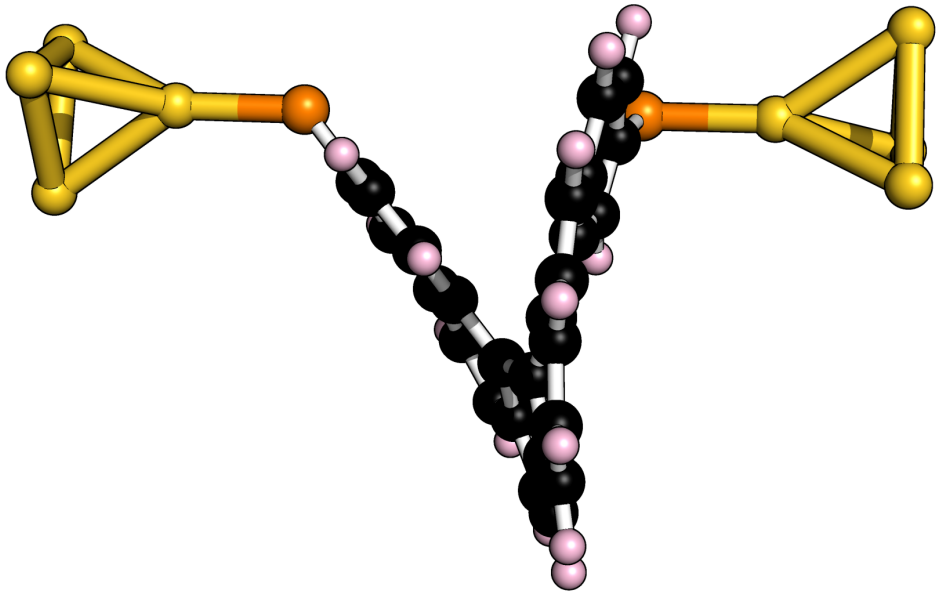

Figure 1.3: This Figure Shows an Electrified Molecular Junction. In This Image a Molecule That ([6]Helicene) Is Sandwiched Between Two Electrodes (Gold) Is Shown. This Is Also the Setup We Use Through out This Dissertation for Calculating Charge Transport.

reconstruct the surface of the electrode, hence make the extended molecule a nice practice.

Conductance as a Transport Process; Landauer Formula

In a typical conductance measurement, in a nano-device, the molecule is connected to two leads that are assumed to act a reservoirs for electrons at a well-defined temperature and chemical potential, as depicted in Figure 1.3. Under some assumptions regarding the many-body aspects of the electron transport process, we can view this phenomenon as a scattering process. This way, the problem can be reduced into dealing with the transmission and reflection probabilities, an idea first introduced in

the seminal work of Landauer. It is worth mentioning that the transport process is limited in this case to a one-electron process that conserves phase coherence. This approach is surprisingly successful in describing the experimental observations, in spite of its relative simplicity. Pedagogically, it is very beneficial to understand the connection between current and transmission intuitively before moving into a more mathematically intensive approach.

Let us imagine that a plane wave, ($\frac{1}{\sqrt{L}}e^{ikx}$) is representing the electrons that are coming from the left electrode towards a potential barrier with length L. Part of this wave will be reflected, with the probability amplitude of r and part of it will be transmitted ($T = |t|^2$).

The current density, J_k, in quantum mechanics is defined as:

$$J_k = \frac{\hbar}{2mi}\big[\psi^*(x)\frac{d\ \psi}{d\ x} - \psi(x)\frac{d\ \psi^*}{d\ x}\big] = \frac{e}{L}\ v(k)\ T(k) \tag{1.5}$$

where $v(k) = frac\hbar km$ is called group velocity. Equation 1.5 is define for an electron with an specific energy while in a real device there are many electrons, with different energies, contributing to the current. Hence, we need to sum over all the positive k values. We also have to take into account the Pauli Principle which results in the introduction of $f_L(k)[1 - f_R(k)]$. $f_R/L(k)$ are the Fermi distribution functions of the electrons. This factor also guarantees that we are only considering transfer from the occupied states on the left electrode into the empty states of the right electrode. Also it can account for the shifts in the chemical potential in the presence of an applied bias voltage. These considerations will give us:

$$J_{L\to R} = \frac{e}{L}\sum_k v(k)T(k)f_L(k)[1 - f_R(k)] \tag{1.6}$$

Next step is to convert the sum into an integral:

$$J_{L\to R} = \frac{e}{L}\int dk\ \ v(k)\ T(k)\ f_L(k)[1 - f_R(k)] \tag{1.7}$$

In solid states physics, the density of states is defined as: $\frac{dk}{dE} = \frac{m}{\hbar^2 k}$. To simplify the equation we change the integration variable from k to E, which results in:

$$J_{L\to R} = \frac{e}{h}\int dE \;\; T(E)\; f_L(E)[1 - f_R(E)] \tag{1.8}$$

Similarly, since the transmission function of crossing from the left side of barrier to the right and vice-versa are the same, we can prove that the current from the right electrode to the left electrode is:

$$J_{R\to L} = \frac{e}{h}\int dE \quad T(E)\; f_R(E)[1 - f_L(E)] \tag{1.9}$$

Finally, the total current is $I = J_{L\to R} - J_{R\to L}$. We have to also double the current because of electron's spin degeneracy. It is worth mentioning that this degeneracy does not always hold and in fact conductance current can be spin-dependent.[118, 33, 49, 219, 22, 150] The final outcome is the simplest version of the eminent Landauer formula and shows the connection between the current and transmission.

$$I(V) = \frac{2e}{h}\int_{-\infty}^{\infty} dE \;\; T(E)\; [f_R(E) - f_L(E)] \tag{1.10}$$

We can see that this is similar to equation 1.14 that is discussed in the next section.

Green's function techniques

At the molecular level, we are assuming that the electron transport can be described as involving an incident plane-wave (or state) propagating from deep in the electrode comes and interacting with the extended molecule potential (scattering region) to be collected a the outgoing wave in the other electrode. This system is described by a Hamiltonian, $\mathcal{H}$, which has an infinite dimension. It is worth mentioning that through this dissertation I use calligraphic letters for matrices with infinite dimension. In the

absence of magnetic field the Hamiltonian can be molded into the form:

$$\mathcal{H} = \begin{pmatrix} H_L & H_{LM} & 0 \\ H_{ML} & H_M & H_{MR} \\ 0 & H_{RM} & H_R \end{pmatrix} \tag{1.11}$$

The retarded Green's function for the whole system, $\mathcal{G}^r$, contains all the information needed for solving this problem. The retarded Green's function can be calculated by solving the Green's function equation:

$$[\epsilon^+ \mathcal{S} - \mathcal{H}]\mathcal{G}^r(E) = \mathcal{I} \tag{1.12}$$

where $\int$ is the overlap matrix and $\epsilon^+ = \lim_{\delta \to 0^+}(E + i\delta)$.

Finding the Green's function, that is an infinite dimensional matrix, can be mapped into a simpler yet equivalent problem by benefiting from Löwdin partitioning technique. This technique was used by Mujica et al to reduce "the infinite dimensional matrix problem into an N $\times$ N problem".[140] The retarded Green's function contains all the information about the extended molecule that is attached to the electrodes. In other words this is a Green's function that corresponds to the effective Hamiltonian of the extended molecule

$$H_{eff} = H_M + \Sigma_L^r(E) + \Sigma_R^r(E) \tag{1.13}$$

with $\sum_{L/R}^r(E)$ is the self-energy of the left and right electrodes. This dimension reduction comes at a price. While 1.11 is hermitian, due to the introduction of the self-energies, the 1.13 is not hermitian anymore.

The current in this framework is given by:[132]

$$I = \frac{2e}{h} \int_{\mu_L}^{\mu_R} dE Tr[\Gamma^L G^a \Gamma^R G^r][f_L(E) - f_R(E)] \tag{1.14}$$

where $f_L(E)$ and$f_R(E)$ are the Fermi functions for the left and the right electrode.

At zero bias, we can calculate the conductance of the system at Fermi level:

$$g(E) = g_0 Tr[\Gamma_L G_M^a \Gamma_R G_M^r] \tag{1.15}$$

where $Tr[\Gamma_L G_M^a \Gamma_R G_M^r]$ is the transmission function ($T(E)$) and $\Gamma_{L/R} = i[\Sigma_{L/R}^r(E) - \Sigma_{L/R}^a(E)]$and g_0 is the quantum of conductance.

In principle, the NEGF (Non-Equilibrium Green's Function) theoretical framework permits the description of elastic and inelastic transport including electron-electron and electron-phonon interaction through an appropriate inclusion of self-energies for each type of interaction. It is however important to consider approximate schemes and the combination of non-equilibrium Green's function method with density functional theory has been extensively used for the approximate description of electron transport in molecular junctions.

Chapter 2

POLARIZABILITY AS A MOLECULAR DESCRIPTOR OF CONDUCTANCE

2.1 Introduction

Organic molecular electronics have garnered tremendous interest[115, 73, 86, 163, 39] due to the possible ability to replace circuit elements such as transistors. [39, 8, 176] This is outshone by the recently explored interface of molecular electronic devices with biochemistry[110] and the study of various phenomena such as charge transfer on the bio-nano interface.[190] One of the key properties for an efficient design is the ability of these molecular structures to transport electrons effectively. There are an endless number of possibilities for the molecular structures.[153] While having a plethora of options for design gives scientists and engineers many opportunities, it can become overwhelming in the absence of a physical parameter that can be used as a screening factor that can a priori discern between desirable and unattractive candidates.[88, 176] For example, such a factor can be very important in finding an optimized reader molecule in a recognition junction since synthesis and measuring or computing the conductance of these is very time consuming.[96, 223]

Traditionally, some rules of thumb have been used to make fast predictions about the conductance in a single molecule junction, parameters such as length,[98] temperature and the energy gap between HOMO (Highest Occupied Molecular Orbital) and LUMO (Lowest Unoccupied Molecular Orbital.[149] But due to the intrinsic complexity of the transport and its relation to molecular electronic structure, these rules do not always hold. [184, 215] Molecular polarizability can be used as a guideline for designing systems with desired transport properties.

The physical plausibility of the connection between conductance and polarizability can be realized from Mujica and coworkers' work that described the spatial profile of the electrostatic potential in a junction by solving Schrödinger and Poisson equation self-consistently by connecting the quantum electronic density to the electrostatic potential.[141]

The picture that emerges from this model is that if many-body and inelastic effects, such as charging and electron-phonon coupling, are neglected, molecules behave to a large extent as a dielectric whose polarization response counteracts the driving field. This leads to a spatial profile that differs substantially from that of a vacuum junction between two electrodes, which is a linear function of the inter-electrode separation as found by solving Poisson equation for zero charge density, and corresponds rather to an S-shape function associated with a spatial profile characterized by the fact that the potential drop occurs essentially at the interfaces between the molecule and the electrodes.[141]

Accepting the crucial role of the molecular bridge in determining the local dielectric properties of a junction; the next conceptual step is to connect the dielectric constant to the molecular polarizability, which I introduce by assuming the validity of the Clausius-Mosotti relation from electromagnetism. Once this is achieved, the missing link is the connection between conductance itself and the molecular polarizability. This is still an open theoretical question, which has been addressed in several articles.[201, 25, 55] . In this work, I approach this problem in its simplest form, using Simmons' tunneling model, which connects the barrier properties, that in turn determine the current and the conductance, to the junction dielectric constant.

The main goal of this study is to explore the robustness of this connection in different design motifs and discuss the domain in which it is applicable. To this end, I have investigated the correlation between calculated molecular polarizabilities

and the experimental zero voltage conductance of different families of molecules used in junctions. The results are remarkably consistent with the qualitative and even quantitative predictions of my simple model.

The structure of this chapter is as follows. First the computational protocol is discussed. In the result section on polarizability, I present several systems and discuss the success of this approach for various families of molecules. I then finish by discussing the limitations and possible application of this correlation in helping the design of next generation nano-electronics components.

2.2 Computational Details

Geometry optimizations and polarizability calculations were carried out at the Density Functional Theory level by using the Becke gradient-corrected exchange functional and Lee-Yang-Parr correlation functional with three parameters (B3LYP) and the 6-31G* basis set by ORCA electronic structure package.[144, 48, 162, 18, 103, 60, 67] The polarizability calculations were also done with aug-cc-pVTZ basis set.[206] The tabulated results show that the trend in polarizability is conserved in spite of the change in the values.

2.3 Results and discussion

As mentioned in the Introduction, I approach the rational design of molecular electronics materials by studying the correlation between polarizability and conductance. It is worth mentioning that since polarizability is a tensor property and conductance is a scalar quantity, in the simplest case I need to use the isotropic molecular polarizability which is defined as:

$$\bar{\alpha} = \frac{1}{3} tr(\alpha) = \frac{1}{3}(\alpha_{xx} + \alpha_{yy} + \alpha_{zz})$$

	α (Å)^3	
System	6-31G*	aug-cc-pVTZ
Aniline	11.6	12.3
Anisole	12.5	13.4
Benzaldehyde	12.4	13.1
Chlorobenzene	11.7	12.6
Fluorobenzene	9.8	10.4
N-methylaniline	13.5	14.4
Nitrobenzene	12.5	13.2
Nitrosobenzene	12.2	12.8
Phenol	10.6	11.3
Toluene	11.7	12.5

Table 2.1: Calculated B3LYP, Isotropic Polarizabilities (α) of Different Substituted Benzenes.

I investigated systems whose experimental conductance has been reported and I tested the correlation between calculated polarizabilities and such measured conductance. I observed that an increase in static polarizability of the molecules results in a decrease in the conductance values. This correlation holds for families of molecules. I classify the results based on different molecular groups and show that the correlation holds within different groups, thus indicating the potential of this molecular property as a general guidance for designing new molecular electronic devices.

2.3.1 Halobenzene, the effect of substituents

The effect of halogen substitution on benzene's conductance is investigated as an initial step. Due to their electronegative nature, halogens are electron withdrawing groups (EWG). Hence they reduce the electron density on the benzene which results in a decrease in the energy of the HOMO orbital in comparison to HOMO energy of benzene.[160] The calculated conductance values reported by Venkataraman and coworkers are plotted against calculated molecular polarizability. Figure 2.1 clearly indicates that the conductance of the molecule decreases as its static polarizability increases by changing the substituents.

2.4 Amine-Gold linked molecular motif

The thiol group has been used extensively as an anchoring group between the molecular bridge and gold electrodes.[188, 6, 98, 163] The strong bond between gold and sulfur is the reason for this general interest towards the Au-S anchoring groups. The main issue with sulfur-gold motif is the dramatic dependence of the conductance on the anchoring groups' geometrical parameters.[160, 47, 159] Nitrogen-based anchoring groups are seemingly a good solution.[224]

Due to the reproducibility and smaller effect of the anchoring groups' geometry on conductance; using this motif in designing the molecular circuits and thermoelectric systems seems to be a sensible path.[200, 160, 158] To investigate the robustness of the proposed signature decaying trend, I calculated the polarizabilities of the diamine family and the bipyridine family and plotted them against the conductance values that were measured.[200, 160, 158] Figure 2.2 summarizes the results. The difference between the conductances of the two families is mainly due to the different nature of

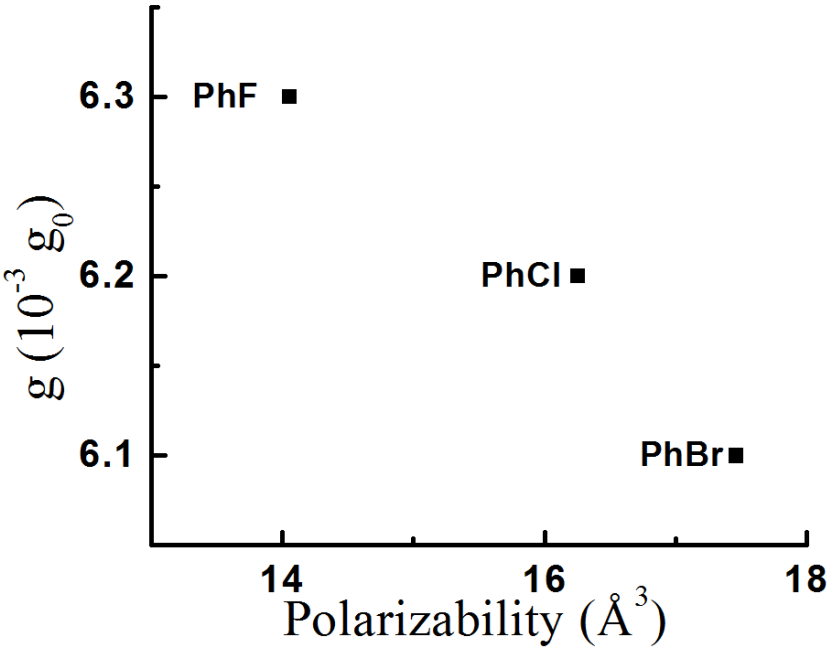

Figure 2.1: The Correlation Between Conductance (*milli* g_0) and Static Polarizability ($Å^3$) Can be Seen. In These Systems The Halogens Affect The Conductance Through Modifying The HOMO of The Molecule. It Can Be Inferred That Polarizability Can Be Used to Predict The Effect of These Substituents on Conductance of Benzene.

their individual anchoring group.

2.5 Thiophene and Furan oligomers

Five-membered heterocycles, in particular thiophene and furan, have been used extensively in organic electronic devices such as organic field effect transistors (OFET) and organic photovoltaics (OPV).[108, 173, 177, 211, 203, 147] The oligomers can be considered as a cis π-conjugated $(CH)_x$ system that are stabilized by a heteroatom.[172] These systems are aromatic. Breslow and coworkers showed that an increase in the (negative) aromatic stabilization energy correlates with the conductance values in

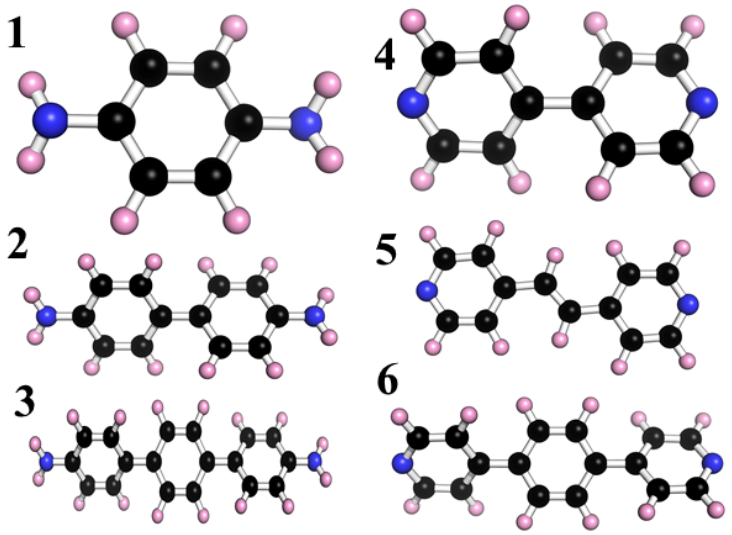

(a) (b)

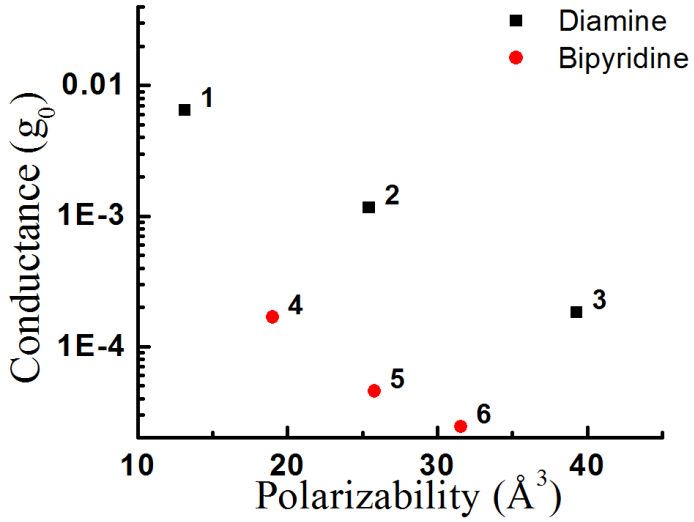

(c)

Figure 2.2: The Structures of the Compounds Are Presented. (A) Structures **1**, **2** and **3** Belong to the Diamine Family Whereas **4**, **5** and **6** Are from the Bipyridine Family of Molecules (B). (C) Measured Conductance, Obtained from Venkataraman and Coworkers Work[200, 160, 158], in the Unit of Quantum of Conductance Are Plotted with Respect to Calculated Polarizability (Å^3). The Figure Suggests That for a Family of Molecules (Molecules That Are Structurally Similar) We Can Use Polarizability as a Descriptor of Conductance to Predict the Electron Transport Properties of a Molecule.

systems with thiophene and furan motifs.[36] I have selected the aromatic systems in Breslow's work, to put the polarizability-based design guideline through a strict test. Compound **7**, **8**, **9** and **10**(named in accord with Breslow's work) are 2,5-bis-(4-aminophenylethinyl)furan, 2,5- bis-(4- aminophenylethinyl)thiophene, 2,5-bis-(4-aminophenyl) furan and 2,5-bis-(4- aminophenylethinyl) thiophene respectively (Figure 2.3-a). The calculated polarizability and measured conductance are presented in Figure 2.3-b. There are two sets of correlations for these systems. First, the correlation between **7** and **9** (**8** and **10**) that are furan (thiophene) based compounds that their structures are modified by addition of alkyne groups. Second, the furan versus thiophene (**7**, **8** and **9**, **10**). It can be seen that for both sets of molecular wires, an increase in polarizability is followed by a decrease in conductance of the heterocyclic molecules. In fact this is not very surprising. It has been shown that an increase in polarizability is an indicator of an increase in the aromaticity of the compound.[45], which has led to several ways of measuring aromaticity based on the static polarizability of the system.[44] It is worth mentioning that increasing the length of a molecular wire by increasing furan/ thiophene units mainly modifies the LUMO and has a negligible effect on the energy of the HOMO, which again points out to the limitations of schemes based on molecular orbitals to predict the behavior of the conductance .[19, 45]

2.6 Hydrogen bond motif

A ubiquitous motif in organic molecular electronics, in particular bio-inspired designs, takes advantage of the unique properties of hydrogen bonding to build low cost, bottom-up organic materials with desirable properties.[52, 54, 12, 59, 82, 222, 214] Nishino et al have measured the conductance through the hydrogen bond and showed that at short distances hydrogen-bonded wires have higher conductance than alkane

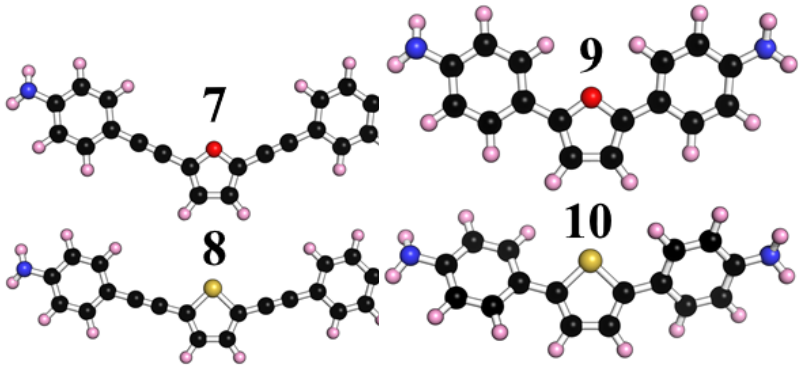

(a) (b)

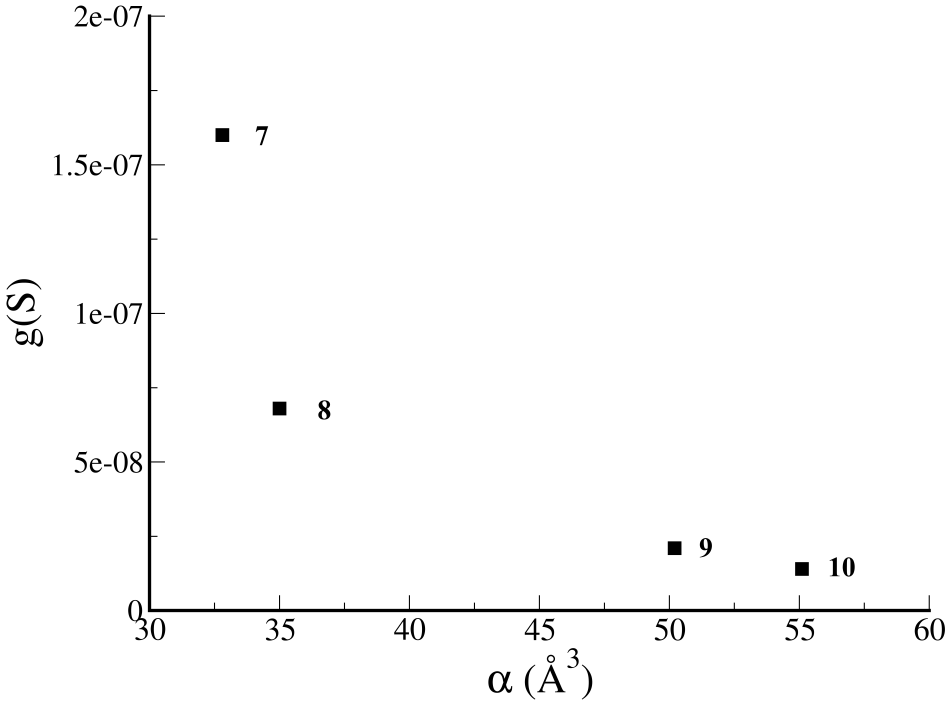

(c)

Figure 2.3: (A) and (B) Shows the Structure of the Compounds **7**, **8**, **9**, and **10**. In the Structures Nitrogen, Oxygen, Sulfur, Carbon and Hydrogen Are Blue, Red, Yellow, Black, and Pink. (C) the Calculated Polarizabilities Versus Experimental Conductance Shows That for the Families of Molecules That Shows the Change in the Polarizability Correlates with the Changes in the Conductance of the Junction.

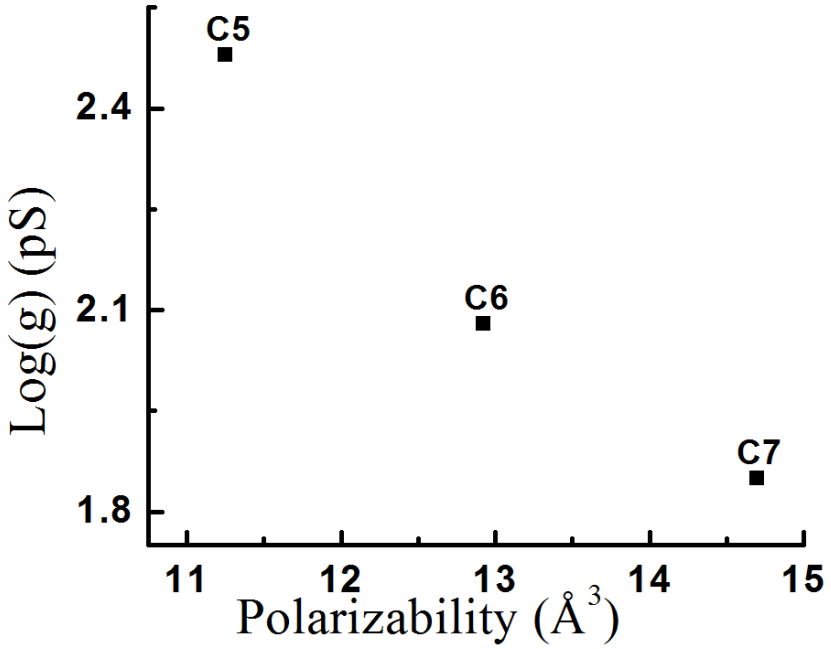

Figure 2.4: The Correlation Between Measured Conductance and Calculated Static Polarizability of Three Hydrogen-bonded Carboxyl Groups ($c_n cooh$) Is Shown in This Plot. The Labels Show the Total Number of Carbons in the Molecular Junction in a Manner Consistent with the Work of Nishino *etal .[148]*

chains.[148] Based on their results, I investigate the connection between polarizability and conductance for the family of carboxylic acid alkane thiols. Figure 2.4 shows the robustness of the correlation between conductance and static molecular polarizability. I have previously shown for a set of biologically-relevant hydrogen-bonded systems, that polarizability can be used as a universal guideline to qualitatively predict conductance through the hydrogen bonded system.[131]

2.7 Barrier model of conductance

To explore the connection between polarizability and conductance I consider a model of molecular conductance as a tunneling process, which essentially ignores all the many-body and inelastic aspects of the transport process and assumes that the molecule acts as a one-dimensional tunneling barrier, specified by two parameters: the height and the width of the barrier. Simmons' model, which includes image charges and dielectric effects, has been extensively used for the description of tunneling through metal-molecule interfaces with remarkable success.[181] I am particularly interested in the expression for the height of the tunneling barrier, which has been shown in the Simmons model to be related to the dielectric constant as:[181]

$$\bar{\phi} = \phi_0 - qV\frac{s_1 + s_2}{2x} - \frac{1.15\lambda x}{\Delta s} ln(\frac{s_2(x - s_1)}{s_1(x - s_2)}).\frac{1}{\epsilon_r} \tag{2.1}$$

with λ defined by:

$$\lambda = \frac{q^2 ln2}{8\pi\epsilon_0 x} \tag{2.2}$$

Where q is the electron charge, V is the bias voltage, ϕ_0 barrier height, s_1 and s_2 are the turning points in the barrier shape, $\Delta s = s_2 - s_1$, x is the nominal width of the barrier, ϵ_0 is the vacuum permittivity and ϵ_r is the dielectric.

The relation between the current and the voltage in the tunneling junction can be recast in the following form:

$$\begin{aligned} J &= J_0(\bar{\phi}\ e^{-A\sqrt{\bar{\phi}}} - (\bar{\phi} + qV)\ e^{-A\sqrt{\bar{\phi}+qV}}) \\ J_0 &= \tfrac{q}{2\pi h(\sigma\Delta s)^2} \\ A &= (\tfrac{4\pi\Delta s}{h}\sqrt{2m_e}) \end{aligned} \tag{2.3}$$

where σ is a correction factor as described by Simmons and is usually around 1.[181] On the other hand the most straightforward connection between the dielectric constant ϵ_r of an electrified interface and the molecular polarizability α of the intervening

medium is given by Clausius-Mossotti equation:

$$\begin{aligned} \epsilon_r &= \tfrac{\epsilon_0+2\gamma\alpha}{\epsilon_0-\gamma\alpha} \\ \gamma &= \tfrac{N_A d}{3M} \end{aligned} \tag{2.4}$$

with N_A being the Avogadro number, ϵ_0 vacuum permittivity, M is the molar mass of the material and d is its density. It applies to the dielectric constant of a bulk dielectric material that is homogeneous and isotropic, and it connects the static polarizability of a single molecule with the susceptibility of a three-dimensional molecular material. The basic microscopic premise of this relation is that in a uniform electric field, each molecule is represented as a polarizable point dipole that experiences the external field inducing a polarization response. These conditions might seem too simplistic to describe a molecular junction, but the nanoscopic validity of the Clausius- Mossotti equation has been systematically explored by Natan et al. [143] and it corresponds to a well-defined limit that provides us with a physically reasonable starting point, that is only applicable for simple junction where tunneling is the dominant transport mechanism. The inclusion of hopping or hybrid transport mechanisms, like those present in DNA, is well beyond the validity of my simple model.

The combined use of Equations 2.4 and 2.1 results in the desired connection between the effective barrier's height and the polarizability:

$$\bar{\phi} = \phi_0 - qV\frac{s_1+s_2}{2x} - B(\frac{\epsilon_0-\gamma\alpha}{\epsilon_0+2\gamma\alpha}) \tag{2.5}$$

where $B = \frac{1.15\lambda x}{\Delta s} ln(\frac{s_2(x-s_1)}{s_1(x-s_2)})$. The differential conductance g is defined as:

$$g(V) = \frac{\partial J}{\partial V} \tag{2.6}$$

And the differential conductance in the limit of zero voltage can be obtained straightforwardly from Equation (2.3).

$$\lim_{V\to 0} g(V) = -qJ_0 e^{-A\sqrt{\bar{\phi}}}\left(1 - \frac{A\sqrt{\bar{\phi}}}{2}\right) \tag{2.7}$$

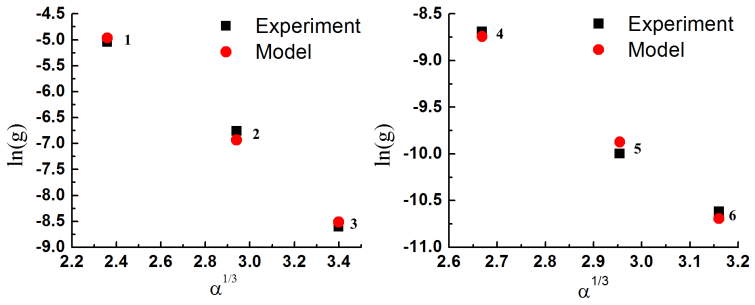

(a) (b)

Figure 2.5: Plot of ln of Conductance Versus Third Root of Polarizability for Diamine (a) and Bipyridine (B). I Used the Following Values and Fitted the Equation 2.8. I Used the Following Values to Fitting. (A) for Diamine I Used $g_1 = 11.26$, $c = .01$ and $\beta_1 = 3.76$. (B) for Bipyridine Family, I Used $g_1 = 2.75$, $c = .01$ and $\beta_1 = 4.31$

In deriving Equation 2.7, I assumed that the molecular polarizability is not dependent on the bias voltage. Expanding the barrier in terms of polarizability and insert it into the equation 2.7 gives:

$$g = g_1 e^{-\beta_1 \alpha} \left(C - \frac{\beta_1}{2}\alpha + \dots \right) \tag{2.8}$$

where $\beta_1 = \frac{AB\gamma}{2\epsilon_0\sqrt{\phi_0 - B}}$, $g_1 = -J_0 q e^{-A\sqrt{\phi_0 - B}}$ and $C = 1 - \frac{A}{2}\sqrt{\phi_0 - B}$. Inspired by the correlation between polarizability and volume of the molecule, I write $\alpha \simeq L^3$. Figure 2.5 plots natural log of conductance versus $\alpha^{1/3}$ and compares it with conductance values calculated via equation 2.8 for the diamine and bipyridine systems (Figure2.2).

2.8 Conclusions

In this work I have explored the rather substantial evidence of an existing correlation between the static isotropic molecular polarizability and the molecular contribution to the zero-voltage conductance of a molecular junction. I have also examined

the physical origin of such a correlation via a model that connects the local dielectric properties of the junction to its transport behavior via changes in the effective shape of the associated tunneling barrier.

While my model is clearly not a first-principle theory, it does incorporate strong physical plausibility arguments and provides a rationale for the apparent correlation between experimental conductances and calculated molecular polarizabilites. It also relates to recent efforts by Ratner, Marks and co-workers to use the dielectric constant as a single variable characterizing the extent of electric network connectivity at the molecular level.[21, 76, 75] Finally, these findings strongly suggests, together with the already demonstrated connection between conductance and electron transfer rate, that it should be possible to reformulate Marcus theory of electron transfer in terms of response functions associated to the frequency-dependent polarizabilities, a subject I am currently working on and that is related to the original approach taken by Marcus to this subject[123, 121]

Chapter 3

ELECTRON TRANSPORT THROUGH HYDROGEN BOND

3.1 Introduction

Designing and developing new functional electronic devices at nano scale based on supramolecular self-assembly and controlled organization have mustered immense interest.[207, 209, 208, 220, 94, 154, 105]

The recent demand for electronics in biomedical applications is in part the driving force of this trend.[110] Despite substantial progress in nucleotide sensing technologies, there have been very few studies on electron transport through molecular systems that have non-covalent interactions.[35, 213, 80, 182] Therefore we believe there is a need for systematic studying of electron transport through hydrogen bond. Despite their small interaction energies, in particular through their cooperative and collective effects, hydrogen bonds have shown promising results in direct monitoring of chemical processes.[137, 142, 126]

Hydrogen bonds are also known for their relatively high polarizability and hyperpolarizabilities.[90] Their polarizabilities further increase in the presence of external field.[53] For electron transport through hydrogen bond this is indeed a very important feature, because the more polarizable systems have a soft electron cloud that responds to the external bias which in turn can modulate and modify the barrier shape and height.

Ultimately the change in the barrier parameters, directly changes the tunneling current. Weiss and coworkers have shown that by studying the changes in the conductance of molecules adsorbed on gold electrodes, we can measure their

polarizabilities.[139] As it was shown in the previous chapter, based on the correlation between polarizability and the measured conductance of hydrogen-bonded systems, we were inspired to look systematically into the important, yet somewhat neglected[148, 197, 29, 185], ubiquitous weak interaction. We have investigated the effect of factors such as hydrogen bond geometry, strength, polarizability and electronic couplings on electron transport. In this study, we focus on biologically-relevant hydrogen bond between O,N,S, and H.

3.2 Computational Details

Geometries of all the hydrogen-bonded structures and their monomers were DFT-optimized by using B3LYP functional. We have also used two different basis sets, 6-311++G(2d,2p) and 6-31G*, which we will refer to as large and small basis sets to calculate the electronic structure of these molecules. [144, 61, 48, 162, 18, 103, 60] This level of calculation has been shown to be successful at describing hydrogen-bonded systems' properties. For interaction energies, we have used Boys and Bernardi counterpoise correction to consider the basis set superposition error.[27]

In this chapter, I use atomic polarizabilities by partitioning the static molecular polarizability components into atomic components by using Hirshfeld population analysis.[125]

$$\alpha_{\gamma\gamma} = \sum_i \alpha_{\gamma\gamma i} \tag{3.1}$$

where $\alpha_{\gamma\gamma i}$ is defined as:

$$\alpha_{\gamma\gamma i} = \lim_{F_\gamma \to 0} \frac{\mu_\gamma(F_\gamma) - \mu_\gamma(0)}{F_\gamma} \tag{3.2}$$

In this equation, $\mu_\gamma(F_\gamma)$ and $\mu_\gamma(0)$ are the distributed contributions to the dipole moment. These parameters are obtained from Hirshfeld population analysis. F_γ is the magnitude of the auxiliary field that is used for polarizability calculations. On

the other hand the spherically averaged molecular polarizability can be computed as:

$$\alpha_{\gamma\gamma} = \left(\frac{\partial \mu_\gamma}{\partial F_\gamma}\right)_{F_\gamma \to 0} \tag{3.3}$$

where γ is the x, y, and/or z. The static polarizability tensor can be recovered by summation over all the individual atomic polarizabilities.

For the electron transport calculations we used Non-Equilibrium Green's Function (NEGF) formalism combined with density functional as implemented in the TranSiesta 3.1.5 package.[183, 43, 57] The devices were set up in usual left electrode, molecule, right electrode form and a minimal single-ζ basis set [92] at the local density approximation (LDA) parametrized in the Perdew-Zunger form were used for all calculations. The electrodes were modeled as Au (111) crystal lattice [97], each unit cell consisted of three sub-layers of 3, 7 and 3 gold atoms in a ABCABC order. We used a $3 \times 3 \times 100$ Monkhorst [138] type k-grid to sample the Brillouin zone for the leads and only the gamma point was calculated for the device region. For the real space grid, a mesh cut off were set to 380 Ry and a 30 $\mathring{A}$ space in the plane perpendicular to the direction of transport to prevent interactions between the super-cells. Figure 1.3 shows the computational setup of an organic molecular sandwiched between to metal (gold) electrodes.

3.3 Results and Discussion

3.3.1 Geometries and Energies

Interaction energies of the hydrogen-bonded systems follow an expected pattern of: (N$-$H$\cdots$O $<$ N$-$H$\cdots$N $<$ O$-$H$\cdots$O $<$ O$-$H$\cdots$N). Our calculations show, Tables 3.1 and 3.2, that the smaller basis set produce similar trends in energy and distances as of the larger basis set. Interestingly, the strongest hydrogen bond, O$-$H$\cdots$N, is not a very common hydrogen bond in natural systems.[91]

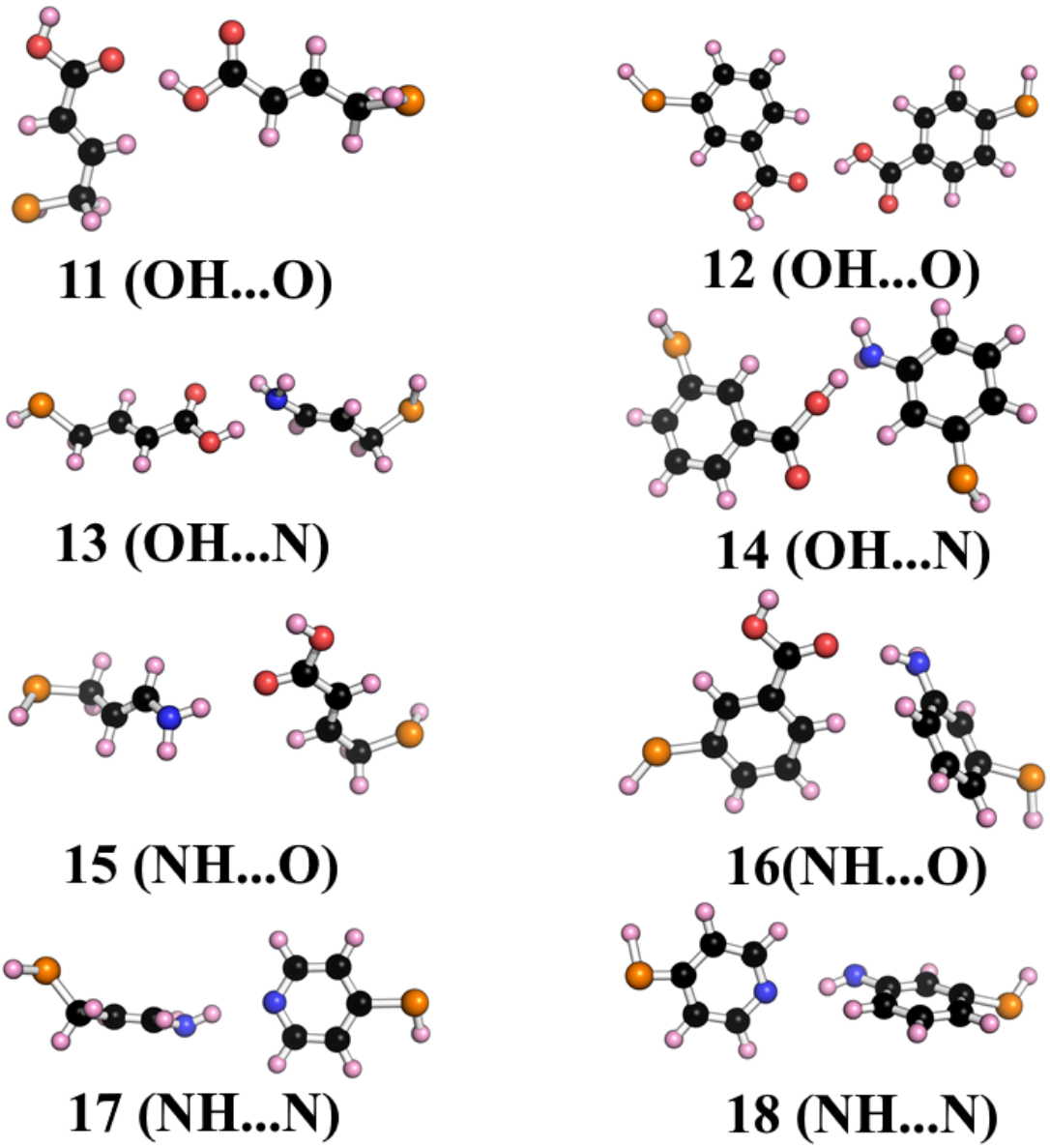

Figure 3.1: Structures Are Made By Combining Crotonic Acid **C**, Benzoic Acid **B**, Aniline **A**, and Pyridine **Py**.

	6-31+G*			6-311++G(2d,2p)		
System	$r_{D...A}$	r_{D-H}	$r_{A...H}$	$r_{D...A}$	r_{D-H}	$r_{A...H}$
11(O-H...O)	2.793	0.984	1.840	2.792	0.981	1.839
12(O-H...O)	2.806	0.982	1.845	2.804	0.979	1.846
13(O-H...N)	2.809	1.001	1.828	2.816	0.995	1.840
14(O-H...N)	2.808	1.000	1.824	2.818	0.994	1.839
15(N-H...O)	3.127	1.015	2.128	3.175	1.010	2.166
16(N-H...O)	3.130	1.015	2.126	3.151	1.010	2.142
17(N-H...N)	3.149	1.019	2.151	3.158	1.015	2.160
18(N-H...N)	3.140	1.019	2.153	3.147	1.015	2.162
11D(O-H...O)2	2.702	0.999	1.704	2.654	1.001	1.653
12D(O-H...O)2	2.694	0.999	1.695	2.648	1.001	1.647

Table 3.1: Geometrical Parameters of B3lyp-optimized Hydrogen-bonded Systems. The Distances Are in the Unit Of $\mathring{A}$.

The accuracy of our calculations are bolstered by the nice agreement between our calculated interaction energies for the benzoic acid dimer and values reported in the literature.[2] Of course it is not surprising that the interaction energy is higher for the dimeric system in comparison with the single hydrogen bond formed in the linear set up.

Tables 3.1 and 3.2 shows that there is almost no correlation between the strength and length of hydrogen bond. It is known that in most cases, the closer the hydrogen bond angle to 180° the higher the chances of forming a stronger hydrogen bond. But as we discussed in previous chapter for electron transport within the limits of hydrogen bond length , the process is mostly controlled by quantum tunneling through the

	6-31+G*		6-311++G(2d,2p)	
System	ΔE	ΔE_B	ΔE	ΔE_B
11(O-H...O)	-6.3	-5.5	-5.5	-5.1
12(O-H...O)	-6.1	-5.2	-5.3	-4.9
13(O-H...N)	-10.1	-8.8	-8.6	-8.2
14(O-H...N)	-10.0	-8.6	-8.3	-8.0
15(N-H...O)	-3.7	-3.2	-2.8	-2.6
16(N-H...O)	-4.0	-3.2	-3.3	-3.0
17(N-H...N)	-4.5	-4.0	-3.9	-3.7
18(N-H...N)	-4.8	-4.2	-4.2	-4.0
11D(O-H...O)2	-16.8	-15.4	-15.8	-15.2
12D(O-H...O)2	-17.1	-15.6	-16.0	-15.4

Table 3.2: The Interaction Energies Are Calculated at B3lyp Level of Theory and Are Reported in the Unit of Kcal. Δe and ΔE_b Are Interaction Energy with and Without Bsse Correction. D, A Stand for Donor and Acceptor.

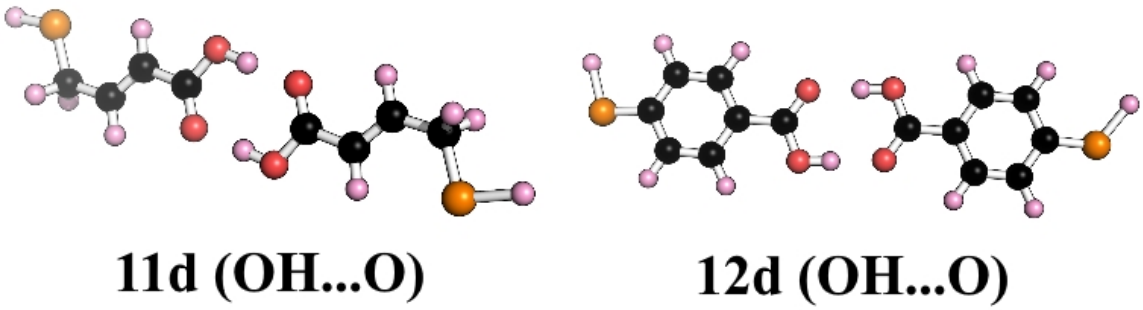

Figure 3.2: B3LYP/6-311++G(2d,2p) Optimized Structures of The Crotonic (**11d**) and Benzoic (**12d**) Acid Dimers.

barrier.

The most important issue in the transmission of the electron through the barrier is the barriers shape which is dictated by the length of the hydrogen bond.

3.3.2 Electron Transport through Hydrogen Bond

In justifying transport properties of material, one of the first parameters to look at is the frontier molecular orbitals. Hence, it is informative to look at the FMOs of these hydrogen-bonded complexes to gain a preliminary insight into the systems.

The monomers all have similar HOMO-LUMO gaps (Table 3.4). In these systems, the nitrogen atom in propenyl amine and aniline, acts as the hydrogen bond donor and acceptor, but the nitrogen atom in the pyridine is merely a hydrogen bond acceptor.

For carboxyl group, the oxygen can behave as donor in the form of hydroxyl and it behaves as an acceptor in the form of carbonyl.

It is worth noting the relative polarizabilties of the hydrogen bond donor and acceptor atoms. Relatively, the atomic polarizability of the hydrogen bond donor atoms is substantially lower than the acceptor atom. The covalent bond between the donor atom and hydrogen might be the reason for this observation.

Table 3.6 summarizes all the electronic and transport information for the complexes studied in this section. It has been shown experimentally, that at short distances and at bias, the conductance of the experimentally observed conductance of hydrogen-bonded ω-carboxyl ethanethiol (HS-$(CH_2)_2$COOH) dimer is 1.5 nS, in comparison with octanedithiol molecular junction (0.99 nS)[148]

While many have reported correlation between HOMO energy or the HOMO-LUMO gap energy and molecular conductance, Table 3.6 clearly shows an absence of this correlation with our systems. It is also noted that, the aromatic molecules consistently show lower conductance than the double bonded systems.

	6-31+G*			6-311++G(2d,2p)					
System	H	L	α	H	L	α	α_D	α_H	α_A
Crotonic Acid	-7.7	-1.6	41	-7.7	-1.6	44	4.3	4.7	6.3
Propenyl Amine	-5.5	0.1	35	-5.6	-0.2	38	3.4	3.7/4.8	3.4
Benzoic Acid	-7.4	-1.8	61	-7.5	-1.8	63	3.7	5.1	7.7
Aniline	-5.7	-0.3	56	-5.8	-0.4	58	3.8	4.6/4.6	3.8
Pyridine	-7.2	-1.1	45	-7.2	-1.1	46			5.8

Table 3.4: Calculated B3LYP Orbital Energies, Molecular and Atomic Polarizabilities of Different Hydrogen-bonded Systems. HOMO (Highest Occupied Molecular Orbital) and LUMO (Lowest Unoccupied Molecular Orbital) Energies Are in eV. α Is The Static Molecular Polarizability in Atomic Units(a.u.). α_D, α_H, and α_A Are The Polarizabilities (a.u.) of The Donor, Hydrogen, And Acceptor Atoms in The Various Monomers.

Given the relation between conductance and polarizabilities, we plot the calculated molecular polarizabilties and the corresponding conductances in Figure 3.3. It is obvious from the plot that for complexes exhibiting identical hydrogen bonding interactions, an enhanced conductivity is associated with a smaller polarizability.

On an interesting note, we can see that larger values of conductance directly correspond to a smaller atomic polarizability of the acceptor atom. This correlation is put into the spotlight in subsequent sections.

This is indeed another piece of evidence, that even when HOMO/LUMO are not informative, polarizability can be used as a molecular descriptor of conductance.

	6-31+G*		6-311++G(2d,2p)				
System	α	G	α_D	α_H	α_A	α	G
11	83	3.0	1.8	1.7	1.9	87	3.9
12	124	0.3	0.0	0.3	4.8	127	0.8
13	77	0.5	3.2	2.0	0.2	82	1.4
14	118	0.4	2.7	2.0	0.5	121	0.1
15	76	6.6	1.7	1.7	2.0	82	0.3
16	117	1.0	2.8	2.0	3.2	121	0.4
17	81	2.2	1.1	1.6	1.2	85	1.9
18	101	0.3	1.7	1.9	0.5	105	0.2
11D	84	41.4	3.4	1.8	2.5	88	9.4
12D	125	12.6	2.7	1.8	2.4	129	5.8

Table 3.6: α Is The Static Molecular Polarizability in Atomic Units(a.u.). α_D, α_H, and α_A Are The Polarizabilities (a.u.) of The Donor, Hydrogen, and Acceptor Atoms. The Molecular Conductance (G) Is in Units of NanoSiemens (nS).

3.3.3 Quinone- Imidazole: A Model System

The hydrogen bond between *p*-benzosemiquinone and imidazole is critical in the role of electron transfer in energy conversion reactions involving most biological systems including photosystem II.[130] Therefore we examine the nature of charge transport across this hydrogen bond. Substituent effects have a very well-known effect on electron transfer processes. With this in mind, we also investigated the effect of substituents on the nature of hydrogen bond and charge transport through hydrogen bond.

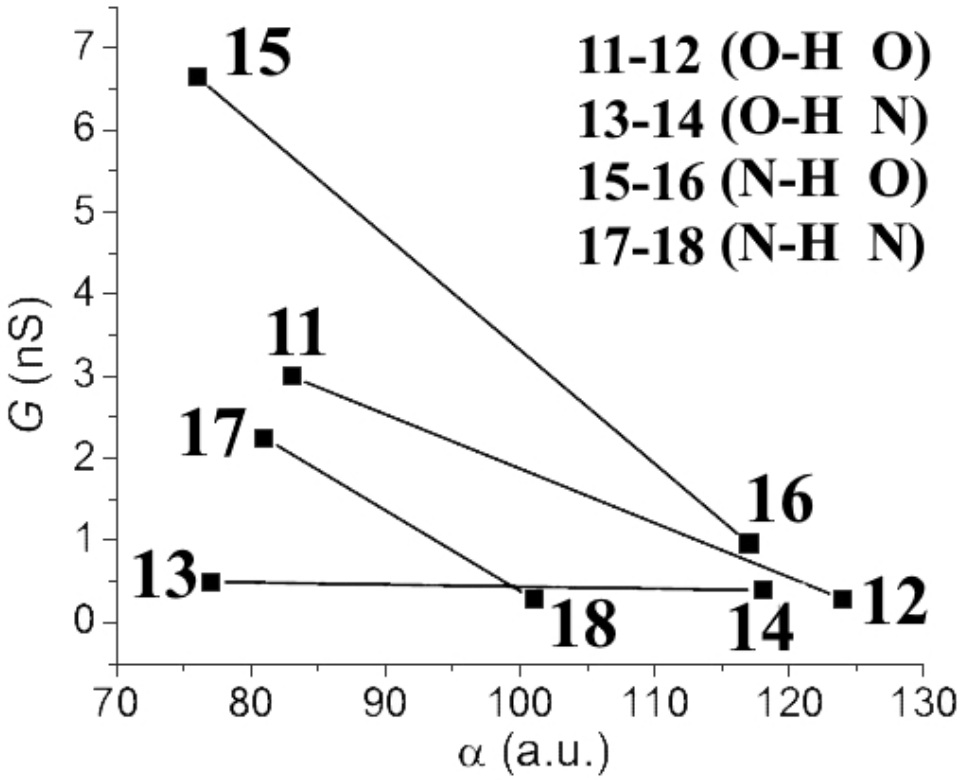

Figure 3.3: Correlation Between The Calculated Molecular Polarizabilities (a.u.) And The Molecular Conductances (nS) of All The Hydrogen-bonded Complexes.

I use an electron withdrawing (NO_2) and electron donating (NH_2) groups on the imidazole and/or the *ortho* and *meta* positions of the phenyl ring. Figure 3.4, the B3LYP/6-31+G* optimized structures of the various substituted *p*-benzosemiquinone-imidazole complexes. Also these complexes are positively charged and are open-shell spin doublets.

Since the interaction energies, HOMO-LUMO gaps are not very informative on the nature of electron transport, only the polarizabilties, geometrical parameters, and the conductance values are reported in Table 3.7.

An electron-withdrawing or an electron-donating substituent on the imidazole ring has negligible effect conductances. However, positioning an electron-withdrawing

System	α_N	α_H	α_O	α	G
111	-0.4	1.2	3.3	87	18.7
112	-0.6	0.9	4.0	99	2.4
113	-0.8	1.0	5.1	99	77.8
114	0.0	1.2	2.8	100	7.3
115	-0.5	1.2	3.0	94	44.0
116	-0.6	1.3	4.4	96	6.9
117	-0.1	1.1	2.4	95	8.1

Table 3.7: Calculated Polarizabilties, Selected Geometrical Parameters, and Molecular Conductance of the P-benzosemiquinone-imidazole Hydrogen-bonded System. The Molecular Conductance (G) Is in Units of Nanosiemens (Ns).

group at the *meta* position or an electron-donating group at the *ortho* position of the phenyl ring enhances conductance. While this effect can be comprehended in the context of activating and deactivating groups in electrophilic aromatic substitution reactions, we should understand this more in the context of electrostatic potential effects. Thus, the electron withdrawing (NO_2) group at the *ortho* position leads to a partial positive charge on the carbon attached to acceptor oxygen atom. This results in a decrease in the electron density of the acceptor oxygen atom and results in a weakening of the $O \cdots H-N$ hydrogen bond. The enhancement of the condutance in **15** can be explained.

Electron density on the acceptor oxygen atom is influenced by the presence of the substituents, it can be expected that its polarizability would reflect the observed conductance. It can indeed be seen in Figure 3.5, that the polarizabilities of the acceptor oxygen atom exhibit an inverse correlation to the observed conductance.

3.4 Future work

The first line of research is the obvious inclusion of S hydrogen bonds that are very peculiar and there is not a universally accepted trend for their strengths in literature. In some systems they form very strong hydrogen bonds with nitrogen. They are also involved, as methionine and cytosine, in biological systems. Our initial results show very strong hydrogen bond that is formed between nitrogen and sulfur.

Next, we have to investigate the effect of metal ions on the hydrogen bond. Charge effects can be considered in two themes: one through weak interactions. In fact in an study, it has been shown experimentally that presence of an ion increases the conductance of hydrogen-bonded system; second, we can study the effect of coordination to a metal on the electron transport. This opens up a venue to expand, cautiously, the results obtained from electron transport to electron transfer in organometallic systems.

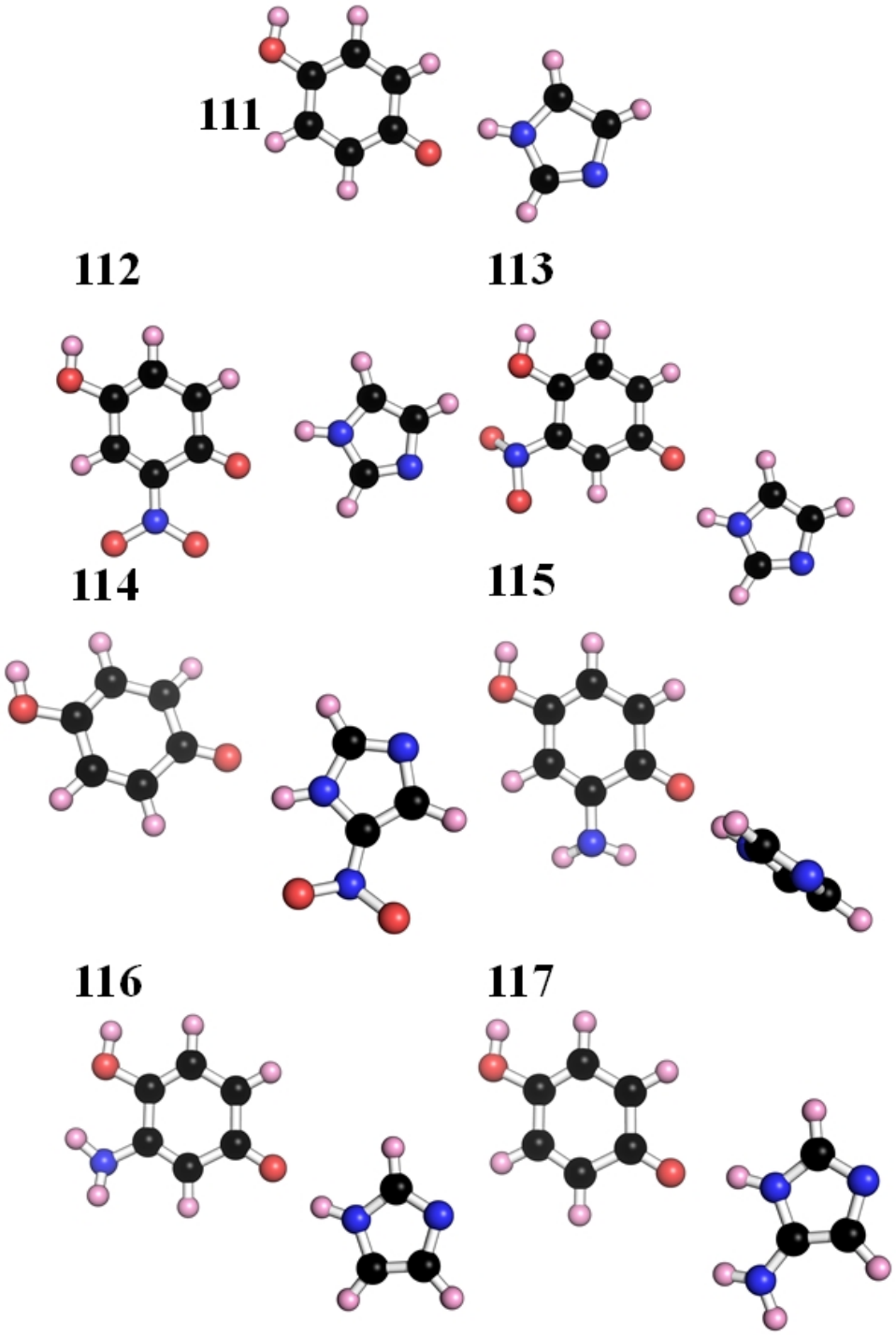

Figure 3.4: B3LYP/6-31+G* Optimized Structures of All The p-benzosemiquinone-imidazole Hydrogen- bonded Complexes.

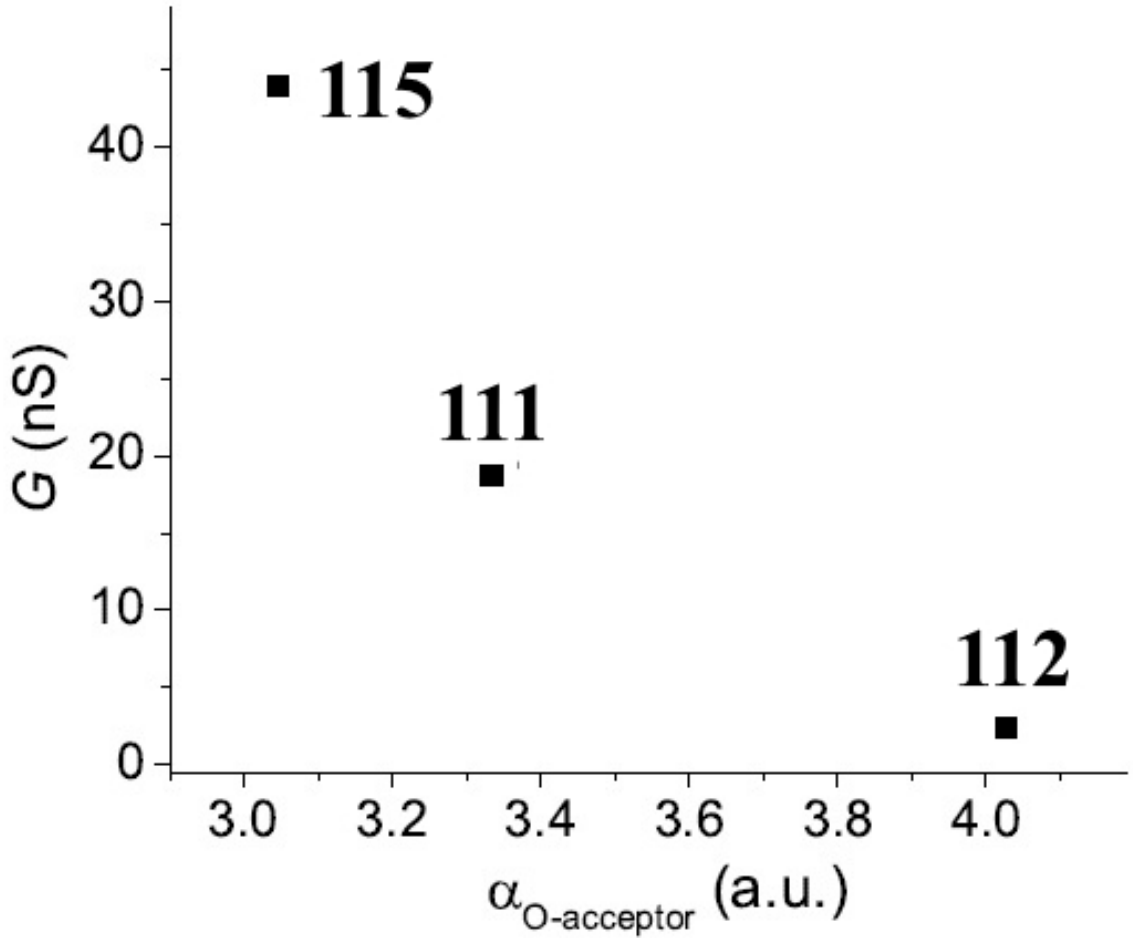

Figure 3.5: Correlation of the Calculated Atomic Polarizabilities (A.U.) Of the Acceptor Oxygen Atom and the Molecular Conductances (Ns) of Ortho-substituted P-benzosemiquinone-imidazole Hydrogen-bonded Complexes.

Chapter 4

ELECTRON TRANSFER AND HYDROGEN REDUCTION CATALYST

The experimental results of this chapter are not done by this author and are purely work of professor Jone's group. The reader is referred to Papers [62] and [175] for the complete discussion of the experiments.

4.1 Introduction

Climate change and energy crisis, while seemingly different, can both be addressed by a single silver bullet: renewable energy.[225, 78] One viable option to produce a renewable fuel that can be easily stored is hydrogen. It is proven challenging to mass-produce hydrogen in the scale of global energy consumption. An ideal catalyst has a very high turnover frequency and preferably use abundant and non-precious metals. Hydrogenase, is an enzyme that reversibly catalyses the proton reduction reaction with high turnover frequencies (over 1000 s^{-1}) with extremely low overpotentials.[119] The hydrogenase performance is even more impressive when considering that they only use first row transition metals, i.e. Fe and Ni, work in aqueous solutions and under weak acidic condition. So it is not a surprise that a broad spectrum of researchers have been studying hydrogenase.[71, 9, 81, 204]

Although a number of heterogeneous catalysts, such as nickel nanomaterials, are reported to catalyse hydrogen production reaction; molecular catalysts are superior and more desirable for the facile modification of the catalytic behavior of these systems.[7] It is worth mentioning that while there are many studies that use noble metals, such as Pd and Pt[202, 146], for hydrogen generation, in order to make a catalyst that can be practically used in future, it should be based on cheap and abundant

metals. To this end, scientific community has moved towards preparing and studying molecular systems their catalytic moiety is Co, Ni or Fe based. In other words, earth abundant first row transition metal complexes.[4, 50]

In understanding the catalytic process, it is necessary to assess if the molecular structure of the catalyst is retained or is transformed into active metallic particles.[7] To this end, we can apply the mercury poisoning test to see if Hg(0) poisons the Ni nanoclusters. Most of the studies showed that mercury amalgamates with cobalt and nickel. While these results alone are not conclusive, the lack of lag phase in the kinetic study of hydrogen evolution and the system-dependent (linear or quadratic) relation between the concentration of cobalt and the H_2 production rate that presents distinctive mechanistic features, are all pointing away from the degradation and transformation of the molecular catalyst into a metallic, active nanocluster. Although iron powder is inactive as a catalyst, several studies have shown that both iron and nickel nanoparticles are capable of being used as hydrogen production catalysts in aqueous solutions.[217, 95]

The presence of an electrode in electrochemical experiments make them inevitably heterogeneous. We can put these experiments in to three different categories. First, electrode only acts as a source of electron to the molecular catalyst (electro-assisted catalysis). Second, the electrode itself acts as a catalyst by interacting with the substrate (electrocatalysis). Third, the molecular catalyst is chemisorbed on the surface of the electrode. In this thesis, electrocatalysis is used as a general term that encompasses all the three categories.

Based on the active site of the di-iron [Fe-Fe] and [Ni-Fe] hydrogenase, a plethora of macrocyclic and pincer nickel and iron and cobalt complexes are reported in the literature.[116, 117, 174, 40] Most of the catalytically active compounds are not bio-mimicked but bio-inspired. And among those the catalysts usually deactivate after a

few dozens of turnovers. The degradation of catalyst may form catalytically inactive species and compounds. The molecular catalysts have been re-characterized and the robustness of the compound was approved.[34] But one might be cautious in drawing conclusions from these studies since during the bulk electrocatalytic experiments, only molecules that are inside the diffusion layer around the electrode are active and a large number of the catalyst do not cycle.

Some studies show that some of the hydrogen production catalysts that were reported in before are not truly a molecular catalyst; meticulous studying of the surface of the electrode proved that in fact the metal atoms are adsorbing on the electrode surface, modifying it and producing hydrogen over a considerable pH range.[20, 5] These studies cast doubts on the success and relevance of the well-designed organic ligands, if the final result is going to be a metal that is electrochemically deposited and formed nanoparticles at even neutral pH in aqueous surroundings. Fortunately, chemisorption of these complexes on a solid material can stabilize them.

All of the aforementioned instances point to the complex nature of this process and proves that no generalization is possible and each situation needs a particular systematic analysis. To this end, in a collaboration with Prof. Jones' group we have applied several computational tools, such as frontier orbital analysis, charge analysis, charge decomposition analysis, to clarify and understand the underlying mechanism of Fe, [Fe-Fe] ,and [Ni-Fe] hydrogen evolution catalysts. The results of these calculations and correlations and corroborations from the experiments done by Jones and coworkers are presented in the following sections. Finally, I show some promising correlations that can be used to as design guidelines to amp up the search for the next best hydrogen evolution catalyst.

4.2 A nickel phosphine complex as a fast and efficient hydrogen production catalyst

[1] [2]

4.2.1 Introduction

The successful bioinspired catalysts have set some design guidelines that can be used in producing an effective and efficient hydrogen evolution catalyst. For instant, an internal proton relay in a nickel phosphine complex was used by DuBois and coworkers, in the outer sphere, that resulted in an exceptionally fast catalyst.[157, 30] McNamara et al. have investigated the role of non-innocent ligands such as benzenedithiolate (bdt) as internal redox systems that provide the reducing equivalent necessary in the two-electron reaction.[128, 129] Ott and coworkers have systematically studied and synthesized a series of mononuclear, unsaturated complexes that by the support of bdt, a CO and chelating phosphine to produce hydrogen and relatively high rates and small overpotentials.[23, 93] Also Jones and coworkers have used 1,1'-bis(diphenylphosphino)ferrocene, dppf, that is a sterically prohibitive ligand with unsaturated coordinations around the iron complex and proved that it can perform at low overpotentials. This complex will be discussed in the next section of this thesis.

A combination of these design motifs resulted in a nickel complex that can efficiently reduce proton from a weak acid in THF in a surprisingly low overpotential. In this complex, the Ni is covalently bonded to thiolate and phosphine. The thiolates come in the form of a bdt, which can be a non-innocent ligand, and the phosphines are a part of the dppf sterically demanding ligand. Not only the bdt moiety can act

[1] The figures of this section are adapted with permission from reference[62] Copyright 2015 American Chemical Society.

[2] The experimental results of this chapter are not done by this author and are purely work of professor Jone's group. The reader is referred to the complete paper [62] for the further discussion of the experimental results.

as a redox non-innocent ligand but also it might act as an internal proton transfer conduit.A combination of theoretical calculations, spectroscopic data and electrochemical information is used to characterize this compound and explain its reaction mechanism.

4.2.2 Computational Detail

Geometry optimizations were carried out at the Density Functional Theory level by using the Becke gradient-corrected exchange functional and Lee-Yang-Parr correlation functional with three parameters (B3LYP) and the 6-31G* basis set. The crystal structures were used as the initial structure for **1** and **2**. The calculations were performed by ORCA and Gaussian electronic structure suits.[144, 61, 48, 162, 18, 103, 60, 67] The calculations were also done at BP86/def2-TZVP level.[206] Scalar relativistic effects were introduced by using zeroth-order regular approximation (ZORA) as implemented in ORCA.[198, 199] This level of theory have been shown to yield energies and spectroscopic parameters comparable to those obtained at higher levels of theory and larger basis sets.[180, 171, 46] The synchronous transit-guided quasi-Newton (STQN) method was applied to found the transition state.[11]

4.2.3 Results and Discussion

Ni(bdt)(dppf) complex, **1**, was synthesised with a 45% yield in two steps. A second compound, Ni(bdt)(dppe) (dppe = 1,2-bis(diphenylphosphino)ethane), **2**, was also made. The second compound's, **2**, dppe is a less restrictive phosphine. Table 4.1 shows the comparison between selected geometrical parameters as calculated by DFT and crystallography data.

The nickel is in the square planar coordination environment. The iron nickel distance is about 4.257 $\mathring{A}$. All the distances and angles are within an acceptable range

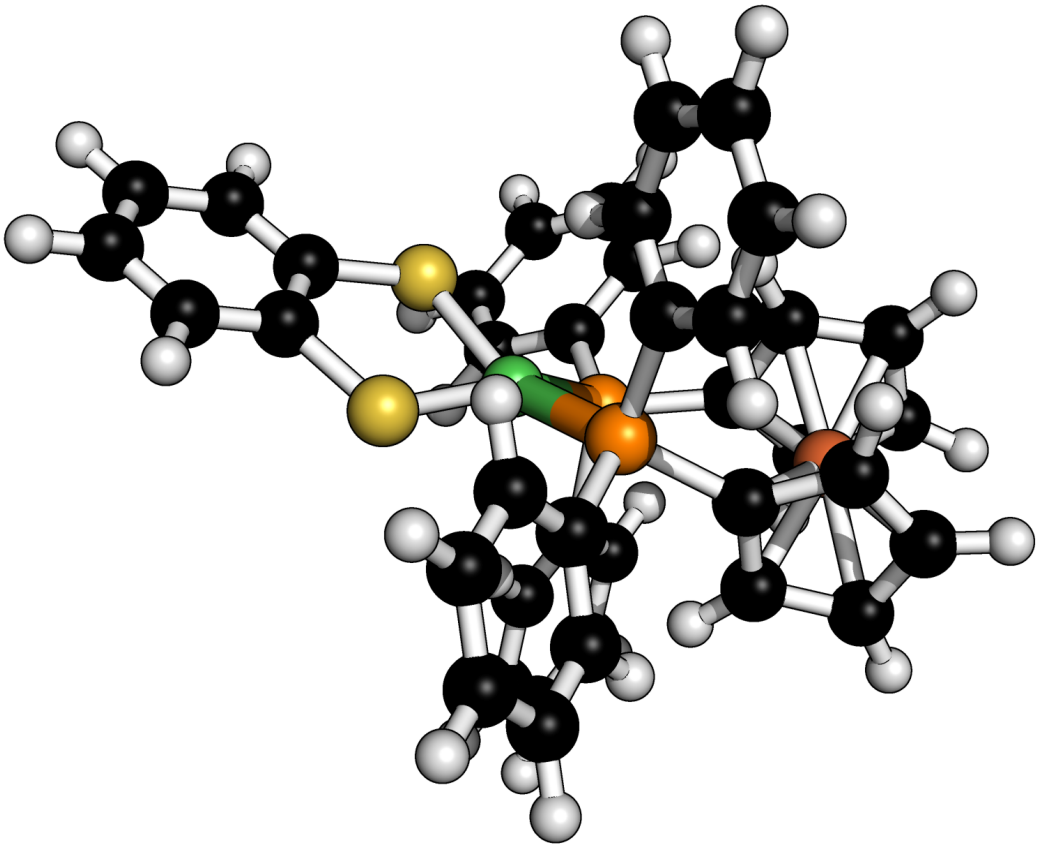

Figure 4.1: The Structure of **1**.

for a square planar nickel complex. Experiments (X-ray absorption spectra and X-ray differaction) shows geometry of **1** appear to be similar in THF solution and crystal structure. The relatively low dielectric constant of the THF solvent ($\epsilon = 7.58$) means that the structure obtained from the gas phase calculations should correlate well with the crystallographic parameters. This is indeed the case, in particular, when we use the ZORA approach to include relativistic effects into our calculations. The error in the bond lengths for the B3LYP/6-31G* relative to the crystal structure is around 2% and when BP86(ZORA)/def2-TZVP functional and basis sets are used the error in the bond lengths goes down to less than 0.1 %.

Figure 4.2 shows the UV-vis spectrum of the complex **1**. Based on Laporte se-

	1	20	31	32	41	42	50	TS	Exp.
Bond Length (Å)									
Ni-S1	2.195	2.304	2.208	2.450	2.291	2.263	2.240	2.200	2.1661
Ni-S2	2.191	2.303	2.235	2.254	2.283	2.386	2.286	2.206	2.1657
Ni-P1	2.224	2.203	2.335	2.224	2.222	2.092	2.235	2.204	2.2228
Ni-P2	2.240	2.203	2.242	2.242	2.190	2.091	2.443	2.203	2.2264
Ni-Fe	4.294	4.255	4.225	4.212	4.131	4.131	4.339	4.253	4.2570
Ni-H			1.468		1.470		1.464		
S-H				1.352		1.363			
H-H							1.286	0.745	
Bond Angles (°)									
S1-Ni-S2	90.5	91.5	92.3	89.6	90.4	89.2	90.4	91.5	90.66
P1-Ni-P2	103.1	105.9	106.4	105.9	112.0	112.4	101.1	106.1	101.43
Td- dihedral (°)									
	32.1	66.8	75.7	81.1	88.0	86.5	73.7	45.8	-

Table 4.1: The "Td dihedral" is the angle between the normal vectors of the S1-Ni-S2 and P1-Ni-P2 planes. The short code written to calculate this is available in the appendix.

lection rules, transitions such as $d \rightarrow d$, which their parity does not change through the transition, are forbidden, hence these forbidden transitions have small transition amplitude, or ε (extinction coefficient).[107, 102]

The strong transitions(4.2) are standard feature of charge transfer band. The charge transfer bands are due to the change in the charge distribution between the central metal and the ligand. This high intensity is due to high probability of this

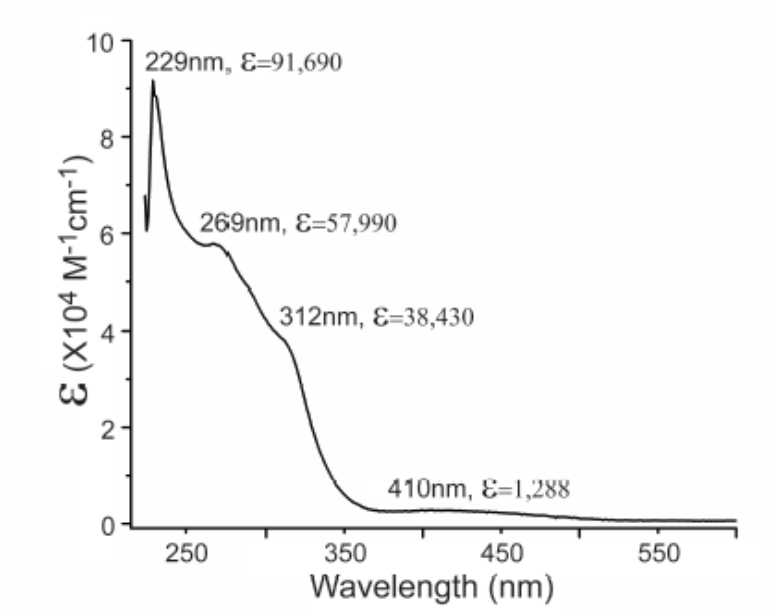

Figure 4.2: The UV-vis Absorbance Spectrum From a 0.01 mM Solution of **1** in Dichloromethane.[62]

transition of these metal to ligand (Ni to P and Ni to S) charge transfers. The lower intensity peaks are $\pi \rightarrow \pi^*$ transitions. The mass of the evidence from XAF, NMR ,and UV-visible spectrum clearly proves the structure of **1** in solution is similar to the reported crystal structure and gas phase quantum chemical calculations. The electron density of the cyclopentadienyl rings is affected by the phosphines that form bond to the nickel. This presents itself in the downfield shift in the proton NMR of the cyclopentadienyl protons relative to those of dppf.

Figure 4.3 shows the voltagramms of the **1**.All the potentials are reported against the saturated calomel electrode (SCE) It can be seen that there is a reversible reducing reaction at $E_{1/2} = -1.280$ $(VvsSCE)$. This reversible peak can be assigned to Ni^{II}/Ni^{I} couple. The complex was stable under continuous potential cycling around the Ni^{II}/Ni^{I} for 30 min. There is also a partially reversible oxidation peak around $E = +0.744$ $(VvsSCE)$ that can be attributed to the oxidation of ferrocenyl iron

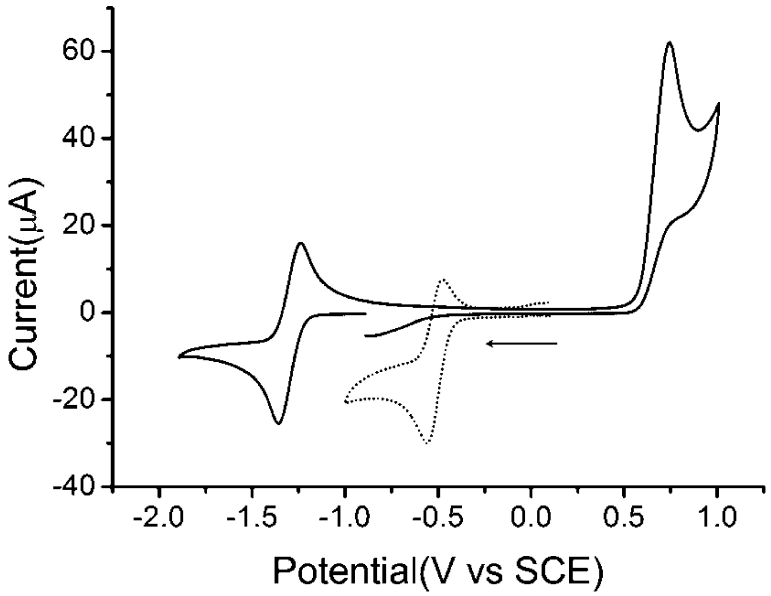

Figure 4.3: Cyclic Voltammograms of 3 mM **1** and 2.7 mM **2** in THF at a Potential Scan Rate of 100 mVS^{-1} Where The Solid Line Represents **1** and The Dotted Line Denotes Compound **2**. The Supporting Electrolyte Is 0.3 $TBAPF_6$. The Arrow Denotes The Starting Point and Direction of The Potential Cycle.[62]

from Fe^{II}/Fe^{III}. This has been observed in other ferrocene phosphine complexes. This decomposition results in irreversible reaction.[38, 155]

The CV of **2** shows a reversible peak at -0.518 V corresponds Ni^{II}/Ni^{I}. I would like to point to the 0.75 V difference in the reduction potential for Ni^{II}/Ni^{I} between complex **1** and **2** which are structurally close. The dppf is a stronger donor which can destabilize the reduced form of **1**, but this alone can not account for 0.75 V of difference. Electronic structure studies of these two complexes clarifies and shows how the change in the LUMO (Lowest Unoccupied Molecular Orbital) from **1** and **2** can justify this result. Table 4.2 summarizes the results of higher level calculations.

Looking at these results, one can notice that the biggest difference between the two complexes is in their P-Ni-P fragment. In fact both angles and lengths and

	1	2
Bond Length		($\AA$)
Ni-S1	2.165	2.161
Ni-S2	2.161	2.159
Ni-P1	2.208	2.153
Ni-P2	2.221	2.156
Bond Angles (°)		
S1-Ni-S2	90.4	92.2
P1-Ni-P2	103.7	90.5
Bond Orders		
Ni-S1	0.96	0.89
Ni-S2	0.97	0.90
Ni-P1	0.91	0.95
Ni-P2	0.85	0.94
HOMO/LUMO Energies (eV)		
HOMO	-4.4	-4.4
LUMO	-1.4	-1.3

Table 4.2: Selected geometrical parameters, Mayer's bond orders, and HOMO/LUMO energies of complexes **1** and **2** are shown. These parameters are calculated at a higher level of theory and relativistic effects are considered by the ZORA method.

more importantly bond orders hints at the fact that the culprit in the relatively huge difference between the two comes from the difference in their ligands.

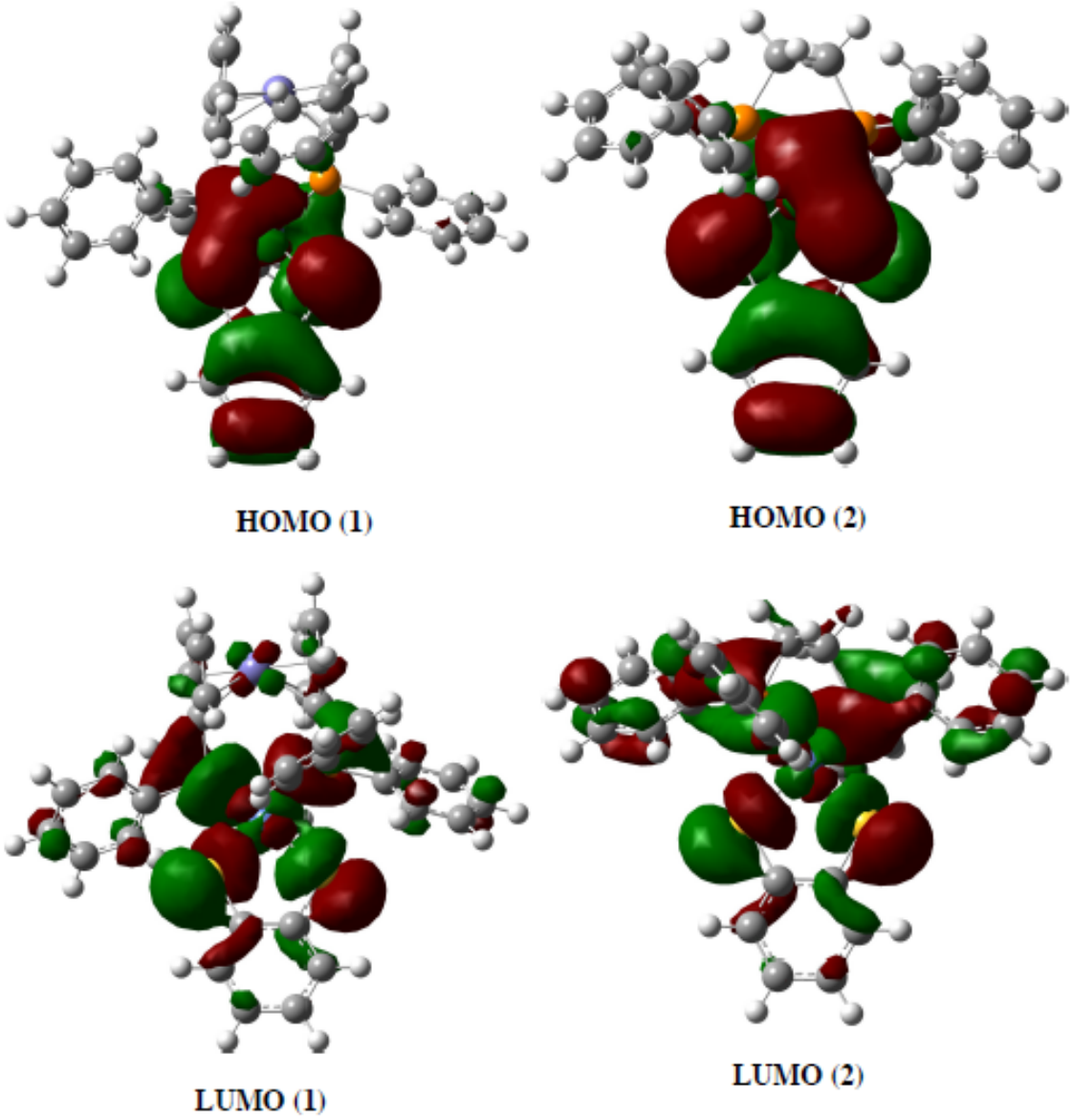

Figure 4.4: Frontier Molecular Orbitals (FMO) of **1** and **2**. The Difference in Delocalization of The LUMO Between The Two Complexes is Considerable.

This ligand difference, which manifests itself geometrically, has effected the LUMO energy of the two compounds more than their HOMO. Table 4.2 shows that the calculated HOMO energies are identical but the LUMO energy of the **2** is slightly more positive than **1**. This may result in the more positive reduction potential.

Figure 4.4 shows the Frontier Molecular Orbitals (FMO) of the two complexes. It is worth noting that while the two complexes present almost similar HOMOs, their LUMOs are very different. In fact the LUMO of **2** is extremely more delocalized than **1**. The LUMO in **2** is distributed into the phenyl rings.

4.2.4 Electrocatalytic Hydrogen Production by 1

As indicated in the Introduction of this chapter, to guarantee that the catalyst plays major role in producing hydrogen and not other factors, further experiments are performed.

The addition of acetic acid to the electrochemical experiment in the presence of **1** results in an increase in the current of the cathode at the reduction potential of Ni. It also causes the oxidation peak to disappear. The unidirectional increase in the current the characteristic feature of electrocatalysis.

Under exactly similar conditions, but without **1**, the proton reduction by the glassy carbon electrode was insignificant. This ensured us that the catalytic process happens because of the complex **1**. To rule out electrocatalysis as a result of degradation of the NiFe complex and deposition of nanoparticles on the glassy carbon electrode,the working electrode was transferred to a fresh acidic solution in the absence of **1**. Catalysis was not observed for this second without complex **1**. The stability of the catalyst during the experiment was also confirmed qualitatively and semi-quantitatively. Qualitatively, the color of the solution was unchanged throughout the experiment. Also, the UV-vis spectrum of **1** did not change after 4 hours of

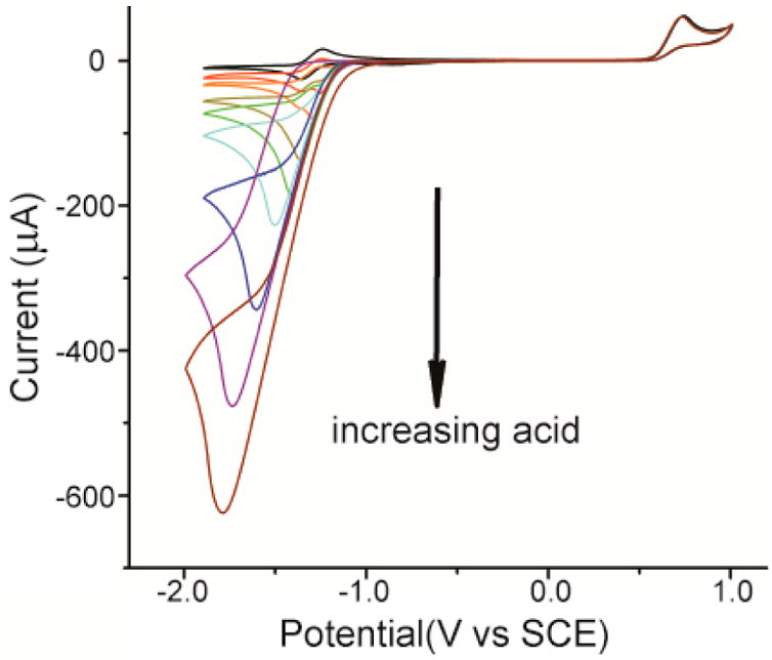

Figure 4.5: Cyclic Voltammograms of **1** and Different Concentrations of Acetic Acid. The Concentrations Are 0.0, 6.0, 8.0, 12.0, 16.0, 20.0, 30.0, 40.0, and 50.0 mM.

exposure to acetic acid (Figure 4.6).

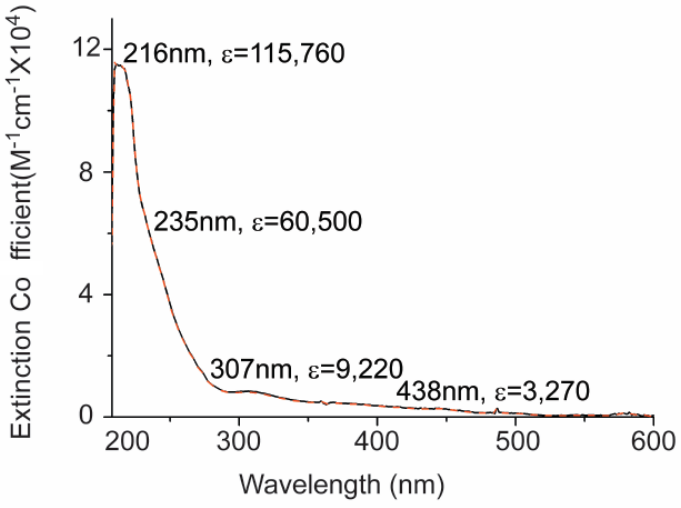

Figure 4.6: UV-visible Spectrum of **1** (Black Line) and After Being Mixed With 0.5 mM Solution of Acetic Acid For Four Hours (Red Line).

Unusually, **2** did not show any sign of catalysis in acetic acid or in p-tolunesulfonic acid which is significantly stronger. Notably, **1** showed catalytic activity in the *p*-tolunesulfonic acid with a higher turnover frequency but was not stable enough and rapidly decomposed.

The current for the reduction of **1** in the presence of acetic acid (i_c) and in the absence of acetic acid, i_p is shown in Figure 4.7. From 0 to 50 equivalent of acetic acid there is a linear relation between the i_c/i_p and the concentration of the acid. This implies that there is a first order kinetic relation between the two. Beyond this range the increase in the concentration of acetic acid does not change the i_c/i_p ratio. This means that the concentration of proton is high enough and there is no depletion in the concentration of the proton due to the catalytic activity of catalyst. This implies a pseudo zeroth order reaction with respect to the concentration of the proton.

Figures 4.8 and 4.9 show the robustness of this behavior under various scan rates and concentrations of the catalyst.

The rate constant for this reaction can be calculated from:

$$\frac{i_c}{i_p} = \frac{n}{0.4463}\sqrt{\frac{RTk}{F\nu}} \tag{4.1}$$

where k is the reaction rate, ν is the scan rate, n is the number of electrons (2 for hydrogen evolution reaction), R is the universal gas constant, T is the temperature, and F is the Faraday's constant.[16] For the concentration independent section, we find the Turn Over Frequency, TOF, to be $1240s^{-1}$. The TOF is in the same range for different scan rates. This very fast hydrogen evolution reaction is higher than the biological counterpart, hydrogenase. The TOF is a very important metric in assessing a catalyst. While high TOFs are desirable, we must know that at what expense we are achieving these high values. This concern is reflected in the electrochemical overpotential values. The overpotential is the activation energy and energy penalty

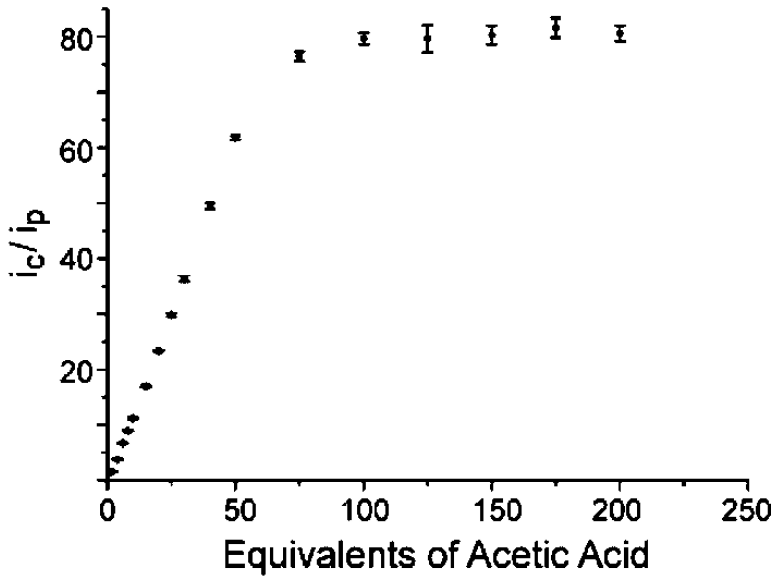

Figure 4.7: Dependence of Normalized Catalytic Current on Concentration of Acetic Acid. Currents Were Extracted from Voltammograms Such as Those Shown in Figure 3 That Were Collected under the Following Experimental Conditions: 2.0 mM 1 in THF, .3 M TBAPF6 and an Electrochemical Potential Scan Rate of 100 mv S^1. Error Bars Indicate the Standard Deviation Calculated from Three Independent Measurements.

that we pay over the thermodynamics to achieve those rates. In nature, hydrogen evolution occurs with high TOF and very low over potentials. Under different experimental conditions, the overpotential of the half of the overall catalytic current is in the range of 265 mV to 500 mV in low and high acetic acid concentrations.

The favorable combination of low overpotential and high turnover frequency makes **1** an efficient catalyst for H_2 production.

*4.2.5 Reaction of **1** Hydrogen Gas*

The small overpotential of the catalytic reaction of **1** and protons, which suggests that the reaction happens close to the thermodynamic equilibrium, raises the question

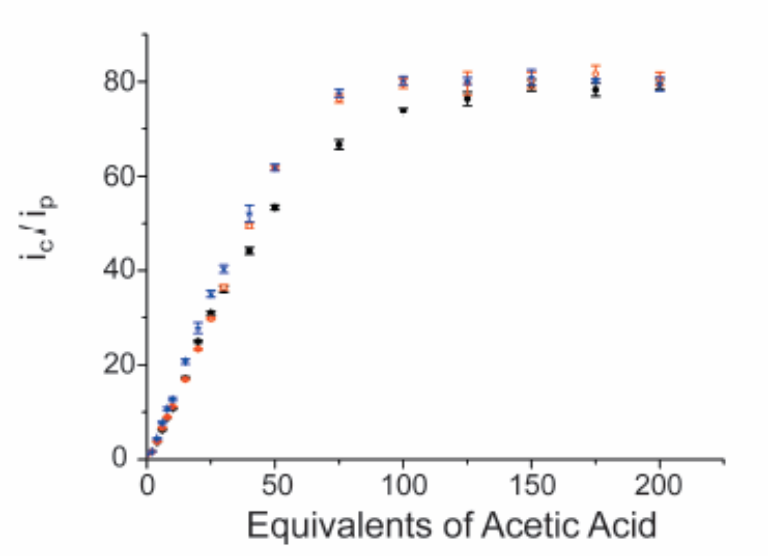

Figure 4.8: Dependence of Normalized Catalytic Current on Conecntration of Acetic Acid. The Black, Red and Blue Points Are Experiments With 1mM, 2mM and 3mM of **1** Respectively. Error Bars Represent One Standard Deviation From Three Independent Measurements.

that how does **1** interact with hydrogen? Figure 4.10 shows that in the presence of the H_2 the reduction potential for the Ni^{II}/Ni^{I} shifts from -1.280 V to -1.009 V. There is also a suppression of the oxidation peak. Figure 4.11 shows that the reduction potential of Fe in the ferrocene is unchanged.

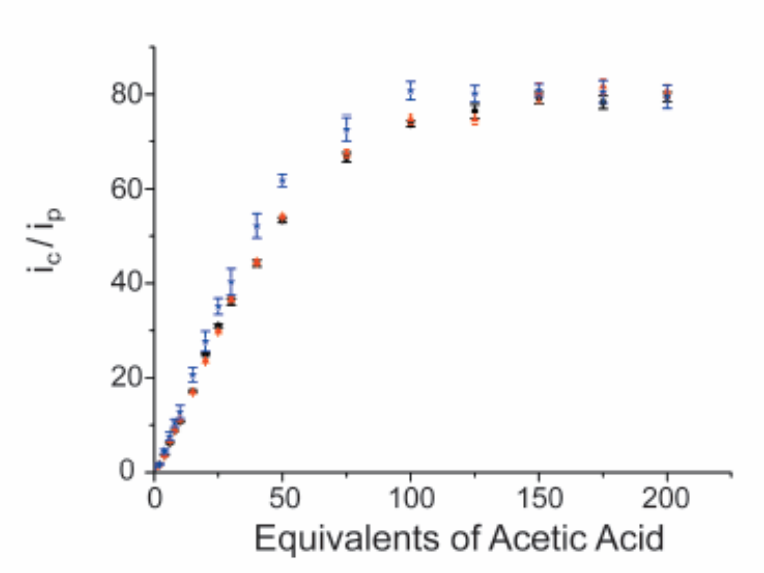

Figure 4.9: Dependence of Normalized Catalytic Current on Concentration of Acetic Acid. The Scan Rates of 10 mVS^{-1}, 100 mVS^{-1}, and 5 VS^{-1} Correspond to Red, Black and Blue Points. Error Bars Represent One Standard Deviation From Three Independent Measurements.

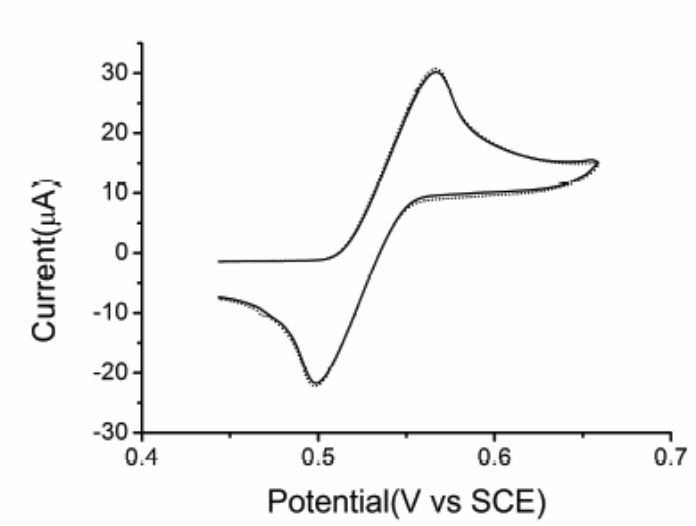

Figure 4.11: The Solid Lines Correspond to the Cyclic Voltammogram of **1** in the Absence of Hydrogen Gas and the Dash Line Is the Cv in a Solution Saturated with Hydrogen in 1 Atm Pressure That Corresponds to the Reduction of Fe.

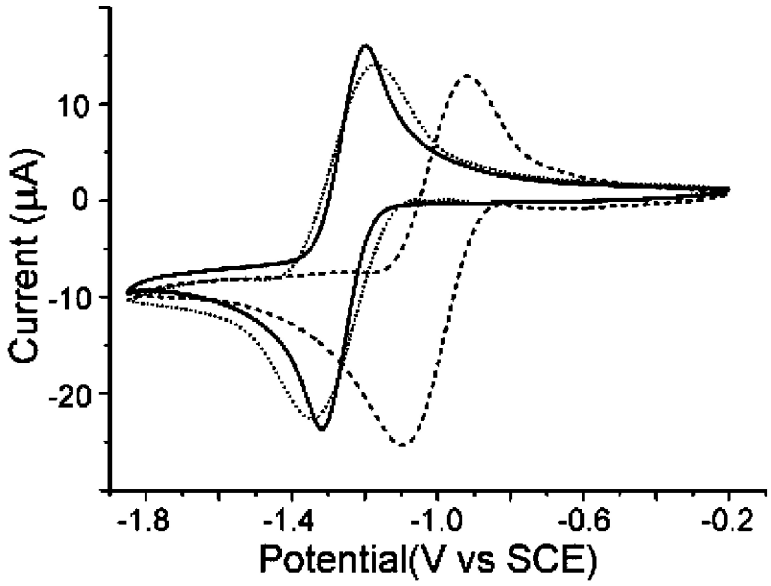

Figure 4.10: The Solid Lines Correspond to the Cyclic Voltammogram of **1** in the Absence of Hydrogen Gas and the Dash Line Is the Cv in a Solution Saturated with Hydrogen in 1 atm Pressure.

This means that the change in the reduction potential of**1** is not the result of change in the ferrocene. In a computational study, it was hypothesized that the H_2 molecule is bridging between the two metals Ni and Fe.[72] The lack of any change in the reduction potential of the ferrocene moiety and also the absence of any considerable change in the ^1H NMR of the Ni(II)-H_2 are pointing against this hypothesis. Moreover the interaction between the hydrogen molecule and **1** is very reversible. In fact a flow of argon gas in the solution returns the reduction potential peak back to the -1.280 V, with a small change in the oxidative signal.

The change in the reduction potential translates to the fact that the it is considerably easier to reduce the nickel moiety when it is interacting with H_2. We can conclude that the hydrogen ligand, either directly or indirectly, withdraws the electron density from nickel. This in effect, stabilizes the Ni(I). We explored the possible

mechanism that governs this catalytic process and also attempt to gain more insight into this process.

4.2.6 What is the catalytic mechanism?

The data presented in previous sections signifies that in this two-electron process, initially there is an electron process that reduces the complex and then **1** goes through a protonation step that is the rate-determining step of the reaction. We propose and investigate the mechanism is electrochemical/chemical electrochemical/ chemical reaction (ECEC). This mechanism is consistent with the experiments that are mentioned in previous sections.

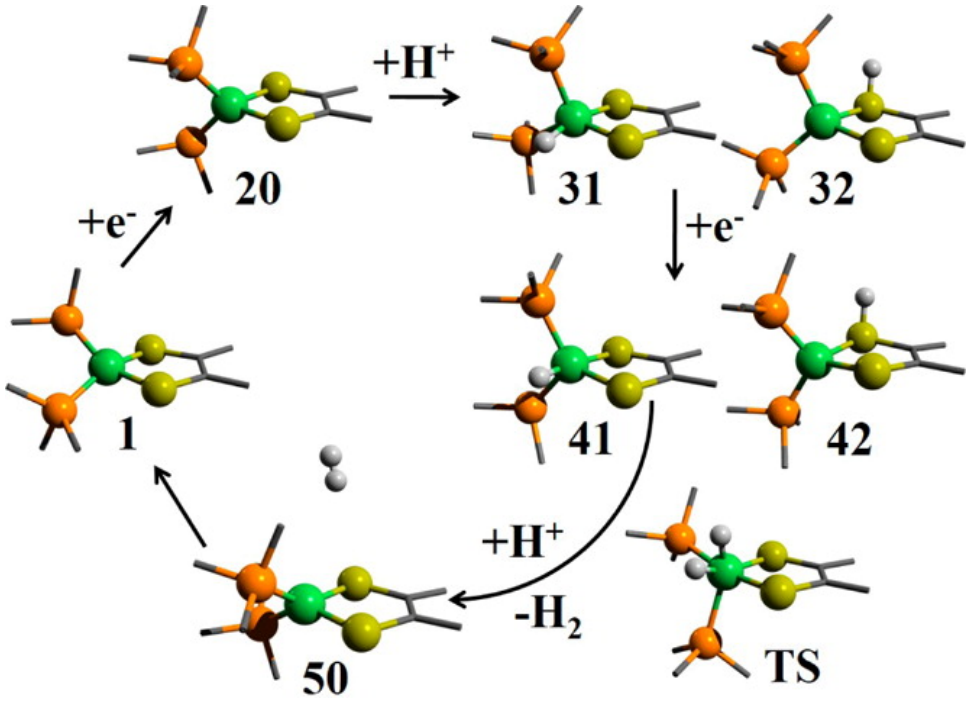

Figure 4.12: Hypothesized Mechanism of Action of **1** in Hydrogen Production Reaction. Nickel, Phosphorus, and Sulfur Are Green, Orange, and Yellow Respectively.

Tables 4.4 and 4.6, show the HOMO and LUMO energy of the compounds that are discussed in the Figure 4.12. Also, in these tables present the contribution percentage of each fragment to the HOMO/ LUMO of the complexes.

	HOMO							LUMO						
	1	20	31	32	41	42	5	1	2	31	32	41	42	5
α	-4.4	-0.7	-4.3	-4.4	-0.6	-0.6	-4.5	-1.4	1.9	-1.4	-0.7	1.9	2.2	-1.8
β	-4.4	-0.8	-4.8	-4.1	-0.6	-0.6	-4.5	-1.4	1.9	-2.0	-0.9	1.9	2.2	-1.8
Ni(s)	0	0	0	2	0	1	0	0	0	1	0	0	0	0
Ni(p)	5	1	1	6	0	8	5	3	0	3	8	0	0	5
Ni(d)	9	14	7	57	26	48	12	41	1	53	35	1	1	38
d_{z^2}	0	0	0	4	0	2	0	0	0	2	1	0	0	0
d_{xz}	1	1	0	44	2	2	2	1	0	2	0	0	0	0
d_{yz}	8	0	0	7	0	0	10	1	0	7	3	0	0	1
$d_{x^2-y^2}$	0	1	5	1	1	2	0	28	0	31	30	0	0	22
d_{xy}	0	12	1	0	22	42	0	11	1	11	0	0	0	15
S1(s)	0	0	0	0	0	0	0	0	0	0	0	0	0	0
S1(p)	19	25	25	5	26	1	20	12	0	11	1	0	0	11
S1(d)	0	0	0	0	0	0	0	0	0	0	0	0	0	0
S2(s)	0	0	0	0	0	0	0	0	0	0	0	0	0	0
S2(p)	24	25	24	15	17	15	25	12	0	7	3	0	0	11
S2(d)	0	0	0	0	0	0	0	0	0	0	0	0	0	0
P1(s)	0	1	1	-1	1	-1	0	1	0	1	0	0	0	1
P1(p)	2	3	4	4	3	5	2	4	2	5	5	0	0	5
P1(d)	0	0	0	1	0	1	0	1	1	0	1	0	0	1
P2(s)	0	1	0	0	1	0	0	1	0	0	-1	0	0	1
P2(p)	2	3	2	1	2	4	2	4	0	2	4	5	4	6
P2(d)	0	0	0	0	0	0	0	1	1	0	1	2	2	1

Table 4.4: HOMO/LUMO energies (eV) and contributions of different fragments (on and around nickel moiety) to the corresponding HOMO and LUMO.

	HOMO							LUMO						
	1	20	31	32	41	42	5	1	2	31	32	41	42	5
α	-4.4	-0.7	-4.3	-4.4	-0.6	-0.6	-4.5	-1.4	1.9	-1.4	-0.7	1.9	2.2	-1.8
β	-4.4	-0.8	-4.8	-4.1	-0.6	-0.6	-4.5	-1.4	1.9	-2.0	-0.9	1.9	2.2	-1.8
Fe(s)	0	0	0	0	0	0	0	0	0	0	0	0	0	0
Fe(p)	0	0	0	0	0	0	0	0	0	0	0	0	0	0
Fe(d)	0	1	1	0	1	1	0	2	1	1	1	1	1	2
phenyl	34	20	31	4	17	6	30	3	0	5	7	0	0	3
cyclo	0	2	1	0	1	1	0	3	4	2	2	4	3	3
rings	3	4	3	3	5	9	3	11	87	7	31	87	90	13
H/H2			0	0	0	1	0			0	2	0	0	0
phenyl(s)	0	0	0	0	0	0	0	0	0	0	0	0	0	0
phenyl(p)	34	19	30	3	17	6	29	2	0	5	7	0	0	3
phenyl(d)	1	1	1	0	0	0	1	0	0	0	0	0	0	0
cyclo(s)	0	0	0	0	0	0	0	0	1	0	1	1	1	1
cyclo(p)	0	1	1	0	1	1	0	3	2	2	1	3	2	3
cyclo(d)	0	0	0	0	0	0	0	0	0	0	0	0	0	0
rings(s)	1	0	1	1	1	1	1	1	1	0	1	1	1	0
rings(p)	2	3	2	3	4	7	2	9	84	7	29	84	87	12
rings(d)	0	0	0	0	0	0	0	0	2	0	1	2	2	0

Table 4.6: HOMO/LUMO energies (eV) and contributions of different fragments (not coordinated to the nickel moiety) to the corresponding HOMO and LUMO.

As Table 4.6 shows there is an insignificant contribution, 0%, from the iron atom in the ferrocene moiety. This hints that the reactivity of **1** depends almost exclusively on the Ni and the bidithiolate. This means that the **1** is in nature closer to a mononuclear Ni complex than to a [NiFe] complexes.[111, 17, 51, 161]

Firstly, **1** gains an electron which reduces the nickel into a d^9 nickel complex (**20**). This extra electron manifests itself in changes in the bond lengths and bond orders (Table 4.1). In particular, the phosphorus bonds strengths increase which reduces the distance between the Ni and Fe, from 4.294 to 4.255 angstrom, as well as shortening the Ni-P bonds.

The other effect of this geometry distortion is that the two phosphorus atoms become indistinguishable and identical in terms of bond order and length. These minute structural changes facilitate the protonation of Ni in the next step. There has been studies that show that the protonation can occur on the thiolate site as well as Ni.[104, 210]

Complexes **31** and **32** are the results of protonation of complex **20** on Ni and sulfur sites respectively. Energetically, protonation of Ni is 3.6 kcal/mol more stable than **32**. While this is a considerable difference in energy, we do not discard the hypothesized **32** yet. The next step in our EC/EC mechanism is the reduction of complexes **31** and **32**. The result of this reduction are complexes **41** and **42**. The energy difference between these two complexes is significantly larger, 15.3 kcal/mol. This proves that the protonation of the bdt ligand is energetically undesirable (and improbable). Interestingly, protonation of both **41** and **42** will form complex **50**; where the H_2 is produced and left the nickel site. While this mechanism is fully supported by all the aforementioned experimental results, finding a transition state can give us more insight into how does the final step of this process, hydrogen evolution, happen?

To find the transition state (TS), we performed Synchronous Transit-guided Quasi-Newton (STQN2) calculation, where **41** and **50** are used as initial and final structures. The results of this calculation was very interesting. The **TS** shows that the second hydrogen will also bind to the Ni, but in order to facilitate this, the complex goes through a geometry change. The **TS** forms a pseudo-octahedral structure. Table 4.1 shows that the Ni−S bonds and Ni−P bonds are, 0.1 $\mathring{A}$ and 0.15 $\mathring{A}$ longer in comparison to **1**. There is also a staggering 40° change in the dihedral angle. This hints that the rearrangement in the geometry is likely a critical step that aids the attachment of the second hydrogen to nickel by providing an open coordination site in the juxtaposition of the first and second hydrogen. To sum up, this structural change can be a key factor in the efficiency of this catalyst. It is also worth mentioning that, analyzing the Mayer's bond orders, also confirms the formation of a covalent nickel-hydride bond during the proposed mechanism.

4.3 Conclusion and Future work

To understand the functionality of **1**, it is better to consider it as a mononuclear nickel complex even though it is a [NiFe] bimetallic compound. Density functional theory based results show that effectively there is no bonding interaction between nickel and iron moieties. In fact, the bite angle of the ddpf ligand and its rigidity are likely more relevant factors. These properties of the ligand not only enforce a certain geometry on the Ni(II) but also tune the redox properties of the complex by modifying the LUMO energy and construction.

An efficient hydrogen evolution catalyst that can function in water at pH close to 7 and also be energetically desirable, are crucial ingredients that can make a proton reduction catalyst economically feasible. Complex **1**, on the other hand, is water insoluble. However the structure of our catalyst makes it easily modifiable.

Synthetically, tuning the ligands to make **1** water soluble is the clear next step. From a theoretical point of view, I believe that the difference between the LUMO energies of complexes **1** and **2** is not large enough to account for the significant difference in the reduction potential of Ni^{II}/Ni^{I}. This means that further calculations are essential into justifying this. It has already been an attempt in looking into this problem[72], but this study comes short by ignoring some of the crucial experimental results such as H-NMR results. Also, rational computationally-guided designing and searching for ligands that can tune the water-solubility of **1** without interrupting the mechanistic steps of this catalytic reaction can amp up and speed up reaching our ultimate product.

4.4 Catalytic Hydrogen Production by Fe(II) complex

[3]

4.4.1 Introduction

As we discussed previously, one way to address the global energy crisis is through finding a sustainable energy source. An enticing opportunity seems to be producing hydrogen from solar energy which can make a storable renewable fuel. Bio-inspired by hydrogenases, that is the biological catalysts for hydrogen evolution, many efforts have been made into using organometallic model systems of hydrogenases' active sites such as [NiFe] or [FeFe]. However, the synthetic model systems rarely come close to natural hydrogenases' performance of 1000 s^{-1} at close to zero overpotential.

[FeFe]-hydrogenases' H-cluster is a distinct six-iron cluster comprised of an iron-sulfur cluster ,Fe_4S_4 an a diiron site. These two sites are related by two bridging cysteinyl thiolate groups. The diiron site is a biologically interesting complex as it resembles many organometallic complexes. A bridging dithiolate ligand, CO, and CN^- are on each iron center.

It is worth mentioning that it is not very common to have CO and CN^-, both very strong π-acceptors, in biological systems. Figure 4.13 shows the H-cluster of two different categories of hydrogenase. It is clear from the figure that we have two distinct irons: One which is closer to the iron sulfur cluster and is called proximal iron, Fe_p; and second the distal iron, Fe_d, that is a five-coordinated ,pseudosquare pyramidal center. Fe_d has electron deficiency and a terminal open coordination site where the hydrogen production reaction takes place.

[3]The experimental results of this chapter are not done by this author and are purely work of professor Jone's group. The reader is referred to the complete paper [175] for the further discussion of the experimental results.

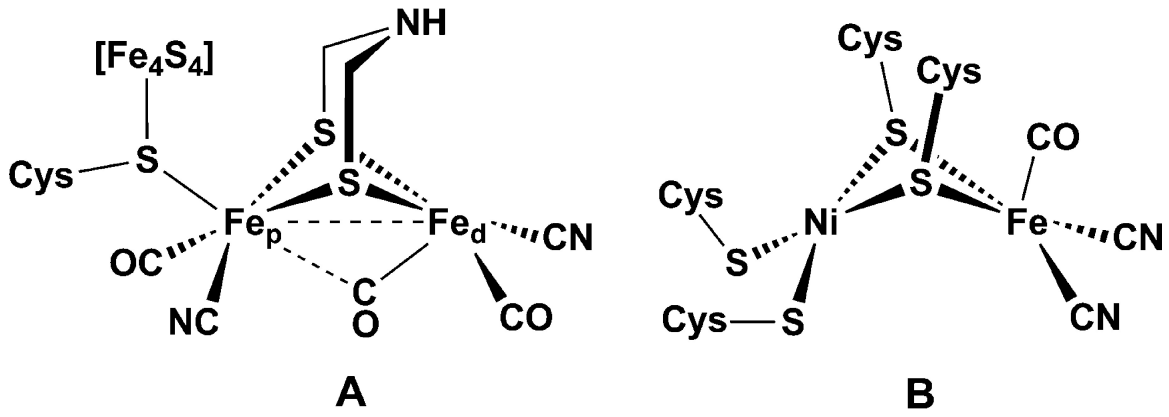

Figure 4.13: Active Sites of [FeFe] (A) And [NiFe] (B) Hydrogenase.

Organometallic complexes that have a $[(\mu{-}SR_2)Fe_2(CO)_6$] and their close relatives that the CO ligands are substituted by phosphines (σ-donor ligand), have been widely used as structural/functional bio-mimic alternatives to [FeFe] hydrogenase.[191, 56, 65] Many of the model complexes are poor catalysts for hydrogen production, due to their high overpotentials. In many of these complexes it is believed that the hydrogen bridges, as a hydride, between the irons. In principle, a mononuclear iron complex with an open terminal coordination site should be able to mimic the reactivity of the distal iron of the natural enzyme, provided, the electronic environment and geometrical constraints of the ligands imitate the diiron counterparts.

Followed by the determining of the crystal structure of [FeFe]- hydrogenase, many have synthesized hexa-coordinated iron compounds that resembled the [FeFe]- hydrogenase which were mostly used as a model for spectroscopic studies.[99, 85, 42] The synthesis of a 16-electron Fe(II) complex,$[Fe(CO)_2(CN)(SNH{-}C_6H_4)]$ and its tendency to form a saturated coordination (sometimes by forming a dimer[109] have started a realm for investigation for other groups.[112, 179] The bdt ligand was later used by Sellman and coworkers to make $[Fe(bdt)(PMe_3)_2(CO)_2]$. Interestingly, they observed that this complex is readily losing a CO ligand to form an unsaturated,

penta-coordinate complex.[178]

This complex inspired other inorganic chemists to create other iron complexes in particular as a spectroscopic model of the H-cluster in hydrogenase.[164] None of these studies investigated the electrocatalytic proton reduction; until recently, where the distal iron site of the hydrogenase was modeled with bdt and chelating phosphine ligands bonded to Fe and could undergo an electrocatalytic proton reduction.[63, 23, 152]

In this section, we discuss [(κ_2−dppf)Fe(CO)(κ_2−bdt)], **1** which is capable of reducing proton at a very small over-potential. We have also compared this complex with [(κ_2−NP_2)Fe(CO)(κ_2−bdt)], **2**, where NP2 stands for methyl-2-bis (diphenylphosphinomethyl) amino. Computationally, we aimed at utilizing several methods at Density Functional Theory level of theory to explain the different behavior of **1** and **2** in reducing proton and their reactivity towards binding with CO.

4.4.2 Computational Details

All the structures were optimized at the DFT level of theory with B3LYP functional and 6-31G* basis set. This level of theory has been shown to give reliable geometrical parameters and vibrational frequencies.[87, 189] We have also benchmarked the calculations using different functionals and larger basis sets. These results are presented in the Computational Studies section. We have also performed overlap population analysis to understand the nature of the interactions between the fragments of the compounds.

4.4.3 Results and Discussion

The details of synthesis of these compounds can be found elsewhere and are not within the scope of this thesis.[175] The bdt ligand is a natural π-donor and it is a

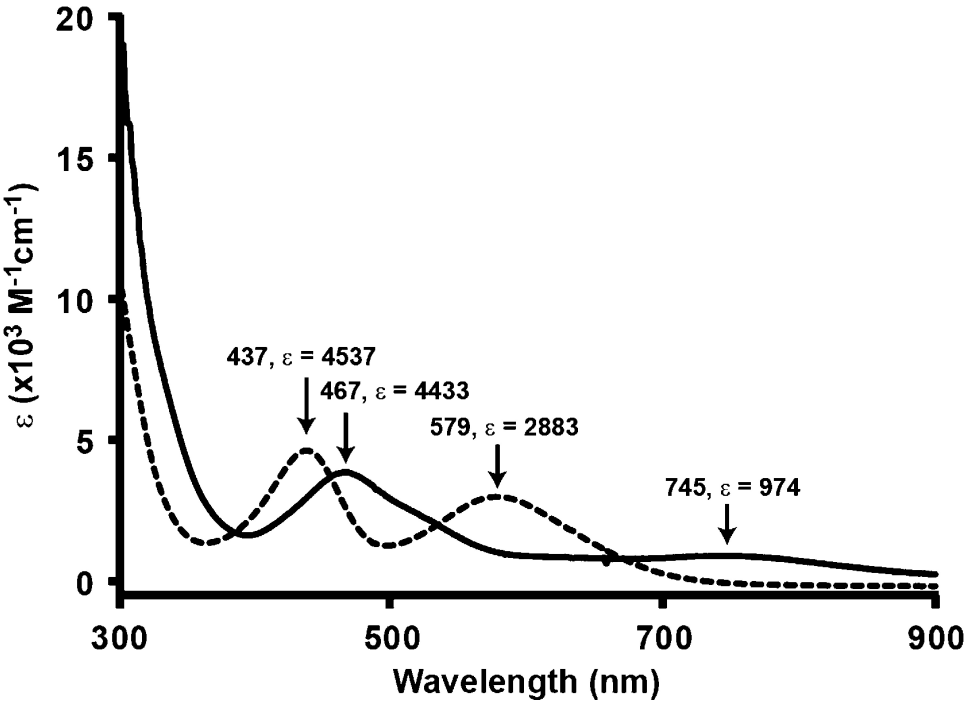

Figure 4.14: The Solid Line and Dashed Line Are the Uv-vis Spectra of Complexes **1** and **2** Respectively in A .1 Mm Solution in THF.

redox non-innocent ligand. The dppf has an interesting bite angle. This wide bite angle has a considerable effect on the structure and function of the complex.[14, 15, 114]. Complex **2** was made so that we can compare the effects of the wide bite angle of dppf on catalytic properties of the iron center.

Figure 4.14 shows the UV-Vis spectra of the two complexes. Complex **1** absorbes at 467 and 745 nm. The 467 nm peak, corresponds to a super blue color, is assigned to two charge transfer processes even though the ε is not as high as what is normally expected for charge transfer UV-vis features. The 745 nm band is assigned to d-d transition. The relatively low ε is a signature of a forbidden d-d transition.

IR spectra of **1** and **2** presents a peak at 1918 and 1915 cm^{-1} that corresponds to the stretching of the CO. The minimal difference between the CO-stretching IR peak shows that the two different ligands have almost negligible difference on the CO

bond. This point is reflected in the very similar CO bond length in the DFT studies as can be seen in Table 4.7.

Crystal Structure

Tables 4.7 and 4.8 summarize the geometrical parameters obtained from single crystal X-ray diffraction of **1** and **2**. The geometries of **1** and **2** are completely different around the central iron. Complex **1** has a distorted trigonal bipyramidal (TBP) structure and complex **2** has a distorted square pyramidal structure (SP). CO ligand is in an axial position in **2** and in an equatorial position in **1**. Addison's τ value, is defined as:

$$\tau = \frac{\beta - \alpha}{60}$$

where β is the larger of the angles between the trans aligands on the basal plane in SP and/or the angle between the two axial ligands of a TBP; α is the smaller angle between the trans ligands in SP and/or the larger of the basal angles in a TBP complex.[1] τ is a factor that shows how much is the geometry of a pentacoordinate complex distorted from the ideal SP ($\tau = 0$) and TBP ($\tau = 1$).

The Addison's parameters of 0.099 and 0.721 was obtained for **2** and **1** which bolsters the assigned structures. Important for computational studies, it was confirmed that **1** is diamagnetic. The perfect TBP geometry doesn't allow a diamagnetic ground state for a d^6, Fe(II), but a ground state with multiplicity of one is consistent with the distorted geometry.[85, 145] Also the benzene rings on the bdt have an alternative bond lengths. The two C−S bonds have different bond lengths in both complexes and are slightly shorter than the normal carbon sulfur bond lengths in bdt, suggesting the bond orders are greater than a single bond.[168, 166, 165] The charge on the iron center in **1** and **2** is less than +2 as it can be seen in the computational section.

Bond Length	X-ray Structure		Calculated (B3LYP/6-31G*					
$\mathring{A}$	1	2	1	2	$1(H)^+$	$2(H)^+$	$[1(H)\text{-}CO]^+$	$[2(H)\text{-}CO]^+$
Fe1-S1	2.1719	2.2007	2.218	2.229	2.194	2.357	2.384	2.394
Fe1-S2	2.2243	2.1767	2.285	2.239	2.386	2.192	2.408	2.374
Fe1-P1	2.2405	2.2222	2.297	2.263	2.320	2.284	2.404	2.310
Fe1-P2	2.2241	2.2249	2.256	2.256	2.321	2.288	2.362	2.316
Fe1-C1	1.732	1.715	1.735	1.706	1.742	1.733	1.809	1.805
C1-O1	1.162	1.154	1.162	1.165	1.158	1.157	1.150	1.150
Fe1-C2	-	-	-	-	-	-	1.826	1.835
C2-O2	-	-	-	-	-	-	1.147	1.144
C1-C6	1.398	1.412	1.407	1.411	1.404	1.397	1.408	1.400
C1-C2	1.404	1.386	1.407	1.409	1.399	1.399	1.403	1.405
C2-C3	1.410	1.407	1.409	1.409	1.397	1.404	1.400	1.408
C3-C4	1.365	1.373	1.388	1.391	1.394	1.393	1.391	1.391
C4-C5	1.401	1.394	1.405	1.407	1.399	1.399	1.400	1.400
C5-C6	1.380	1.385	1.389	1.391	1.393	1.394	1.391	1.391
C1-S1	1.745	1.746	1.764	1.757	1.780	1.794	1.770	1.800
C2-S2	1.735	1.757	1.757	1.758	1.794	1.781	1.796	1.771

Table 4.7: The comparison between bond lengths ($\mathring{A}$ obtained from DFT calculations and X-ray structures.

Bond Angles	X-ray Structure		Calculated (B3LYP/6-31G*					
°	1	2	1	2	$1(H)^+$	$2(H)^+$	$[1(H)\text{-}CO]^+$	$[2(H)\text{-}CO]^+$
P2-Fe-P1	101.18	87.49	102.4	89.3	100.8	92.9	98.0	91.8
S1-Fe1-S2	89.21	89.31	88.4	89.3	87.2	86.9	85.9	87.3
C1-Fe1-S1	134.57	101.30	137.9	102.4	130.4	93.3	89.1	88.6
C1-Fe1-S2	88.52	106.58	86.3	99.1	89.4	119.5	81.6	84.5
C1-Fe1-P1	90.19	94.11	89.9	96.0	89.5	92.8	90.1	93.4
C1-Fe1-P2	96.69	93.28	97.0	97.9	96.3	93.8	97.9	96.6
S1-Fe1-P2	128.48	165.14	124.7	159.7	132.9	172.6	176.1	178.0
S2-Fe1-P1	171.74	159.2	168.8	164.9	171.8	147.6	171.1	176.4
O1-C1-Fe1	173.4	176.7	172.6	173.4	170.5	173.0	173.1	173.3
O2-C2-Fe1	-	-	-	-	-	-	173.4	173.9

Table 4.8: The comparison between bond angles obtained from DFT calculations and X-ray structures.

Reaction with CO

1 and **2** were reacted with CO to assess whether the open coordination site on them is sn accessible binding site. Figure 4.15 presents the IR spectra of **1** when exposed to CO, bubbled through the solution of **1**. As a result two new bands are observed for CO at 1996 and 2020 cm^{-1}. These peaks are an indication of formation of **1-CO** complex. Original, the presence of two peaks was interpreted as a sign that the CO are in Cis conformation.[175] But the computational studies shows that the trans structure is energetically favorable. One hypothesis is that the reaction is under kinetic control, but on the other hand 4.7 shows that even in the trans conformation

the calculated bond lengths for the two CO are slightly different which can account for the presence of two CO bands.

The phosphorus NMR spectra also shows two peaks at 66.32 ppm and 62.59 ppm that can be a further proof for the formation of **1-CO** These peaks disappeared after purging removing the CO from the environment, which indicates the reversibility of the CO binding. Under similar conditions, similar behavior was observed for **2** with two IR peaks at 1995 and 2021 cm^{-1} (4.15). It is worth mentioning that the reaction of **2** with CO is not as complete as **1**. Accepting the hypothesis 1, cis conformation, then the difference in the reactivities can be explained by the substantial change in the geometry that is necessary for the formation of the cis conformer, meanwhile **1** can form the bond more readily.

However, the reaction performance was improved by adding a strong acid, $HBF_4 \cdot OEt_2$. This new complex, $[1\,(H)-CO]^+$, has also two CO vibrations at 2089 and 2043 cm$^-$1. Adding a base to the solution and purging the CO out of the solution will reversibly form **1**. We believe that the acid protonates one of the sulfurs on the bdt, which will in return weaken the bonding between the metal-ligand character. This will be discussed in detail in the next section. The electrocatalytic properties of these two compounds are discussed elsewhere [175]

Computational Studies

New studies have shown good performance of BP86 and TPPS functionals in particular for first row transition metals.[218, 212, 28] Hence the geometrical parameters of **2** are calculated and compared with these functionals and with larger basis set (TZVPP). The results show a good agreement with the chosen B3LYP/6-31G* method. Table4.9 summarizes the results.

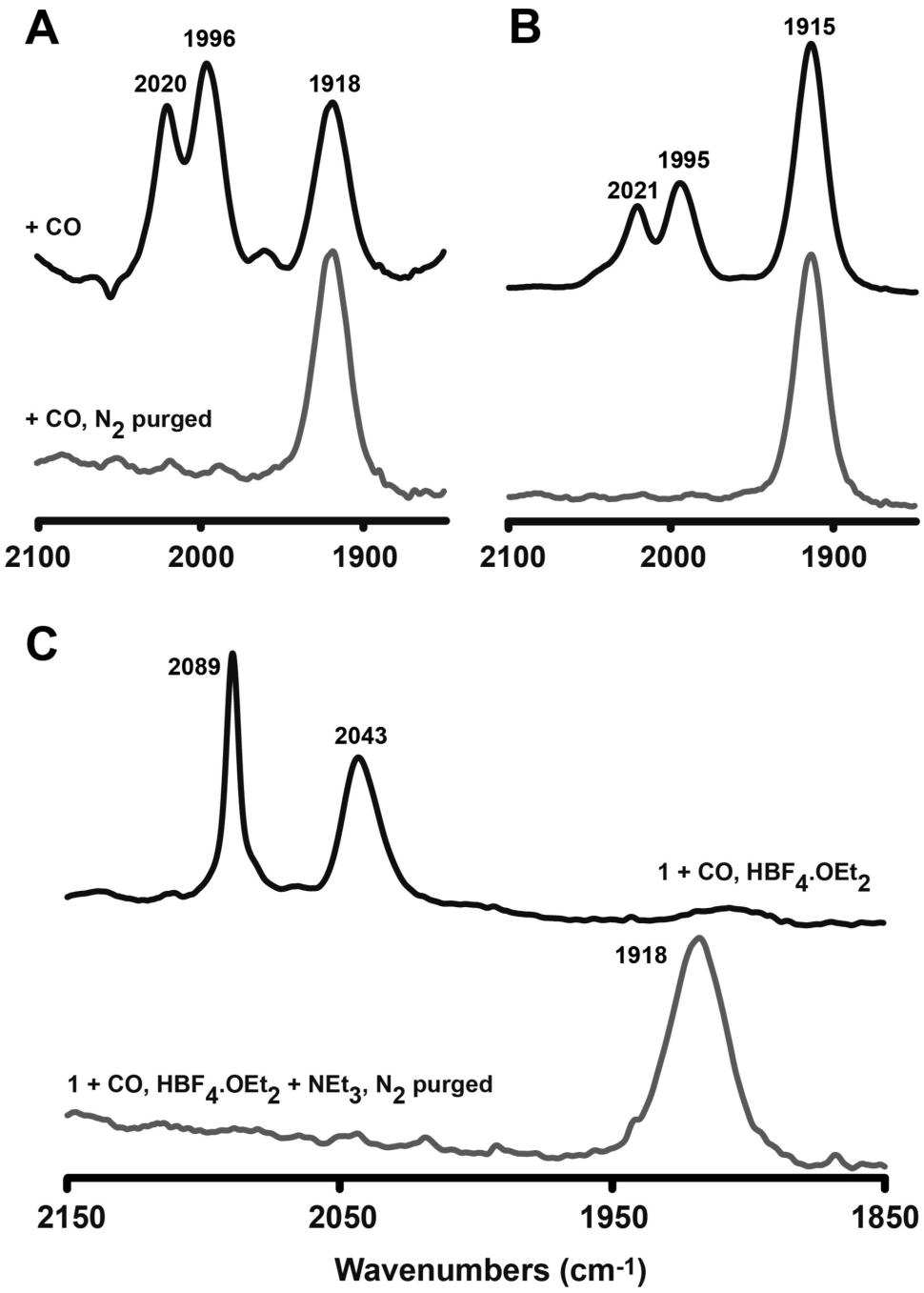

Figure 4.15: IR Spectra of **1** and **2** Are Presented in the Absence (a) and (B) and in the Acidic Environment with CO Gas Bubbling Through the Solution.

Parameters	X-ray	BP86		TPPS		B3LYP
		6-31G*	TZVPP	6-31G*	TZVPP	6-31G*
Fe1-S1	2.201	2.211	2.211	2.208	2.206	2.227
Fe1-S2	2.177	2.202	2.199	2.206	2.198	2.222
Fe1-P1	2.225	2.232	2.230	2.229	2.229	2.292
Fe1-P2	2.222	2.237	2.236	2.229	2.224	2.285
Fe1-C1	1.715	1.709	1.711	1.716	1.716	1.723
C1-O1	1.154	1.185	1.173	1.182	1.170	1.164
P2-Fe-P1	87.5	91.1	90.1	89.0	88.9	91.1
S1-Fe-S2	89.3	88.8	88.8	89.1	89.0	88.9
C1-Fe-S1	101.3	101.5	101.5	102.3	101.8	100.0
C1-Fe-S2	106.6	106.8	105.8	104.6	105.1	103.3
C1-Fe-P1	94.1	94.8	96.1	95.2	95.8	96.7
C1-Fe-P2	93.3	94.1	93.4	94.4	94.3	94.6
S1-Fe-P2	165.1	163.7	165.1	162.2	163.9	163.3
S2-Fe-P1	159.2	159.1	158.1	161.0	159.0	162.1
O1-C1-Fe	176.7	175.8	175.5	175.9	175.7	175.9

Table 4.9: The comparison between geometrical parameters with different functionals and basis sets. The bond lengths are measured in angstrom and the bond angles are in degree units.

1, **2**, **1(H)**+, **2(H)**+, [**1(H)-CO**]+, and [**2(H)-CO**]+ are all optimized at DFT level of theory. Tables 4.7 and 4.8 show that the crystal structures and B3LYP-optimized structures are in good agreement with each other.

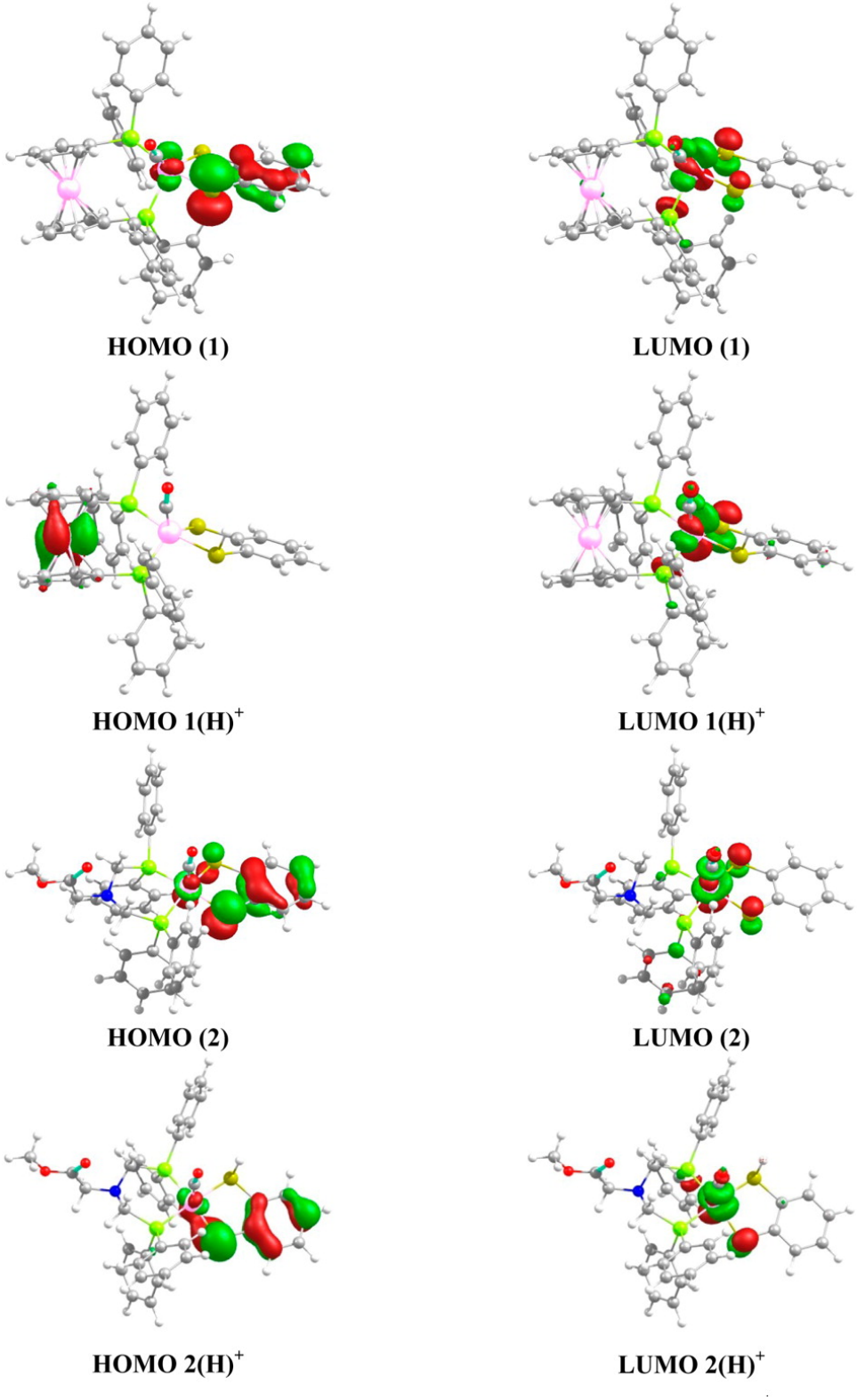

Figure 4.16: Electron Density Profiles of The HOMOs and LUMOs of 1, 1(H)+, 2, and 2(H)+.

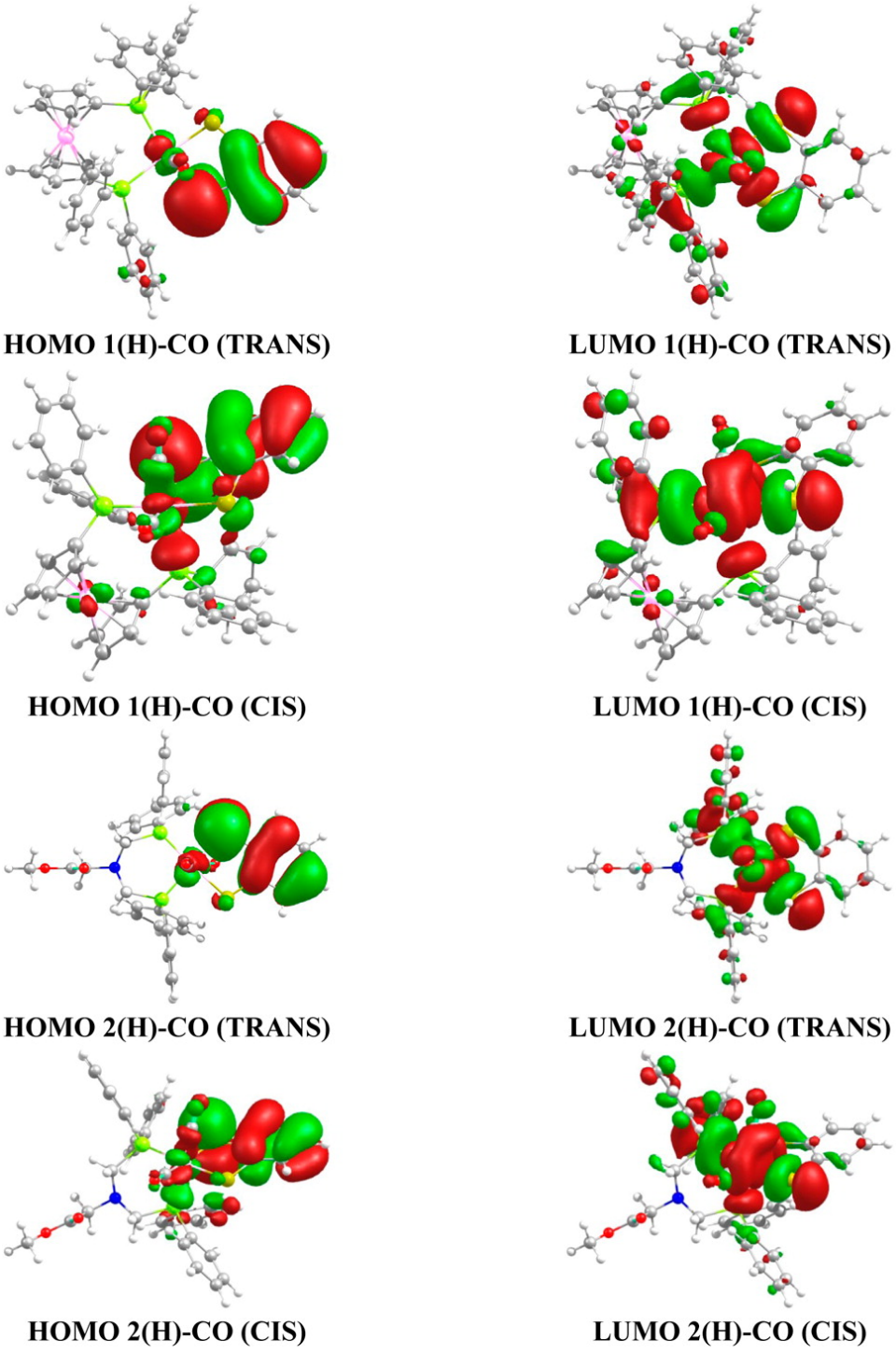

Figure 4.17: Electron Density Profiles of The HOMOs and LUMOs of The Cis And Trans Conformers of [1(H)-CO]+ And [2(H)-CO]+.

HOMOs of both **1** and **2** are delocalized on the central iron and the bdt ligand. This hints to the partial oxidization of the bdt ligand that make it to exhibit π-radical character and justifies its distortion.

The HOMOs are comprised of a bonding interaction between Fe d orbitals and S p(π) orbitals and an antibonding interaction between S and the nearby carbons. This implies delocalization of the electrons over iron and bdt. To further investigate this bonding pattern, we applied "overlap population" analysis. These parameters are listed in Table 4.10. The overlap populations are a semi-quantitative measure for quantifying the nature of the orbital interactions.[68, 79, 192, 64] A positive overlap population implies a bonding combination, the negative overlap analysis means there is an anti-bonding interaction and a zero overlap represents negligible bonding between the fragments. The overlap parameters of **1** and **2** and their protonated counterparts are tabulated in Table 4.10

	HOMO				LUMO			
	1	1(H)+	2	2(H)+	1	1(H)+	2	2(H)+
Fe1-S1	0.00	0.00	0.02	-0.01	-0.08	-0.08	-0.07	0.02
Fe1-S2	0.02	0.00	0.04	0.04	-0.04	0.01	-0.07	-0.08
Fe-C	0.00	0.00	-0.01	-0.01	0.02	0.00	0.00	0.01
Fe-P1	0.03	0.00	0.02	0.01	0.00	0.04	0.05	0.03
Fe-P2	0.00	0.00	0.01	0.01	-0.04	0.02	0.05	0.04

Table 4.10: Overlap populations of different fragments of **1** and **2** and their protonated form.

Interestingly, there two S atoms are not identical from an FMO point of view. The HOMO of **1** shows bonding interactions only with the axial sulfur, another manifestation of the peculiar geometry of **1**. Contrary to **1**, both S of the bdt ligand have contributes to the bonding interaction substantially. More over, the HOMO of **1** and **2** have an uncanny resemblance with SOMO, Singly Occupied Molecular Orbital, of the π-radical anion form of a free bdt ligand.[169, 167] The overwhelming evidence from molecular orbital theory calculations shows that the interaction between iron and dithiolate ligand can be justified as a result of charge (density) transfer from the ligand to the empty d orbital of the iron center. This likely causes the ligand to metal charge transfer peaks in the UV-vis spectra.

The Lowest Unoccupied Molecular Orbitals, Figure 4.16, along with the orbital decomposition results, Table 4.11, show that the LUMOs of both compounds are dominated predominantly by Fe center with small contributions from phosphine and bdt. These convey that reducing the complex, causes a charge localization and accumulation on the iron center. In other words, reduction of the compounds will cause a very basic site, Fe, make it a suitable site for interacting with the protons in the acidic environment. It is worth mentioning that the heavy contribution from Fe to the LUMOs in both **1** and **2** is consistent with the reactivity of these complexes with CO.

		HOMO				LUMO			
		1	$1(H)^+$	2	$2(H)^+$	1	$1(H)^+$	2	$2(H)^+$
Energy (eV)		-4.79	-8.16	-4.81	-8.47	-1.72	-5.06	-1.48	-4.96
Fe1	s	0	0	0	1	1	0	0	0
	p	3	0	5	3	4	8	7	9
	dz^2	10	0	11	6	11	23	21	36
	d_{xz}	3	0	0	0	2	3	22	10
	dyz	0	0	1	1	12	9	0	2
	dx2-y2	0	0	0	1	22	19	0	0
	dxy	6	0	0	1	4	0	0	4
	Total d	19	0	12	9	51	55	43	52
Fe (ferrocene)	s	0	0	-	-	0	0	-	-
	p	0	0	-	-	0	0	-	-
	d	0	79	-	-	1	1	-	-
S1	s	0	0	0	0	0	0	0	0
	p	0	0	9	1	8	9	8	2
	d	0	0	0	0	0	0	0	0
S2	s	0	0	0	0	0	0	0	0
	p	41	0	26	37	6	1	7	10
	d	0	0	0	0	0	0	0	0
CO	s	0	0	0	0	1	2	4	4
	p	0	0	1	1	2	2	2	2
	d	0	0	0	0	0	0	0	0
P1	s	0	0	0	0	0	0	0	0
	p	1	0	2	1	2	2	4	5
	d	0	0	0	0	0	0	1	0
P2	s	0	0	0	0	1	0	0	0
	p	0	0	1	1	7	6	4	3
	d	0	0	0	0	1	0	1	0
Phenyl ring (bdt)	Total	32	0	40	39	5	5	4	5
Cp rings	Total	0	20	0	0	2	1	0	0
Phosphine phenyls	Total	2	1	3	7	9	5	16	5
Proton (H)	Total	-	0	-	0	-	1	-	1

Table 4.11: Orbital contribution percentages.

In order to estimate the charge transfer between different fragments of the compounds, we used Mulliken charge decomposition analysis.I discussed Mulliken charge decomposition framework and briefly discussed its limitations in appendix A.

	1	2	1-H+	2-H+	t1-HCO+	c1-HCO+	t1-HCO+	c1-HCO+
Fe1	25.64	25.65	25.60	25.65	25.77	25.72	25.78	25.73
Fe2	25.54		25.52		25.53	25.53		
S1	16.20	16.17	16.12	15.98	16.13	16.16	16.14	16.15
S2	16.17	16.18	16.00	16.11	15.99	15.97	15.98	15.97
CO1	14.11	14.09	14.07	14.05	13.97	14.03	13.98	14.02
CO2					13.97	13.96	13.94	13.97
P1	14.69	14.69	14.68	14.65	14.60	14.60	14.61	14.61
P2	14.63	14.69	14.65	14.66	14.62	14.60	14.63	14.61
bdt phenyl	40.20	40.21	40.04	40.05	40.07	40.07	40.07	40.09
CP/glycine	68.70	62.19	68.57	62.10	68.58	68.59	62.10	62.09
P-phenyls	164.13	164.13	163.91	163.90	163.93	163.93	163.93	163.91
Proton (H)			0.84	0.84	0.84	0.84	0.84	0.85

Table 4.12: Mulliken Charge Decomposition analysis.

The Mulliken partial charges are presented in Table 4.12 and they are in accord with the FMO description of the systems. The ferrocenyl's iron (Fe(II)) in **1** can be used as an internal standard to assign a charge to the Fe center. The central Fe always has a smaller charge which is yet another proof for the ligand to metal electron transfer which results in a less than +2 oxidation state for Fe.

Next, we try to understand the reactivity of **1** and **2** towards the CO. To this aim, we study two more complexes that are protonated, because of the acidic condition in the experiment.

Two main sites can be hypothesized for the protonation of **1**, the iron center and the S in bdt that shows the highest contribution to the HOMO.[113]

Compound **2** has more possibilities, since both S are involved in the HOMO and it has an amine group in its ligand that can (and probably will) become protonated.

Protonation of **1** on the S is 13 kcal/mol more stable than the Fe center. Similarly for **2**, sulfur is the preferred protonation site since it is 6.4 kcal/mol more stable than the protonated amine. So logically, all the other calculations are performed on the structures that the protonation occurred on the thiolate site.

The structure of 1(H)+ shows only negligible changes around the iron center. Particularly, the Addison value of this structure (0.65), shows minor distortion in comparison to 0.72 of the original complex.

Contrary, protonation of **2** starkly distorts the structure from a square pyramidal geometry ($\tau = 0.09$) to an intermediate structure between SP and TBP ($\tau = 0.42$). More importantly, the frontier molecular orbitals of the 1(H)+ and 2(H)+ exposes major distinctions that are crucial in explaining the diverse reactivity behavior of them towards the CO.

Ferrocene moiety harbors almost entirely the HOMO of 1(H)+; whereas the HOMO in 2(H)+ is delocalized ove the bdt ligand (almost exclusively with small contribution from the iron center). The bdt ligand shows a bonding pattern, combined with the orbital contributions of the HOMO, we can deduce that bdt is partially oxidized in the 2(H)+. The Mulliken charges show a considerable change in the thiolate's partial charge between **2** and 2(H)+ complex. Also the aromatic fragment of the bdt has smaller negative charge.

Indeed the most interesting change happens in **1**, where protonation of the complex breaches the electron delocalization between the iron and the bdt ligand. This re-

establish the aromaticity of the benzene ring in the bdt. This charge rearrangement helps 1(H)+ to act as a typical coordinatively unsaturated d^6 iron (II).

The distinction between electronic structures of 1(H)+ and 2(H)+ can explain why the CO uptake is observed mostly for **1** in acidic solution. We can also see the stronger CO interaction with 1(H)+ than with 2(H)+. The lower LUMO energy in the 1(H)+ (0.1 eV in comparison to LUMO of 2(H)+) can make a stronger bond to the HOMO of CO. Also we should notice that addition of CO to 1(H)+ or/and 2(H)+ saturates the Fe and will result in the complexes to maintain an octahedral structure with a sp^3d^3 hybridization, where the d_{z^2} and $d_{d^2-y^2}$ orbitals form the hybridized orbitals. This is clear, from the increased contribution of the d_{z^2} and $d_{d^2-y^2}$ to the LUMO of 1(H)+. This also makes it more likely, and more favorable, for 1(H)+ to form a bond with CO.

		HOMO				LUMO			
		1CO trans	1CO cis	2CO trans	2CO cis	1CO trans	1CO cis	2CO trans	2CO cis
Energy (eV)		-7.83	-7.97	-7.80	-7.80	-4.44	-4.58	-4.34	-4.43
Fe1	s	0	0	0	0	1	1	1	2
	p	0	0	0	0	1	1	0	1
	dz^2	0	2	1	1	1	7	2	5
	d$_{xz}$	2	1	2	1	0	13	1	16
	dyz	5	1	4	2	1	0	3	4
	dx2-y2	0	2	0	1	13	36	0	11
	dxy	0	0	0	1	41	1	43	17
	Total d	7	6	7	5	56	57	49	52
Fe2	s	0	0	-	-	0	0	-	-
	p	0	0	-	-	0	0	-	-
	d	0	1	-	-	1	1	-	-
S1	s	0	0	0	0	0	0	0	0
	p	53	51	54	53	5	2	4	2
	d	0	0	0	0	0	0	0	0
S2	s	0	0	0	0	1	1	2	1
	p	0	1	0	0	8	9	9	9
	d	0	0	0	0	0	1	0	0
CO1	s	0	0	0	0	0	1	0	1
	p	0	1	0	1	3	1	6	1
	d	0	0	0	0	0	0	0	0
CO2	s	0	0	0	0	0	1	0	1
	p	1	1	0	1	3	1	6	3
	d	0	0	0	0	0	0	0	0
P1	s	0	0	0	0	1	2	1	2
	p	0	0	0	0	4	7	4	7
	d	0	0	0	0	0	1	1	1
P2	s	0	0	0	0	1	0	0	0
	p	0	2	0	1	3	1	3	1
	d	0	0	0	0	0	0	0	0
Ring (bdt)	Total	36	32	36	34	2	2	2	2
Cp rings	Total	0	1	0	0	2	2	1	1
Phenyls	Total	1	3	1	3	7	7	11	12
Proton (H)	Total	0	0	0	0	0	0	0	0

Table 4.13: Orbital contribution percentages for trans-$[1-(H)CO]^+$, cis-$[1-(H)CO]^+$, trans-$[2-(H)CO]^+$, and cis-$[2-(H)CO]^+$

4.4.4 Conclusion

In short,two pentacoordinate $Fe_{II}(CO)P_2S_2$ complexes with benzene-1,2-dithiol and two different chelating bis-phosphine ligands: NP2 and dppf. The electronic structures of both complexes are similar, but the different geometrical constraints imposed by the two phosphine ligands make two complexes with very different reactivity. We have utilized various computational tools to explain the spectroscopic and reactivity of this two complexes. While, we haven't discussed the electrocatalytic activity of these complexes in this dissertation, it is worth noting that **1** reduces protons at a very low overpotential.

4.5 Future Works: Towards a Molecular Descriptor for Hydrogen Evolution Catalyst

With the ever increasing pressure on chemical industry and academia to produce and develop products and results at the shortest time with minimum cost and the relative scarcity of the funding sources, there is more need than ever to produce new ideas and increase the success rate of the scientific endeavors. There are two methods that have proven to be helpful and were initially embraced by the pharmaceutical companies to escalate and optimize their efforts in drug discovery. They had a 10^{200} drug-like chemical space and it seemed as if all the low-lying drugs were already been harvested. With such a huge space to cover and search, there is a need for massive parallelization and use of high-throughput methods as well as using molecular descriptors that can, with the help of data manipulation and machine learning methods, quickly search a big part of chemical space and screen the undesirable molecules and produce a handful of candidates. These "brute force" approaches to material discovery can be classified as : Combinatorial methods and computational approaches.[32]

4.5.1 Combinatorial Methods

Combinatorial methods are based on an iterative process for material discovery. Firstly, a library of candidates with relatively similar structures is synthesized. It is essential that in this step the synthetic process has only few steps with high yields so that it can be automated by use of a robot-synthesizer. Secondly, the synthesized candidates are tested to find which one has the desirable catalytic properties (Figure of Merit, FOM). This step is normally parallelized as well. Typically FOMs are product selectivity, enantioselectivity, and price. In the case of hydrogen evolution catalysts, the FOMs are turnover frequency, overpotential and perhaps water solubility. Finally, it is time for using data analysis. By using data-science tools, we search for relations between the FOM and different chemical properties. Within this three-step framework the search for a new homogeneous catalyst can be mapped into a search for an optimal region in a multi-dimensional space. Combinatorial methods well-suit the problems were the large search space make the conventional methods improvident. Once an initial desirable candidate is found, then a new library is constructed around that compound to sample this smaller region with a higher resolution!

It is worth noting that, as it is the case in computational chemistry, there is a trade-off between the quantitative precision and screening time and cost. Although, this field is still in its maturation time, it has been successfully applied and resulted in many discoveries.[106, 84, 205, 3, 156]

4.5.2 Computational Approaches

The theoretical approaches and calculations have grown exponentially in recent decades. Once exclusively a scientific and academic interest, theoretical calculations of catalytic reactions is now at the stage of solving commercial problems. These

endeavors are primarily focused on modifying the ligands to make the catalysts more selective and more efficient.

The biggest challenge in theoretical modeling of catalysts, in particular the ones with transition metals, is choosing the right model system. Experimental setups are normally too complicated to model. They are comprised of precursors, catalysts, solvents, counter-ions, electrodes, substrates and etc. It is impractical to model all of this; moreover it does not necessarily improve our insight and understanding. Also, in case of transition metals, appropriately modeling the d orbitals (and electrons) or have the right molecular mechanic's parameters for these metals is also challenging. Also, we should note that catalysis, in its very nature, a kinetic problem. Hence, inevitably, the transition state, its structure/function, are of paramount importance, because it governs the activation energy and rate of the reaction. A single model, can not deal with all of these parameters. So practically, we choose a smaller and 'hopefully' representative system.

Combinatorial design is based on finding the fastest way to calculate a **molecular descriptor**, that can uniquely distinguish between structures and correlates with the FOM. The Quantitative Structure-Activity Relationship (QSAR) equation is our predictive model that correlates the experimental results to the molecular descriptor.

Ab initio calculations are assumed to be very expensive for screening enormous libraries. While this is true, we can benchmark the lower-level calculations for particular forms of catalysts and use the less exact methods that preserve the trends, in a qualitative/semi-quantitative manner, for the molecular descriptor. Also with the increase in the computational power, as it was discussed in previous chapters, the computational cost of QM-related methods are becoming less important and less problematic. Another venue is the realization of quantum computers and quantum computation. Quantum computers are ideal for doing parallel search. by utilizing

quantum mechanic's peculiarities, and are also perfect for solving quantum problems. Hence, in parallel with developing and relying on soft computational methods it is worth exploring ab initio and quantum mechanical descriptors in catalysis. This was the main incentive for using polarizability as a descriptor for quantum transport in the first section of this dissertation.

Soft computational methods suffer from the fact that the model may not comprise of all the crucial parameters. Currently, the way around this problem is to calculate as many descriptors as possible and by using "chemical intuition" and benefiting from statistical methods choose the most relevant ones. So it is obvious that these structure/function relationships are purely empirical and lack the foundation that an ab initio method will give us based on the energies and FMOs.[32]

Tolman proposed the first stereo-electronic 3D-descriptors for catalysis as early as seventies.[196, 195, 193, 194, 26] He correlated the basicity and acidity of phosphorus ligands to the CO stretching frequency of the coordinated to metal in Nickel complexes. He defined a measure called cone angle, θ, which was defind as the angle of a cylindrical cone that has an origin at 2.28 $\mathring{A}$ from the center of P in monodentate ligands. This concept was further developed and expanded to include asymmetrical ligands as well. While this is generally a useful measure to predict the structure, it has some limitations specially in the case of bulky ligands where a more stable structure can be formed by distortions from the perfect structures. Similar to the case we studied in last section(**1**).

An trade-off between ab initio method calculations and soft computation is using the Semi-empirical quantum mechanical methods. These methods are faster than first principle calculation and can be used to categorize and screen a mid-size (100 to 1000) libraries in a reasonable time. For instance, a two dimensional stereo-electronic map for characterizing phosphines and phosphates was developed in the early 2000s

based on semi-empirical methods.[37] More recent attempts have been made in using computational tools such as electrostatic potential calculations to categorize ligands and make predictions for organometallic compounds.[127, 187, 58] It is important to know the limitations of each of these methods. For example, while the electrostatic potential maps are very useful, they are not very representative and accurate for core electrostatic characteristics of a complex with bulky ligands. In case of bidentate phosphine ligands, there is a theoretical measure, called flexibility, based on the bite angle range of a ligand in an energy range close to the minimum is proposed. Unlike bite angle that is measurable, this is completely theoretical and can be used as how easily a ligand can accommodate different coordination state in a catalytic cycle by changing its bite angle without a huge energy penalty.

4.5.3 Preliminary Results: New Descriptor?

The machine-learning and linear regression modeling approaches have been successfully applied to material discovery for solar energy and even hydrogen evolution catalysts. But it the field of hydrogen evolution catalysts, most of these efforts are concentrated on heterogeneous hydrogen evolution catalysts.[41, 31, 89, 120, 83, 151, 70, 77, 186] Hence, We still have a big challenge facing us in designing a hydrogen evolution catalyst that is inexpensive, made from abundant metals that is fast and have a small overpotential and can act in an aqueous solution. It seems that we can successfully synthesis a complex that has a high turnover frequency or has a very small overpotential and not both simultaneously. Recently, we have found that in pentacoordinate Fe complexes, such as the ones discussed in this section, there is a correlation between the overpotential and the LUMO energy of these compounds (Correlation Coefficient = 0.98). We have also found that the same correlation (0.98) is obtained for the overpotential of these structures with their HOMO-LUMO gap.

This raises the question of whether we can use the LUMO and HOMO/LUMO gap as a design guideline for a rational and computationally-assisted design of iron-based hydrogen production catalysts.

I believe since, these compounds are structurally related, their reorganization energy in the course of electron transfer steps should be comparable. In this case, it has been shown that we can correlate the experimental reduction potential of organic compounds to their HOMO/LUMO energy. Further investigation is needed to make this deduction an statistically reliable result.[133, 134]

Developing quantum-mechanical based descriptors, ab initio or semi-empirical, are particularly helpful in understanding reaction mechanisms. Also, they usually have a definite physical meaning which make it easier to assess their limitations (for instant see A). But the main disadvantage of these methods is that quantum chemical calculations are done most often than not on the most stable structure. Also they are at zero temperature and zero pressure (it should be noted that these two conditions are addressed within the DFT framework). As a result, the quantum mechanical descriptors do not account for the entropic or temperature effects.

In short, although there are some obstacles that need to be addressed, the search for Quantum Mechanical, 3-dimensional molecular descriptors and synchronously benefiting from the improvements and progress in the statistical methods, can help reducing the time needed for material discovery.

REFERENCES

[1] Anthony W Addison, T Nageswara Rao, Jan Reedijk, Jacobus van Rijn, and Gerrit C. Verschoor. Synthesis, structure, and spectroscopic properties of copper(II) compounds containing nitrogen?sulphur donor ligands; the crystal and molecular structure of aqua[1,7-bis(N-methylbenzimidazol-2?-yl)-2,6-dithiaheptane]copper(II) perchlorate. *J. Chem. Soc. Dalt. Trans.*, (7):1349, 1984.

[2] G Allen, J G Watkinson, and K H Webb. An infra-red study of the association of benzoic acid in the vapour phase, and in dilute solution in non-polar solvents. *Spectrochim. Acta*, 22(5):807–814, 1966.

[3] T.S. Almeida, a.R. Van Wassen, R.B. VanDover, a.R. de Andrade, and H.D. Abruña. Combinatorial PtSnM (M = Fe, Ni, Ru and Pd) nanoparticle catalyst library toward ethanol electrooxidation. *J. Power Sources*, 284:623–630, 2015.

[4] Eugen S. Andreiadis, Pierre-André Jacques, Phong D. Tran, Adeline Leyris, Murielle Chavarot-Kerlidou, Bruno Jousselme, Muriel Matheron, Jacques Pécaut, Serge Palacin, Marc Fontecave, and Vincent Artero. Molecular engineering of a cobalt-based electrocatalytic nanomaterial for H2 evolution under fully aqueous conditions. *Nat. Chem.*, 5(1):48–53, oct 2012.

[5] Elodie Anxolabéhère-Mallart, Cyrille Costentin, Maxime Fournier, Sophie Nowak, Marc Robert, and Jean-Michel Savéant. Boron-Capped Tris(glyoximato) Cobalt Clathrochelate as a Precursor for the Electrodeposition of Nanoparticles Catalyzing H 2 Evolution in Water. *J. Am. Chem. Soc.*, 134(14):6104–6107, apr 2012.

[6] Sriharsha V Aradhya and Latha Venkataraman. Single-molecule junctions beyond electronic transport. *Nat. Nanotechnol.*, 8(6):399–410, 2013.

[7] Vincent Artero and Marc Fontecave. Solar fuels generation and molecular systems: is it homogeneous or heterogeneous catalysis? *Chem. Soc. Rev.*, 42(6):2338–2356, 2013.

[8] Kamal Asadi, Ilias Katsouras, Jan Harkema, Fatemeh Gholamrezaie, Edsger C.P. Smits, Fabio Biscarini, Paul W.M. Blom, and Dago M. de Leeuw. Organic field-effect transistors as a test-bed for molecular electronics: A combined study with large-area molecular junctions. *Org. Electron.*, 13(11):2502–2507, nov 2012.

[9] Philip a. Ash, Juan Liu, Nathan Coutard, Nina Heidary, Marius Horch, Ingvild Gudim, Thomas Simler, Ingo Zebger, Oliver Lenz, and Kylie a. Vincent. Electrochemical and Infrared Spectroscopic Studies Provide Insight into Reactions of the NiFe Regulatory Hydrogenase from Ralstonia eutropha with O 2 and CO. *J. Phys. Chem. B*, page 150710061549008, jul 2015.

[10] Arieh Aviram and M.A. Ratner. Molecular rectifiers. *Chem. Phys. Lett.*, 29(2):277, 1974.

[11] Philippe Y Ayala and H Bernhard Schlegel. A combined method for determining reaction paths, minima, and transition state geometries. *J. Chem. Phys.*, 107(2):375, 1997.

[12] Sukumaran Santhosh Babu, Seelam Prasanthkumar, and Ayyappanpillai Ajayaghosh. Self-assembled gelators for organic electronics. *Angew. Chemie - Int. Ed.*, 51(8):1766–1776, 2012.

[13] Andreas Bachmeier and Fraser Armstrong. Solar-driven proton and carbon dioxide reduction to fuels lessons from metalloenzymes. *Curr. Opin. Chem. Biol.*, 25:141–151, apr 2015.

[14] Giuliano Bandoli and Alessandro Dolmella. Ligating ability of 1,1-bis(diphenylphosphino)ferrocene: a structural survey (1994-1998). *Coord. Chem. Rev.*, 209(1):161–196, 2000.

[15] Giuliano Bandoli, Guendalina Trovo, Alessandro Dolmella, and Bruno Longato. cis-Bis(phosphine)platinum(II) complexes with pyrimidyl nucleobases. Synthesis, characterization, and crystal structures of cis-(1-methylthyminato-N3)(N,N-dimethylformamide-O)(1,1'-bis(diphenylphosphino)ferrocene)platinum(II) tetrafluoroborate-dichloromet. *Inorg. Chem.*, 31(1):45–51, jan 1992.

[16] Allen J Bard, Larry R Faulkner, and Others. Fundamentals and applications. *Electrochem. Methods, 2nd ed.; Wiley New York*, 2001.

[17] Bryan E. Barton and Thomas B. Rauchfuss. Hydride-containing models for the active site of the nickel-iron hydrogenases. *J. Am. Chem. Soc.*, 132(42):14877–14885, 2010.

[18] Axel D. Becke. Density-functional thermochemistry.III. The role of exact exchange. *J. Chem. Phys.*, 98(7):5648, 1993.

[19] Stephen Bell and Trevor J Dines. Advanced Chemistry Classroom and Laboratory Using Modern Electronic Structure Methods. *J. Chem. Educ.*, 84(8):1364–1370, 2007.

[20] Louise a Berben and Jonas C Peters. Hydrogen evolution by cobalt tetraiminecatalysts adsorbed on electrode surfaces. *Chem. Commun.*, 46(3):398–400, 2010.

[21] Justin P Bergfield, Henry M Heitzer, Colin Van Dyck, Tobin J Marks, and Mark a Ratner. Harnessing Quantum Interference in Molecular Dielectric Materials. *ACS Nano*, 9(6):6412–6418, jun 2015.

[22] Justin P. Bergfield and Mark a. Ratner. Forty years of molecular electronics: Non-equilibrium heat and charge transport at the nanoscale. *Phys. Status Solidi*, 250(11):2249–2266, 2013.

[23] Maryline Beyler, Salah Ezzaher, Michael Karnahl, Marie-Pierre Santoni, Reiner Lomoth, and Sascha Ott. Pentacoordinate iron complexes as functional models of the distal iron in [FeFe] hydrogenases. *Chem. Commun.*, 47(42):11662, 2011.

[24] Jochen Blumberger. Recent Advances in the Theory and Molecular Simulation of Biological Electron Transfer reactions. *Chem. Rev.*, 182:112–130, 2015.

[25] P. Bokes and R. W. Godby. Conductance and polarization in quantum junctions. *Phys. Rev. B - Condens. Matter Mater. Phys.*, 69(24):1–8, 2004.

[26] James R. Bolton, Keith G. Bircher, William Tumas, and Chadwick a. Tolman. Figures-of-merit for the technical development and application of advanced oxidation technologies for both electric- and solar-driven systems (IUPAC Technical Report). *Pure Appl. Chem.*, 73(4):627–637, 2001.

[27] SF Boys and F Bernardi. The calculation of small molecular interactions by the differences of separate total energies. Some procedures with reduced errors. *Mol. Phys.*, 8976(May 2012):553–566, 1970.

[28] Scott M. Brothers, Marcetta Y. Darensbourg, and Michael B. Hall. Modeling structures and vibrational frequencies for dinitrosyl iron complexes (DNICs) with density functional theory. *Inorg. Chem.*, 50:8532–8540, 2011.

[29] Phuc Tan Bui and Tomoaki Nishino. Electron transfer through coordination bond interaction between single molecules: conductance switching by a metal ion. *Phys. Chem. Chem. Phys.*, 16(12):5490–4, 2014.

[30] R. Morris Bullock, Aaron M. Appel, and Monte L. Helm. Production of hydrogen by electrocatalysis: making the HH bond by combining protons and hydrides. *Chem. Commun.*, 50(24):3125, 2014.

[31] Enrico Burello and Gadi Rothenberg. Topological mapping of bidentate ligands: A fast approach for screening homogeneous catalysts. *Adv. Synth. Catal.*, 347(15):1969–1977, 2005.

[32] Enrico Burello and Gadi Rothenberg. In silico design in homogeneous catalysis using descriptor modelling. *Int. J. Mol. Sci.*, 7(9):375–404, 2006.

[33] W. H. Butler, X.-G. Zhang, T. C. Schulthess, and J. M. MacLaren. Spin-dependent tunneling conductance of FeMgOFe sandwiches. *Phys. Rev. B*, 63(5):054416, 2001.

[34] Sigolane Canaguier, Loredana Vaccaro, Vincent Artero, Rainer Ostermann, Jacques PA, Martina J. Field, and Marc Fontecave. Cyclopentadienyl Ruthenium€“Nickel Catalysts for Biomimetic Hydrogen Evolution: Electrocatalytic Properties and Mechanistic DFT Studies. *Chem. - A Eur. J.*, 15(37):9350–9364, sep 2009.

[35] Shuai Chang, Jin He, Peiming Zhang, Brett Gyarfas, and Stuart Lindsay. Gap distance and interactions in a molecular tunnel junction. *J. Am. Chem. Soc.*, 133(36):14267–14269, 2011.

[36] Wenbo Chen, Haixing Li, Jonathan R. Widawsky, Chandrakumar Appayee, Latha Venkataraman, and Ronald Breslow. Aromaticity decreases single-molecule junction conductance. *J. Am. Chem. Soc.*, 136(3):918–920, jan 2014.

[37] Katharine D Cooney, Thomas R Cundari, Norris W Hoffman, Karl a Pittard, M Danielle Temple, and Yong Zhao. A priori assessment of the stereoelectronic profile of phosphines and phosphites. *J. Am. Chem. Soc.*, 125(14):4318–24, 2003.

[38] Benedetto Corain, Bruno Longato, Giancarlo Favero, David Ajò, Giuseppe Pilloni, Umberto Russo, and F.R. Kreissl. Heteropolymetallic complexes of 1,1-Bis(diphenylphosphino)ferrocene (dppf). III. Comparative physicochemical properties of (dppf)MCl2 (M = Co, Ni, Pd, Pt, Zn, Cd, Hg). *Inorganica Chim. Acta*, 157(2):259–266, 1989.

[39] Ali Coskun, Jason M. Spruell, Gokhan Barin, William R. Dichtel, Amar H. Flood, Youssry Y. Botros, and J. Fraser Stoddart. High hopes: can molecular electronics realise its potential? *Chem. Soc. Rev.*, 41(14):4827, 2012.

[40] Cyrille Costentin, Marc Robert, and Jean-Michel Savéant. Catalysis of the electrochemical reduction of carbon dioxide. *Chem. Soc. Rev.*, 42(6):2423–2436, 2013.

[41] N. Danilovic, Ram Subbaraman, D. Strmcnik, Kee-Chul Chang, A. P. Paulikas, V. R. Stamenkovic, and Nenad M. Markovic. Enhancing the Alkaline Hydrogen Evolution Reaction Activity through the Bifunctionality of Ni(OH) ¡sub¿2¡/sub¿ /Metal Catalysts. *Angew. Chemie*, 124(50):12663–12666, 2012.

[42] Donald J Darensbourg, Joseph H Reibenspies, Chia-Huei Lai, Way-Zen Lee, and Marcetta Y Darensbourg. Analysis of an Organometallic Iron Site model for the Heterodimetallic Unit of [NiFe]Hydrogenase. *J. Am. Chem. Soc.*, 119(33):7903–7904, 1997.

[43] Supriyo Datta. Nanoscale device modeling: the Greens function method. *Superlattices Microstruct.*, 28(4):253–278, 2000.

[44] Frank De Proft and Paul Geerlings. Conceptual and computational DFT in the study of aromaticity. *Chem. Rev.*, 101(5):1451–1464, 2001.

[45] David Delaere, Minh Tho Nguyen, and Luc G. Vanquickenborne. Influence of building block aromaticity in the determination of electronic properties of five-membered heterocyclic oligomers. *Phys. Chem. Chem. Phys.*, 4(9):1522–1530, 2002.

[46] Mickaël G. Delcey, Kristine Pierloot, Quan M. Phung, Steven Vancoillie, Roland Lindh, and Ulf Ryde. Accurate calculations of geometries and singlet-triplet energy differences for active-site models of [NiFe] hydrogenase. *Phys. Chem. Chem. Phys.*, 16(17):7927–38, 2014.

[47] Emma J. Dell, Brian Capozzi, Kateri H. Dubay, Timothy C. Berkelbach, Jose Ricardo Moreno, David R. Reichman, Latha Venkataraman, and Luis M. Campos. Impact of molecular symmetry on single-molecule conductance. *J. Am. Chem. Soc.*, 135(32):11724–11727, 2013.

[48] F. J. Devlin, J. W. Finley, P. J. Stephens, and M. J. Frisch. Ab Initio Calculation of Vibrational Absorption and Circular Dichroism Spectra Using Density Functional Force Fields: A Comparison of Local, Nonlocal, and Hybrid Density Functionals. *J. Phys. Chem.*, 99(46):16883–16902, 1995.

[49] Massimiliano Di Ventra and Yuriy V. Pershin. Spin physics: DNA spintronics sees the light. *Nat. Nanotechnol.*, 6(4):198–199, 2011.

[50] Pingwu Du and Richard Eisenberg. Catalysts made of earth-abundant elements (Co, Ni, Fe) for water splitting: Recent progress and future challenges. *Energy Environ. Sci.*, 5(3):6012, 2012.

[51] M. Rakowski Dubois and Daniel L. Dubois. Development of molecular electrocatalysts for CO2 reduction and H2 production/oxidation. *Acc. Chem. Res.*, 42(12):1974–1982, 2009.

[52] E. Dujardin and S. Mann. Bio-inspired materials chemistry. *Adv. Mater.*, 14(11):775–788, 2002.

[53] M Eckert and G Zundel. Proton Polarizability, Dipole-Moment, and Proton Transitions of an Ah...B Reversible a-...H+B Proton-Transfer Hydrogen-Bond As a Function of an External Electrical-Field - an Abinitio Scf Treatment. *J. Phys. Chem.*, 91(20):5170–5177, 1986.

[54] Mc Etter. Hydrogen bonds as design elements in organic chemistry. *J. Phys. Chem.*, (8):4601–4610, 1991.

[55] F. Evers, F. Weigend, and M. Koentopp. Conductance of molecular wires and transport calculations based on density-functional theory. *Phys. Rev. B*, 69(23):1–9, 2004.

[56] Greg a N Felton, Charles a. Mebi, Benjamin J. Petro, Aaron K. Vannucci, Dennis H. Evans, Richard S. Glass, and Dennis L. Lichtenberger. Review of electrochemical studies of complexes containing the Fe2S2 core characteristic of [FeFe]-hydrogenases including catalysis by these complexes of the reduction of acids to form dihydrogen. *J. Organomet. Chem.*, 694(17):2681–2699, 2009.

[57] David K Ferry and Stephen Marshall Goodnick. *Transport in nanostructures*. Number 6. Cambridge university press, 1997.

[58] Natalie Fey, Jeremy N Harvey, Guy C. Lloyd-Jones, Paul Murray, a Guy Orpen, Robert Osborne, and Mark Purdie. Computational Descriptors for Chelating P,P- and P,N-Donor Ligands 1. *Organometallics*, 27(7):1372–1383, apr 2008.

[59] Stephen R Forrest. The path to ubiquitous and low-cost organic electronic appliances on plastic. *Nature*, 428(6986):911–918, 2004.

[60] Michelle M Francl, William J Pietro, Warren J Hehre, J Stephen Binkley, Mark S Gordon, Douglas J DeFrees, and John a Pople. Self-consistent molecular orbital methods. XXIII. A polarization-type basis set for second-row elements. *J. Chem. Phys.*, 77(7):3654–3665, 1982.

[61] MJEA Frisch, G W Trucks, Hs B Schlegel, G E Scuseria, M A Robb, J R Cheeseman, G Scalmani, V Barone, B Mennucci, G A Petersson, and Others. Gaussian 09. *Inc., Wallingford, CT*, 200, 2009.

[62] Lu Gan, Thomas L. Groy, Pilarisetty Tarakeshwar, Shobeir K. S. Mazinani, Jason Shearer, Vladimiro Mujica, and Anne K. Jones. A Nickel Phosphine Complex as a Fast and Efficient Hydrogen Production Catalyst. *J. Am. Chem. Soc.*, 137(3):1109–1115, jan 2015.

[63] James M Gardner, Maryline Beyler, Michael Karnahl, Stefanie Tschierlei, Sascha Ott, and Leif Hammarström. Light-driven electron transfer between a photosensitizer and a proton-reducing catalyst co-adsorbed to NiO. *J. Am. Chem. Soc.*, 134(47):19322–5, 2012.

[64] Wingfield V Glassey and Roald Hoffmann. A comparative study of Hamilton and overlap population methods\rfor the analysis of chemical bonding. *J. Chem. Phys.*, 113(5):1698–1704, 2000.

[65] Frédéric Gloaguen and Thomas B. Rauchfuss. Small molecule mimics of hydrogenases: hydrides and redox. *Chem. Soc. Rev.*, 38(1):100–108, 2009.

[66] Carlos Gonzalez, Vladimiro Mujica, and Mark A. Ratner. Modeling the Electrostatic Potential Spatial Profile of Molecular Junctions. *Ann. N. Y. Acad. Sci.*, 960(1):163–176, 2006.

[67] S I Gorelsky. AOMix Program rev. 6.04 http://www. sg-chem. net, Gorelsky, SI; Lever, ABP J. *Organomet. Chem*, 635:187–196, 2001.

[68] S. I. Gorelsky and a. B P Lever. Electronic structure and spectra of ruthenium diimine complexes by density functional theory and INDO/S. Comparison of the two methods. *J. Organomet. Chem.*, 635(1-2):187–196, 2001.

[69] H B Gray and J R Winkler. Electron transfer in proteins. *Annu. Rev. Biochem.*, 65:537–561, 1996.

[70] Jeff Greeley, Thomas F. Jaramillo, Jacob Bonde, Ib Chorkendorff, and Jens K. Nørskov. Computational high-throughput screening of electrocatalytic materials for hydrogen evolution. *Nat. Mater.*, 5(11):909–913, 2006.

[71] Brandon L Greene, Chang-Hao Wu, Patrick M McTernan, Michael W W Adams, and R Brian Dyer. Proton-Coupled Electron Transfer Dynamics in the Catalytic Mechanism of a [NiFe]-Hydrogenase. *J. Am. Chem. Soc.*, 137(13):4558–4566, apr 2015.

[72] Jing GuYan and Steve Y Bollinger. [NiFe] dithiolene diphosphine complex for hydrogen gas activation: a Theoretic Insight. feb 2015.

[73] James R. Heath. Molecular Electronics. *Annu. Rev. Mater. Res.*, 39(1):1–23, 2009.

[74] Tillmann Heinisch and Thomas R Ward. Latest Developments in Metalloenzyme Design and Repurposing. *Eur. J. Inorg. Chem.*, pages n/a—-n/a, 2015.

[75] Henry M Heitzer, Tobin J Marks, and Mark a Ratner. Maximizing the Dielectric Response of Molecular Thin Films via Quantum Chemical Design. *ACS Nano*, 8(12):12587–12600, dec 2014.

[76] Henry M Heitzer, Tobin J Marks, and Mark a Ratner. Molecular Donor-Bridge-Acceptor Strategies for High-Capacitance Organic Dielectric Materials. *J. Am. Chem. Soc.*, 137(22):7189–7196, jun 2015.

[77] Berit Hinnemann, Poul Georg Moses, Jacob Bonde, Kristina P Jorgensen, Jane H Nielsen, Sebastian Horch, Ib Chorkendorff, and Jens K N{\o}rskov. Biomimetic Hydrogen Evolution: \ce{MoS2} Nanoparticles as Catalyst for Hydrogen Evolution. *J. Am. Chem. Soc.*, 127(15):5308–5309, 2005.

[78] M. I. Hoffert. Advanced Technology Paths to Global Climate Stability: Energy for a Greenhouse Planet. *Science (80-.).*, 298(5595):981–987, nov 2002.

[79] Roald Hoffman. Solids and surfaces: a chemist's view of bonding in extended structures. Technical report, DTIC Document, 1988.

[80] R E Holmlin, R F Ismagilov, R Haag, V Mujica, M a Ratner, M a Rampi, and G M Whitesides. Correlating electron transport and molecular structure in organic thin films. *Angew. Chemie-International Ed.*, 40(12):2316–+, 2001.

[81] Marius Horch, Janna Schoknecht, Maria Andrea Mroginski, Oliver Lenz, Peter Hildebrandt, and Ingo Zebger. Resonance Raman Spectroscopy on [NiFe] Hydrogenase Provides Structural Insights into Catalytic Intermediates and Reactions. *J. Am. Chem. Soc.*, 136(28):9870–9873, jul 2014.

[82] Sachio Horiuchi and Yoshinori Tokura. Organic ferroelectrics. *Nat. Mater.*, 7(5):357–366, 2008.

[83] Yidong Hou, Billie L. Abrams, Peter C. K. Vesborg, Mårten E. Björketun, Konrad Herbst, Lone Bech, Alessandro M. Setti, Christian D. Damsgaard, Thomas Pedersen, Ole Hansen, Jan Rossmeisl, Søren Dahl, Jens K. Nørskov, and Ib Chorkendorff. Bioinspired molecular co-catalysts bonded to a silicon photocathode for solar hydrogen evolution. *Nat. Mater.*, 10(6):434–438, 2011.

[84] R a Houghten, C Pinilla, S E Blondelle, J R Appel, C T Dooley, and J H Cuervo. Generation and use of synthetic peptide combinatorial libraries for basic research and drug discovery. *Nature*, 354(6348):84–86, 1991.

[85] Hua-Fen Hsu, Stephen A Koch, Codrina V Popescu, and Eckard. Muenck. Chemistry of iron thiolate complexes with CN- and CO. Models for the [Fe(CO)(CN)2] structural unit in Ni-Fe hydrogenase enzymes. *J. Am. Chem. Soc.*, 119(35):8371–8372, 1997.

[86] Cancan Huang, Alexander V Rudnev, Wenjing Hong, and Thomas Wandlowski. Break junction under electrochemical gating: testbed for single-molecule electronics. *Chem. Soc. Rev.*, 44:889–901, 2015.

[87] Camille Imbert, Hrant P Hratchian, Mauricio Lanznaster, Mary Jane Heeg, Lew M Hryhorczuk, Bruce R McGarvey, H Bernhard Schlegel, and Claudio N Verani. Influence of ligand rigidity and ring substitution on the structural and electronic behavior of trivalent iron and gallium complexes with asymmetric tridentate ligands. *Inorg. Chem.*, 44(21):7414–22, 2005.

[88] Nicholas E. Jackson, Brett M. Savoie, Lin X. Chen, and Mark a. Ratner. A Simple Index for Characterizing Charge Transport in Molecular Materials. *J. Phys. Chem. Lett.*, 1021(1):1018–1021, mar 2015.

[89] Elham Zeini Jahromi and Jürgen Gailer. Probing bioinorganic chemistry processes in the bloodstream to gain new insights into the origin of human diseases. *Dalton Trans.*, (2):329–336, 2010.

[90] R. Janoschek, E. G. Weidemann, H. Pfeiffer, and G. Zundel. Extremely high polarizability of hydrogen bonds. *J. Am. Chem. Soc.*, 94(7):2387–2396, apr 1972.

[91] George A Jeffrey and George A Jeffrey. *An introduction to hydrogen bonding*, volume 12. Oxford university press New York, 1997.

[92] Javier Junquera, Óscar Paz, Daniel Sánchez-Portal, and Emilio Artacho. Numerical atomic orbitals for linear-scaling calculations. *Phys. Rev. B*, 64(23):235111, 2001.

[93] Sandeep Kaur-Ghumaan, Lennart Schwartz, Reiner Lomoth, Matthias Stein, and Sascha Ott. Catalytic hydrogen evolution from mononuclear iron(II) carbonyl complexes as minimal functional models of the [FeFe] hydrogenase active site. *Angew. Chemie Int. Ed.*, 49(43):8033–8036, 2010.

[94] Taeyoung Kim, Hyeongkeun Kim, Soon Woo Kwon, Yena Kim, Won Kyu Park, Dae Ho Yoon, a. Rang Jang, Hyeon Suk Shin, Kwang S. Suh, and Woo Seok Yang. Large-scale graphene micropatterns via self-assembly-mediated process for flexible device application. *Nano Lett.*, 12(2):743–748, 2012.

[95] Hiroaki Kotani, Ryo Hanazaki, Kei Ohkubo, Yusuke Yamada, and Shunichi Fukuzumi. Size- and Shape-Dependent Activity of Metal Nanoparticles as Hydrogen-Evolution Catalysts: Mechanistic Insights into Photocatalytic Hydrogen Evolution. *Chem. - A Eur. J.*, 17(9):2777–2785, feb 2011.

[96] Predrag Krsti, Brian Ashcroft, and Stuart Lindsay. Physical model for recognition tunneling. *Nanotechnology*, 26(8):84001, 2015.

[97] P S Krstić, X-G Zhang, and W H Butler. Generalized conductance formula for the multiband tight-binding model. *Phys. Rev. B*, 66(20):205319, 2002.

[98] Leif Lafferentz, Francisco Ample, Hao Yu, Stefan Hecht, Christian Joachim, and Leonhard Grill. Conductance of a single conjugated polymer as a continuous function of its length. *Science*, 323(5918):1193–1197, 2009.

[99] Chia-huei Lai, Way-zen Lee, Matthew L Miller, Joseph H Reibenspies, Donald J. Darensbourg, and Marcetta Y Darensbourg. Responses of the Fe(CN) 2 (CO) Unit to Electronic Changes as Related to Its Role in [NiFe]Hydrogenase. *J. Am. Chem. Soc.*, 120(39):10103–10114, oct 1998.

[100] R. Landauer. Spatial variation of currents and fields due to localized scatterers in metallic conduction. *IBM J. Res. Dev.*, 44(1.2):251–259, 2000.

[101] Rolf Landauer. Electrical resistance of disordered one-dimensional lattices. *Philos. Mag.*, 21(172):863–867, 1970.

[102] Otto Laporte and William F. Meggers. Some Rules of Spectral Structure. *J. Opt. Soc. Am.*, 11:459, 1925.

[103] Chengteh Lee, Weitao Yang, and Robert G. Parr. Development of the Colle-Salvetti correlation-energy formula into a functional of the electron density. *Phys. Rev. B*, 37(2):785–789, 1988.

[104] Chien-Ming Lee, Chien-Hong Chen, Shyue-Chu Ke, Gene-Hsiang Lee, and Wen-Feng Liaw. Mononuclear nickel(III) and nickel(II) thiolate complexes with intramolecular S-H proton interacting with both sulfur and nickel: relevance to the [NiFe]/[NiFeSe] hydrogenases. *J. Am. Chem. Soc.*, 126(27):8406–12, 2004.

[105] Jean-Marie Lehn. Perspectives in Chemistry-Steps towards Complex Matter. *Angew. Chemie Int. Ed.*, 52(10):2836–2850, 2013.

[106] Richard A Lerner, Rajesh K Grover, Hongkai Zhang, Jia Xie, Kyung Ho Han, Yingjie Peng, and Kyungmoo Yea. Antibodies from combinatorial libraries use functional receptor pleiotropism to regulate cell fates. *Q. Rev. Biophys.*, pages 1–6, 2015.

[107] L. P. Lévy and W. L. Williams. Experimental Test of Laporte's Rule In Atomic Hydrogen. *Phys. Rev. Lett.*, 48(9):607–610, mar 1982.

[108] Yuning Li, Prashant Sonar, Samarendra P. Singh, Wenjin Zeng, and Mui Siang Soh. 3,6-Di(furan-2-yl)pyrrolo[3,4-c]pyrrole-1,4(2H,5H)-dione and bithiophene copolymer with rather disordered chain orientation showing high mobility in organic thin film transistors. *J. Mater. Chem.*, 21(29):10829, 2011.

[109] W F Liaw, N H Lee, C H Chen, C M Lee, G H Lee, and S M Peng. Dinuclear and mononuclear iron(II)-thiolate complexes with mixed CO/CN- ligands: Synthetic advances for iron sites of Fe -only hydrogenases. *J. Am. Chem. Soc.*, 122(3):488–494, 2000.

[110] Stuart Lindsay. Biochemistry and semiconductor electronics-the next big hit for silicon? *J. Phys. Condens. Matter*, 24(16):164201, apr 2012.

[111] Tianbiao Liu, Daniel L. DuBois, and R. Morris Bullock. An iron complex with pendent amines as a molecular electrocatalyst for oxidation of hydrogen. *Nat. Chem.*, 5(3):228–233, 2013.

[112] Tianbiao Liu, Bin Li, Codrina V. Popescu, Andrey Bilko, Lisa M. Pérez, Michael B. Hall, and Marcetta Y. Darensbourg. Analysis of a Pentacoordinate Iron Dicarbonyl as Synthetic Analogue of the Hmd or Mono-Iron Hydrogenase Active Site. *Chem. - A Eur. J.*, 16(10):3083–3089, mar 2010.

[113] Yu-Chiao Liu, Kai-Ti Chu, Ruei-Lin Jhang, Gene-Hsiang Lee, and Ming-Hsi Chiang. [FeFe] hydrogenase active site modeling: a key intermediate bearing a thiolate proton and Fe hydride. *Chem. Commun.*, 49(42):4743–4745, 2013.

[114] Bruno Longato, Giuseppe Pilloni, Giovanni Valle, and Benedetto Corain. Synthesis and solvolytic behavior of cis-[1,1'-bis(diphenylphosphino)ferrocene]platinum(II) and -palladium(II) complexes. X-ray structure of bis-(.mu.-hydroxy)bis[1,1'-bis(diphenylphosphino)ferrocene]diplatinum(II) tetrafluoroborate. *Inorg. Chem.*, 27(5):956–958, 1988.

[115] Emanuel Lörtscher. Wiring molecules into circuits. *Nat. Nanotechnol.*, 8(6):381–4, 2013.

[116] Oana R. Luca, James D. Blakemore, Steven J. Konezny, Jeremy M. Praetorius, Timothy J. Schmeier, Glendon B. Hunsinger, Victor S. Batista, Gary W. Brudvig, Nilay Hazari, and Robert H. Crabtree. Organometallic Ni Pincer Complexes for the Electrocatalytic Production of Hydrogen. *Inorg. Chem.*, 51(16):8704–8709, aug 2012.

[117] Oana R. Luca, Steven J. Konezny, James D. Blakemore, Dominic M. Colosi, Shubhro Saha, Gary W. Brudvig, Victor S. Batista, and Robert H. Crabtree. A tridentate Ni pincer for aqueous electrocatalytic hydrogen production. *New J. Chem.*, 36(5):1149, 2012.

[118] J. M. MacLaren, W. H. Butler, and X.-G. Zhang. Spin-dependent tunneling in epitaxial systems: Band dependence of conductance. *J. Appl. Phys.*, 83(11):6521, 1998.

[119] Christopher Madden, Michael D Vaughn, Ismael Díez-Pérez, Katherine a Brown, Paul W King, Devens Gust, Ana L. Moore, and Thomas a Moore. Catalytic Turnover of [FeFe]-Hydrogenase Based on Single-Molecule Imaging. *J. Am. Chem. Soc.*, 134(3):1577–1582, jan 2012.

[120] Ana G Maldonado and Gadi Rothenberg. Predictive modeling in homogeneous catalysis: a tutorial. *Chem. Soc. Rev.*, 39(6):1891–1902, 2010.

[121] R a Marcus. Electrostatic Free Energy and Other Properties of States Having Nonequilibrium Polarization. I. *J. Chem. Phys.*, 24(5):979, 1956.

[122] R. A. Marcus. On the Theory of Oxidation-Reduction Reactions Involving Electron Transfer. I. *J. Chem. Phys.*, 24(5):966, 1956.

[123] R. a. Marcus. On the Theory of Oxidation-Reduction Reactions Involving Electron Transfer. I. *J. Chem. Phys.*, 24(5):966, 1956.

[124] Rudolph a. Marcus. Electron Transfer Reactions in Chemistry: Theory and Experiment (Nobel Lecture). *Angew. Chemie Int. Ed.*, 32(8):1111–1121, 1993.

[125] Aleksandr V. Marenich, Christopher J. Cramer, and Donald G. Truhlar. Reduced and quenched polarizabilities of interior atoms in molecules. *Chem. Sci.*, 4(6):2349, 2013.

[126] Tal Z Markus, Shirley S Daube, and Ron Naaman. Cooperative effect in the electronic properties of human telomere sequence. *J. Phys. Chem. B*, 114(43):13897–903, 2010.

[127] Jomon Mathew, Tinto Thomas, and Cherumuttathu H Suresh. Quantitative assessment of the stereoelectronic profile of phosphine ligands. *Inorg. Chem.*, 46(25):10800–9, 2007.

[128] W R McNamara, Z Han, C J Yin, W W Brennessel, P L Holland, and R Eisenberg. Cobalt-dithiolene complexes for the photocatalytic and electrocatalytic reduction of protons in aqueous solutions. *Proc Natl Acad Sci U S A*, 109(39):15594–15599, 2012.

[129] William R Mcnamara, Zhiji Han, Paul J Alperin, William W Brennessel, Patrick L Holland, and Richard Eisenberg. A Cobalt Dithiolene Complex for the Photocatalytic and. *J. Am. Chem. Soc.*, 133(Figure 2):15368–15371, 2011.

[130] Jackson D. Megiatto Jr, Dalvin D. Méndez-Hernández, Marely E Tejeda-Ferrari, Anne-Lucie Teillout, Manuel J. Llansola-Portolés, Gerdenis Kodis, Oleg G Poluektov, Tijana Rajh, Vladimiro Mujica, Thomas L Groy, Devens Gust, Thomas A. Moore, and Ana L Moore. A bioinspired redox relay that mimics radical interactions of the Tyr-His pairs of photosystem II. *Nat. Chem.*, 6(5):423–428, feb 2014.

[131] Reza Vatan Meidanshahi, Shobeir K. S. Mazinani, Vladimiro Mujica, and Pilarisetty Tarakeshwar. Electronic transport across hydrogen bonds in organic electronics. *Int. J. Nanotechnol.*, 12, 2015.

[132] Yigal Meir and N.S. Wingreen. Landauer formula for the current through an interacting electron region. *Phys. Rev. Lett.*, 68(16):2512–2515, 1992.

[133] Dalvin Méndez-Hernández, Jason. Gillmore, Luis Montano, Devens Gust, Thomas Moore, Ana Moore, and V. Mujica. Building and testing correlations for the estimation of one-electron reduction potentials of a diverse set of organic molecules. *J. Phys. Org. Chem.*, (January):n/a–n/a, 2015.

[134] Dalvin D Méndez-Hernández, Pilarisetty Tarakeshwar, Devens Gust, Thomas A. Moore, Ana L Moore, and Vladimiro Mujica. Simple and accurate correlation of experimental redox potentials and DFT-calculated HOMO/LUMO energies of polycyclic aromatic hydrocarbons. *J. Mol. Model.*, 19(7):2845–2848, 2013.

[135] Robert M. Metzger. Unimolecular Electronics. *Chem. Rev.*, page 150507090420005, 2015.

[136] Robert M. Metzger, Bo Chen, Ulf Höpfner, M. V. Lakshmikantham, Dominique Vuillaume, Tsuyoshi Kawai, Xiangli Wu, Hiroaki Tachibana, Terry V. Hughes, Hiromi Sakurai, Jeffrey W. Baldwin, Christina Hosch, Michael P. Cava, Ludwig Brehmer, and Geoffrey J. Ashwell. Unimolecular Electrical Rectification in Hexadecylquinolinium Tricyanoquinodimethanide. *J. Am. Chem. Soc.*, 119(43):10455–10466, oct 1997.

[137] Prakash Chandra Mondal, Claudio Fontanesi, David H Waldeck, and Ron Naaman. Field and Chirality Effects on Electrochemical Charge Transfer Rates: Spin Dependent Electrochemistry. *ACS Nano*, 9(3):3377–3384, mar 2015.

[138] Hendrik J Monkhorst and James D Pack. Special points for Brillouin-zone integrations. *Phys. Rev. B*, 13(12):5188, 1976.

[139] Amanda M. Moore, Sina Yeganeh, Yuxing Yao, Shelley a. Claridge, James M. Tour, Mark a. Ratner, and Paul S. Weiss. Polarizabilities of adsorbed and assembled molecules: Measuring the conductance through buried contacts. *ACS Nano*, 4(12):7630–7636, 2010.

[140] V. Mujica, M. Kemp, and M. a. Ratner. Electron conduction in molecular wires. I. A scattering formalism. *J. Chem. Phys.*, 101(8):6849, 1994.

[141] Vladimiro Mujica, Adrian E. Roitberg, and Mark Ratner. Molecular wire conductance: Electrostatic potential spatial profile. *J. Chem. Phys.*, 112(15):6834–6839, 2000.

[142] Ron Naaman and Zeev Vager. C ooperative Electronic and Magnetic Properties of Self-Assembled Monolayers. *MRS Bull.*, 35(June), 2010.

[143] Amir Natan, Natalia Kuritz, and Leeor Kronik. Polarizability, Susceptibility, and Dielectric Constant of Nanometer-Scale Molecular Films: A Microscopic View. *Adv. Funct. Mater.*, 20(13):2077–2084, may 2010.

[144] Frank Neese. The ORCA program system. *Wiley Interdiscip. Rev. Comput. Mol. Sci.*, 2(1):73–78, jan 2012.

[145] D. H. Nguyen, H. F. Hsu, M. Millar, S. A. Koch, C. Achim, E. L. Bominaar, and E. Münck. Nickel (II) Thiolate Complex with Carbon Monoxide and Its Fe (II) Analog: Synthetic Models for CO Adducts of Nickel- Iron-Containing Enzymes. *J. Am. Chem. Soc.*, 118(37):8963–8964, 1996.

[146] Joonas J. Nieminen, Imren Hatay, PeiYu Ge, Manuel A. Méndez, Lasse Murtomäki, and Hubert H. Girault. Hydrogen evolution catalyzed by electrodeposited nanoparticles at the liquid/liquid interface. *Chem. Commun.*, 47(19):5548, 2011.

[147] Kazuki Niimi, Hiroki Mori, Eigo Miyazaki, Itaru Osaka, Hayato Kakizoe, Kazuo Takimiya, and Chihaya Adachi. [2,2]Bi[naphtho[2,3-b]furanyl]: a versatile organic semiconductor with a furan-furan junction. *Chem. Commun.*, 48(47):5892, 2012.

[148] T Nishino, N Hayashi, and P T Bui. Direct measurement of electron transfer through a hydrogen bond between single molecules. *J Am Chem Soc*, 135(12):4592–4595, 2013.

[149] Abraham Nitzan. *Chemical Dynamics in Condensed Phases*. Oxford University Press, New York, 2006.

[150] Abraham Nitzan and Mark a Ratner. Electron transport in molecular wire junctions. *Science*, 300(5624):1384–9, may 2003.

[151] J. K. Nørskov, T. Bligaard, J. Rossmeisl, and C. H. Christensen. Towards the computational design of solid catalysts. *Nat. Chem.*, 1(1):37–46, 2009.

[152] Andreas Orthaber, Michael Karnahl, Stefanie Tschierlei, Daniel Streich, Matthias Stein, and Sascha Ott. Coordination and conformational isomers in mononuclear iron complexes with pertinence to the [FeFe] hydrogenase active site. *Dalton Trans.*, 43(11):4537–49, 2014.

[153] Bala Krishna Pathem, Shelley a Claridge, Yue Bing Zheng, and Paul S Weiss. Molecular switches and motors on surfaces. *Annu. Rev. Phys. Chem.*, 64:605–30, 2013.

[154] a. R. Pease, J. O. Jeppesen, J. F. Stoddart, Y. Luo, C. P. Collier, and J. R. Heath. Switching devices based on interlocked molecules. *Acc. Chem. Res.*, 34(6):433–444, 2001.

[155] Giuseppe Pilloni, Bruno Longato, and Benedetto Corain. Heteropolymetallic complexes of 1,1-bis(diphenylphosphino)ferrocene (dppf). *J. Organomet. Chem.*, 420(1):57–65, nov 1991.

[156] Isabella Pötzelberger, Andrei Ionut Mardare, and Achim Walter Hassel. Screening of catalytic effects on copper-zinc thin film combinatorial libraries for formaldehyde oxidation. *Phys. Status Solidi*, 212(6):1184–1190, 2015.

[157] H Production, M Rakowski Dubois, and Daniel L Dubois. A Synthetic Nickel Electrocatalyst. *Science (80-.).*, (August):863–866, 2011.

[158] S Y Quek, H J Choi, S G Louie, and J B Neaton. Thermopower of Amine - Gold-Linked, Aromatic Molecular Junctions from First Principles. *ACS Nano*, 5(1):551–557, 2011.

[159] Su Ying Quek and Khoong Hong Khoo. Predictive DFT-Based Approaches to Charge and Spin Transport in Single-Molecule Junctions and Two-Dimensional Materials: Successes and Challenges. *Acc. Chem. Res.*, 47:3250–3257, 2014.

[160] Su Ying Quek, Latha Venkataraman, Hyoung Joon Choi, Steven G. Louie, Mark S. Hybertsen, and J. B. Neaton. Amine - Gold linked single-molecule circuits: Experiment and theory. *Nano Lett.*, 7(11):3477–3482, 2007.

[161] M Rakowski DuBois and Daniel L DuBois. The roles of the first and second coordination spheres in the design of molecular catalysts for H2 production and oxidation. *Chem. Soc. Rev.*, 38(1):62–72, 2009.

[162] Vitaly A. Rassolov, John A. Pople, Mark A. Ratner, and Theresa L. Windus. 6-31G basis set for atoms K through Zn. *J. Chem. Phys.*, 109(4):1223, 1998.

[163] Mark Ratner. A brief history of molecular electronics. *Nat. Nanotechnol.*, 8(6):378–381, jun 2013.

[164] T. B. Rauchfuss, S. M. Contakes, S. C N Hsu, M. a. Reynolds, and S. R. Wilson. The influence of cyanide on the carbonylation of Iron(II): Synthesis of Fe-SR-CN-CO centers related to the hydrogenase active sites. *J. Am. Chem. Soc.*, 123(28):6933–6934, 2001.

[165] Kallol Ray, Ameerunisha Begum, Thomas Weyhermüller, Stergios Piligkos, Joris Van Slageren, Frank Neese, and Karl Wieghardt. The electronic structure of the isoelectronic, square-planar complexes [FeII(L)2]2- and [CoIII(L Bu)2]- (L2- and (L Bu)2- = benzene-1,2-dithiolates): An experimental and density functional theoretical study. *J. Am. Chem. Soc.*, 127(12):4403–4415, 2005.

[166] Kallol Ray, Eckhard Bill, Thomas Weyhermüller, and Karl Wieghardt. Redox-Noninnocence of the S,S-Coordinated Ligands in Bis(benzene-1,2-dithiolato)iron Complexes. *J. Am. Chem. Soc.*, 127(15):5641–5654, apr 2005.

[167] Kallol Ray, Taras Petrenko, Karl Wieghardt, and Frank Neese. Joint spectroscopic and theoretical investigations of transition metal complexes involving non-innocent ligands. *Dalt. Trans.*, (16):1552–66, 2007.

[168] Kallol Ray, Thomas Weyhermüller, Anton Goossens, Menno W. J. Crajé, and Karl Wieghardt. Do S,S-Coordinated o -Dithiobenzosemiquinonate(1) Radicals Exist in Coordination Compounds? The [Au III (1,2-C 6 H 4 S 2) 2] 1 - /0 Couple. *Inorg. Chem.*, 42(13):4082–4087, jun 2003.

[169] Kallol Ray, Thomas Weyhermüller, Frank Neese, and Karl Wieghardt. Electronic Structure of Square Planar Bis(benzene-1,2-dithiolato)metal Complexes [M(L)2] z (z = 2-, 1-, 0; M = Ni, Pd, Pt, Cu, Au. *Inorg. Chem.*, 44(15):5345–5360, jul 2005.

[170] Tour Reed, M. a.;C., Zhou;C. J., Muller;T. P., Burgin;J. M. Conductance of a Molecular Junction. *Science (80-.).*, 278(5336):252–254, oct 1997.

[171] Michael Roemelt, Dimitrios Maganas, Serena DeBeer, and Frank Neese. A combined DFT and restricted open-shell configuration interaction method including spin-orbit coupling: application to transition metal L-edge X-ray absorption spectroscopy. *J. Chem. Phys.*, 138(2013):204101, 2013.

[172] J Roncali. Conjugated Poly(thiophenes) - Synthesis, Functionalization, and Applications. *Chem. Rev.*, 92(4):711–738, 1992.

[173] Jean Roncali, Philippe Leriche, and Philippe Blanchard. Molecular materials for organic photovoltaics: Small is beautiful. *Adv. Mater.*, 26(23):3821–3838, 2014.

[174] Michael J Rose, Harry B Gray, and Jay R Winkler. Hydrogen Generation Catalyzed by Fluorinated Diglyoxime-Iron Complexes at Low Overpotentials. *J. Am. Chem. Soc.*, 134(20):8310–8313, may 2012.

[175] Souvik Roy, Shobeir K S Mazinani, Thomas L Groy, Lu Gan, Pilarisetty Tarakeshwar, Vladimiro Mujica, and Anne K Jones. Catalytic Hydrogen Evolution by Fe(II) Carbonyls Featuring a Dithiolate and a Chelating Phosphine. *Inorg. Chem.*, 53(17):8919–8929, sep 2014.

[176] Brett M Savoie, Kevin L Kohlstedt, Nicholas E Jackson, Lin X Chen, Monica Olvera de la Cruz, George C Schatz, Tobin J Marks, and Mark a Ratner. Mesoscale molecular network formation in amorphous organic materials. *Proc. Natl. Acad. Sci. U. S. A.*, 111(28):10055–10060, 2014.

[177] Markus C. Scharber, David Mühlbacher, Markus Koppe, Patrick Denk, Christoph Waldauf, Alan J. Heeger, and Christoph J. Brabec. Design rules for donors in bulk-heterojunction solar cells - Towards 10 % energy-conversion efficiency. *Adv. Mater.*, 18(6):789–794, 2006.

[178] D Sellmann, U Kleinekleffmann, L Zapf, G Huttner, and L Zsolnai. Transition-Metal Complexes With Sulfur Ligands. SYNTHESIS AND STRUCTURE OF THE BENZENEDITHIOLATO-IRON COMPLEXES [ASPH4] 2 [FE (S2C6H4) 2] AND [FE (S2C6H4)(PME3) 3]. *J. Organomet. Chem.*, 263(3):321–331, 1984.

[179] S. Shima, O. Pilak, S. Vogt, M. Schick, M. S. Stagni, W. Meyer-Klaucke, E. Warkentin, R. K. Thauer, and U. Ermler. The Crystal Structure of [Fe]-Hydrogenase Reveals the Geometry of the Active Site. *Science (80-.).*, 321(5888):572–575, jul 2008.

[180] Per E M Siegbahn, Jesse W. Tye, and Michael B. Hall. Computational studies of [NiFe] and [FeFe] hydrogenases. *Chem. Rev.*, 107(10):4414–4435, 2007.

[181] John G. Simmons. Generalized Formula for the Electric Tunnel Effect between Similar Electrodes Separated by a Thin Insulating Film. *J. Appl. Phys.*, 34(6):1793, 1963.

[182] Krzysztof Slowinski, Richard V. Chamberlain, Cary J. Miller, and Marcin Majda. Through-bond and chain-to-chain coupling. Two pathways in electron tunneling through liquid alkanethiol monolayers on mercury electrodes. *J. Am. Chem. Soc.*, 119(17):11910–11919, 1997.

[183] José M Soler, Emilio Artacho, Julian D Gale, Alberto García, Javier Junquera, Pablo Ordejón, and Daniel Sánchez-Portal. The SIESTA method for ab initio order-N materials simulation. *J. Phys. Condens. Matter*, 14(11):2745, 2002.

[184] Gemma C. Solomon, David Q. Andrews, Richard P. Van Duyne, and Mark a. Ratner. When things are not as they seem: Quantum interference turns molecular electron transfer "rules" upside down. *J. Am. Chem. Soc.*, 130(25):7788–7789, 2008.

[185] Yang Song, Zhen Xie, Ming-Zhi Wei, Jian-Cai Leng, Zong-Liang Li, and Chuan-Kui Wang. Rectifying and conductance switch behaviors of molecular devices modulated by intramolecular hydrogen bonding. *Comput. Mater. Sci.*, 108:8–13, 2015.

[186] Jin Suntivich, Hubert A. Gasteiger, Naoaki Yabuuchi, Haruyuki Nakanishi, John B. Goodenough, and Yang Shao-Horn. Design principles for oxygen-reduction activity on perovskite oxide catalysts for fuel cells and metal-air batteries. *Nat. Chem.*, 3(7):546–550, 2011.

[187] Cherumuttathu H Suresh. Molecular Electrostatic Potential Approach to Determining the Steric Effect of Phosphine Ligands in Organometallic Chemistry . *Inorg. Chem.*, 45(13):4982–4986, jun 2006.

[188] N J Tao. Electron transport in molecular junctions. *Nat. Nanotechnol.*, 1(3):173–181, 2006.

[189] P. Tarakeshwar, T. J. Dhilip Kumar, and N. Balakrishnan. Nature of hydrogen interaction and saturation on small titanium clusters. *J. Phys. Chem. A*, 112(13):2846–2854, 2008.

[190] Pilarisetty Tarakeshwar, Julio L. Palma, Gregory P. Holland, Petra Fromme, Jeffery L. Yarger, Vladimiro Mujica, and L Yarger. Probing the Nature of Charge Transfer at Nano-Bio Interfaces: Peptides on Metal Oxide Nanoparticles. *J. Phys. Chem. Lett.*, 5(20):3555–3559, oct 2014.

[191] Cedric Cedric Tard and Christopher J Pickett. Structural and functional analogues of the active sites of the [Fe]-,[NiFe]-, and [FeFe]-hydrogenases. *Chem. Rev.*, 109(6):2245, 2009.

[192] Ken Tokunaga, Shigekazu Ohmori, and Hiroshi Kawabata. Bond overlap population analysis on through-space electron transfer in [3n]cyclophanes (n=2 5). *Thin Solid Films*, 554:170–174, 2014.

[193] C. a. Tolman. Electron donor-acceptor properties of phosphorus ligands. Substituent additivity. *J. Am. Chem. Soc.*, 92(10):2953–2956, 1970.

[194] C A Tolman and D H Gerlach. Triarylphosphine and Ethylene Complexes of Zerovalent Nickel, Palladium, Platinum. *J. Am. Chem. Soc.*, 426(1967):2669–2676, 1971.

[195] Chadwick Tolman. Phosphorus Ligand Exchange Equilibria on Zerovalent Nickel. A Dominant Role for Steric Effects. *J. Am. Chem. Soc.*, 92:2956–2965, 1970.

[196] Chadwick a Tolman. Steric effects of phosphorus ligands in organometallic chemistry and homogeneous catalysis. *Chem. Rev.*, 77(3):313–348, 1977.

[197] Akira Ueda, Shota Yamada, Takayuki Isono, Hiromichi Kamo, Akiko Nakao, Reiji Kumai, Hironori Nakao, Youichi Murakami, Kaoru Yamamoto, Yutaka Nishio, and Hatsumi Mori. Hydrogen-bond-dynamics-based switching of conductivity and magnetism: a phase transition caused by deuterium and electron transfer in a hydrogen-bonded purely organic conductor crystal. *J. Am. Chem. Soc.*, 136(34):12184–92, 2014.

[198] E van Lenthe, J G Snijders, and E J Baerends. The zero-order regular approximation for relativistic effects: The effect of spin-orbit coupling in closed shell molecules. *J. Chem. Phys.*, 105(15):6505, 1996.

[199] Erik van Lenthe, Andreas Ehlers, and Evert-Jan Baerends. Geometry optimizations in the zero order regular approximation for relativistic effects. *J. Chem. Phys.*, 110(18):8943, 1999.

[200] Latha Venkataraman, Jennifer E Klare, Colin Nuckolls, Mark S Hybertsen, and Michael L Steigerwald. Dependence of single-molecule junction conductance on molecular conformation. *Nature*, 442(7105):904–907, 2006.

[201] Matthieu J. Verstraete, P. Bokes, and R. W. Godby. First-principles conductance of nanoscale junctions from the polarizability of finite systems. *J. Chem. Phys.*, 130(12), 2009.

[202] Cheng Wang, Kathryn E. DeKrafft, and Wenbin Lin. Pt Nanoparticles@Photoactive MetalOrganic Frameworks: Efficient Hydrogen Evolution via Synergistic Photoexcitation and Electron Injection. *J. Am. Chem. Soc.*, 134(17):7211–7214, may 2012.

[203] Chengliang Wang, Huanli Dong, Wenping Hu, Yunqi Liu, and Daoben Zhu. Semiconducting ??-conjugated systems in field-effect transistors: A material odyssey of organic electronics. *Chem. Rev.*, 112(4):2208–2267, 2012.

[204] Ning Wang, Mei Wang, Ying Wang, Dehua Zheng, Hongxian Han, Mårten S. G. Ahlquist, and Licheng Sun. Catalytic Activation of H 2 under Mild Conditions by an [FeFe]-Hydrogenase Model via an Active μ-Hydride Species. *J. Am. Chem. Soc.*, 135(37):13688–13691, sep 2013.

[205] Xueshun Wang, Boshi Huang, Xinyong Liu, and Peng Zhan. Discovery of bioactive molecules from CuAAC click-chemistry-based combinatorial libraries. *Drug Discov. Today*, 00(00), 2015.

[206] Florian Weigend and Reinhart Ahlrichs. Balanced basis sets of split valence, triple zeta valence and quadruple zeta valence quality for H to Rn: Design and assessment of accuracy. *Phys. Chem. Chem. Phys.*, 7(18):3297, 2005.

[207] Paul S. Weiss. Functional molecules and assemblies in controlled environments: Formation and measurements. *Acc. Chem. Res.*, 41(12):1772–1781, 2008.

[208] George M Whitesides and Mila Boncheva. Beyond molecules: self-assembly of mesoscopic and macroscopic components. *Proc. Natl. Acad. Sci. U. S. A.*, 99(8):4769–74, 2002.

[209] George M Whitesides and Bartosz Grzybowski. Self-assembly at all scales. *Science (80-.).*, 295(5564):2418–2421, 2002.

[210] Claire Wombwell and Erwin Reisner. Synthesis, structure and reactivity of Ni site models of [NiFeSe] hydrogenases. *Dalton Trans.*, 43(11):4483–93, 2014.

[211] Claire H. Woo, Pierre M. Beaujuge, Thomas W. Holcombe, Olivia P. Lee, and Jean M J Fréchet. Incorporation of furan into low band-gap polymers for efficient solar cells. *J. Am. Chem. Soc.*, 132(44):15547–15549, 2010.

[212] Hong Wu and Michael B. Hall. Density functional theory on the larger active site models for [NiFe] hydrogenases: Two-state reactivity? *Comptes Rendus Chim.*, 11(8):790–804, 2008.

[213] Songmei Wu, Maria Teresa González, Roman Huber, Sergio Grunder, Marcel Mayor, Christian Schönenberger, and Michel Calame. Molecular junctions based on aromatic coupling. *Nat. Nanotechnol.*, 3(9):569–574, 2008.

[214] Fan Xia and Lei Jiang. Bio-inspired, smart, multiscale interfacial materials. *Adv. Mater.*, 20(15):2842–2858, 2008.

[215] Bingqian Q. Xu, Xiulan L. Li, Xiaoyin Y. Xiao, Hiroshi Sakaguchi, and Nongjian J. Tao. Electromechanical and conductance switching properties of single oligothiophene molecules. *Nano Lett.*, 5(7):1491–1495, 2005.

[216] Yongqiang Xue, Supriyo Datta, and Mark a. Ratner. First-principles based matrix Green's function approach to molecular electronic devices: general formalism. *Chem. Phys.*, 281(2-3):151–170, aug 2002.

[217] Yusuke Yamada, Takamitsu Miyahigashi, Hiroaki Kotani, Kei Ohkubo, and Shunichi Fukuzumi. Photocatalytic hydrogen evolution with Ni nanoparticles by using 2-phenyl-4-(1-naphthyl)quinolinium ion as a photocatalyst. *Energy Environ. Sci.*, 5(3):6111, 2012.

[218] Shengfa Ye and Frank Neese. Accurate modeling of spin-state energetics in spin-crossover systems with modern density functional theory. *Inorg. Chem.*, 49(3):772–774, 2010.

[219] Sina Yeganeh, Mark a. Ratner, Ernesto Medina, and Vladimiro Mujica. Chiral electron transport: Scattering through helical potentials. *J. Chem. Phys.*, 131(1):014707, 2009.

[220] T Yokoyama, S Yokoyama, T Kamikado, Y Okuno, and S Mashiko. Selective assembly on a surface of supramolecular aggregates with controlled size and shape. *Nature*, 413(6856):619–621, 2001.

[221] Yang Yu, Chang Cui, Xiaohong Liu, Igor D Petrik, Jiangyun Wang, and Yi Lu. A Designed Metalloenzyme Achieving the Catalytic Rate of a Native Enzyme. *J. Am. Chem. Soc.*, 137(36):11570–11573, sep 2015.

[222] Ming Xing Zhang and Guang Jiu Zhao. Modification of n-type organic semiconductor performance of perylene diimides by substitution in different positions: Two-dimensional ??-stacking and hydrogen bonding. *ChemSusChem*, 5(5):879–887, 2012.

[223] Yanan Zhao, Brian Ashcroft, Peiming Zhang, Hao Liu, Suman Sen, Weisi Song, JongOne Im, Brett Gyarfas, Saikat Manna, Sovan Biswas, Chad Borges, and Stuart Lindsay. Single-molecule spectroscopy of amino acids and peptides by recognition tunnelling. *Nat. Nanotechnol.*, 9(6):466–473, 2014.

[224] Xiao Shun Zhou, Zhao Bin Chen, Sheng Hua Liu, Shan Jin, Ling Liu, Hai Ming Zhang, Zhao Xiong Xie, Yun Bao Jiang, and Bing Wei Mao. Single molecule conductance of dipyridines with conjugated ethene and nonconjugated ethane bridging group. *J. Phys. Chem. C*, 112(10):3935–3940, 2008.

[225] Andreas Züttel, Philippe Mauron, Shunsuke Kato, Elsa Callini, Marco Holzer, and Jianmei Huang. Storage of Renewable Energy by Reduction of CO¡SUB¿2¡/SUB¿ with Hydrogen. *Chim. Int. J. Chem.*, 69(5):264–268, may 2015.

APPENDIX A

MULLIKEN POPULATION ANALYSIS

Population analysis is about looking at the charge distribution within a compound. This is a more rigorous version of the partial charges that chemists use within the domain of Lewis structures. Because partial charges can not be measured experimentally, there is a level of arbitrariness in their definition. But the idea behind all the various models is very simple; one must define the spatial boundaries of atoms in a molecule and integrate over the charge distribution within the volumetric boundary. This causes more fundamental question to arise: where does an atom electron cloud starts?, where does it ends?, Which nucleus does an specific volumetric element of the electron cloud belong to?

Mulliken tried to resolve this question by Partitioning the electrons onto the atoms based on the contribution of atomic orbitals of a specific site to the molecular orbital. This method is benefiting from the theoretical framework of LCAO, Linear Combination of Atomic Orbitals. Within this framework the total number of electrons, N, is:

$$N = \sum_{j} (\sum_{r,s} \int \; c_{jr}\phi_r(r_j) \; c_{js}\phi_s(r_j) \; dr_j) \tag{A.1}$$

where j is the molecular orbital, r and s are atomic indexes of the atomic orbital ϕ. This equation can be recast into:

$$N = \sum_{j} (\sum_{r} c_{jr}^2 + \frac{1}{2} \sum_{r,s} c_{jr}c_{js}S_{rs}) \tag{A.2}$$

This equation consists of two sums, the first summation simply denotes the electrons that belong to one atom. The second summation can be interpreted as the shared electrons between two atoms. In fact this second term is the problematic term and is difficult to handle.

In order to treat the second term Mulliken proposed to break these electrons in half between the two atoms. Here is a very quick red flag for chemists, because Mulliken charges are assigned to atoms by neglecting the electronegativity of the atoms. So,

in Mulliken framework the electrons that belong to atom k are:

$$N_k = \sum_j (\sum_{r \in k} c_{jr}^2 + 0.5 \sum_{r,s \in k} c_{jr} c_{js} S_{rs} + 0.5 \sum_{r,s \notin k} c_{jr} c_{js} S_{rs}) \tag{A.3}$$

The second problem with Mulliken charge can be seen within this equation. Mulliken charges are notoriously basis-set dependent. So they are not meant to be used as a quantitative measure. They are a very nice comparative tool that can give relatively good chemical intuitions into the system at very computationally inexpensive way.

APPENDIX B

CODE USED FOR CALCULATING DIHEDRAL ANGLE

This code calculates the normal vector of the planes that pass through S-Ni-S and P-Ni-P. Then it calculates the angle between the two planes and finally checks to make sure it reports the acute angle.

```
import numpy as np
def bordar(a,b,c):
    vec1=np.array(b)-np.array(a)
    vec2=np.array(c)-np.array(a)
    vec3=np.cross(vec1,vec2)
    return vec3


    Ni=[ -0.248893000, 0.863606000, -0.954728000]
S1=[ -2.143854000, 1.383427000, -2.030408000]
S2=[ -0.697042000, 2.443230000, 0.635116000]
P1=[ 1.859796000, 0.710333000, -0.230978000]
P2=[ -1.181825000, -1.238211000, -0.130040000]
bor1=bordar(Ni,S1,S2)
bor2=bordar(Ni,P1,P2)
ang=np.arccos(np.dot(bor1,bor2)/(np.linalg.norm(bor1)*np.linalg.norm(bor2)))
if np.isnan(ang):
    if np.linalg.norm(bor1)==np.linalg.norm(bor2):
        print 0.0
    else:
        print np.pi*180.0/np.pi
else:
    print ang*180.0/np.pi
```

APPENDIX C

PERMISSION FROM AMERICAN CHEMICAL SOCIETY